

Christof Abfalterer, BSc

**Shallow Landslide Assessment Based on Engineering
Geomorphologic Analyses – A Case Study around the Village of
Sellrain, Tyrol, Austria**

MASTERARBEIT

zur Erlangung des akademischen Grades

Master of Science

Masterstudium Erdwissenschaften

eingereicht an der

Technischen Universität Graz

Betreuer

Ao.Univ.-Prof. Dr.rer.nat. Liu, Qian

Institute of Applied Geosciences

Erdwissenschaften

EIDESSTATTLICHE ERKLÄRUNG

Ich erkläre an Eides statt, dass ich die vorliegende Arbeit selbstständig verfasst, andere als die angegebenen Quellen/Hilfsmittel nicht benutzt, und die den benutzten Quellen wörtlich und inhaltlich entnommenen Stellen als solche kenntlich gemacht habe. Das in TUGRAZonline hochgeladene Textdokument ist mit der vorliegenden Masterarbeit identisch.

Datum

Unterschrift

Shallow Landslide Assessment Based on Engineering Geomorphologic Analyses – A Case Study around the Village of Sellrain, Tyrol, Austria

Master Thesis



Figure 1: Village of Sellrain; © https://de.wikipedia.org/wiki/Sellrain#/media/Datei:Gemeinde_Sellrain.jpg

Department of Earth Sciences
Technical University Graz
Graz, December 2019

Author: Abfalterer Christof, BSc

01217986

Advisor: Ao.Univ.-Prof. Dr. Liu, Qian

Table of Contents

0	List of Figures and Tables	IV
0.1	Figures	IV
0.2	Tables	XI
0.3	Symbols and Variables.....	XII
1	Acknowledgments	1
2	Abstract.....	2
3	Problem Statement.....	3
4	The Study Area	6
4.1	General Information.....	6
4.2	Geology.....	9
4.2.1	Basement geology	10
4.2.2	Quaternary geology.....	14
4.3	Historical Overview of Landslides/Mudslides in the Sellrain Valley	15
5	Review of Previous Approaches.....	18
5.1	Slope Stability and Shallow Landslides	18
5.1.1	Definition of shallow landslides.....	18
5.1.2	Slope stability	19
5.1.3	Modelling shallow landslides	22
5.1.4	A new modelling approach - MEMPS	28
6	Objective of Thesis.....	31
7	Integrated Data	32
7.1	Field Data.....	32
7.2	Open Source Data.....	32
7.3	Non-Public Data Provided by Tyrolean Governmental Agencies	32
8	Methodology.....	33
8.1	Calculation of MEMPS	33
8.1.1	Input parameters	33
8.1.2	MEMPS calculation	34
8.1.3	Error assessment of MEMPS	38

8.2	Field Work.....	38
8.2.1	Drunken trees.....	38
8.2.2	Possible landslides.....	39
8.2.3	Cracks in the road and hummocky topography.....	39
8.2.4	Multi-Part outcrops and others	39
9	Results.....	40
9.1	Field Work.....	40
9.1.1	Outcrop Map	48
9.2	MEMPS.....	49
9.2.1	Input parameters	49
9.2.2	The calculation of MEMPS	50
9.3	Remarks to the Large-Scale Map.....	77
10	Discussion	78
10.1	Concerning results of Category III (Potential instability)	78
10.2	Concerning the Different MEMPS-Calculations	78
10.2.1	Precipitation Period 1 (1980 – 2010)	79
10.2.2	Precipitation Period 2 (2010 – 2016)	80
10.2.3	Precipitation Period 3 (Maximum Precipitation)	80
10.2.4	Comparison of the maps	81
10.3	Reliability of the Field Work and its Comparison with the calculated Model(s) and Literature	81
10.3.1	Example 1 – Outcrops along forest road to Rosskogel and the parallel trail that runs above (Outcrops 12 to 25 and outcrops 93 to 122)	82
10.3.2	Example 2 – Outcrop 141.....	84
10.3.3	Example 3 – Outcrops 152/154	86
10.3.4	Outcrops outside the study area (Outcrops 74 to 80)	87
10.4	Possible Effects of varying Friction Angles	88
11	Conclusions	89
12	References	91
13	Appendix.....	95

13.1	Outcrop Protocol (in German and English)	95
13.2	DEM – maps	102
13.2.1	5m resolution.....	102
13.2.2	10m resolution.....	108
13.3	DTM – maps.....	114
13.3.1	5m resolution.....	114
13.3.2	10m resolution.....	120

0 List of Figures and Tables

0.1 Figures

Figure 1: Village of Sellrain; © https://de.wikipedia.org/wiki/Sellrain#/media/Datei:Gemeinde_Sellrain.jpg	
Figure 2: Aerial photograph of the precipitation event June 7 th , 2015 (Rauth, 2015) © Witting3	
Figure 3: View to the south, in the direction of the Fotscher Valley (alpen.wetter, 2015) © zeitungsfoto.at	3
Figure 4: Map of study area (red); satellite picture taken on July 31 st 2015 , about a month and a half after the event; the result of the precipitation is visible (e.g. west of the Sellrain map marker); base map: © Google Earth	4
Figure 5: Overview of the study area (red) with the water network – selected rivers and streams are named – that is part of the study area and the river Inn outside of it; base map: © Google Earth; water network: © (Land Tirol - data.tirol.gv.at, 2019)	6
Figure 6: Map of the study area with the corresponding water network, which includes Melach, Fotscher Bach additional streams located in the study area and other streams located outside the study area; raw data: © (Land Tirol - data.tirol.gv.at, 2018), orthophoto and water network: © (Land Tirol - data.tirol.gv.at, 2019)	7
Figure 7: Geologic map of the study area (yellow) and of its surroundings; Greywacke zone is orange, the Permomesozoic rocks are red, the Ötztal - Stubai Kristallin is blue, the Northern Calcareous Alps are green, faults and thrust faults are marked black; raw data: © (Land Tirol - data.tirol.gv.at, 2018), orthophoto: © (Land Tirol - data.tirol.gv.at, 2019), geology: © (Geologische Bundesanstalt - geologie.ac.at, 2019)	9
Figure 8: Overview map of the ÖSK (Schmidt, 1965)	10
Figure 9: Amphibolite found near Längenfeld , Ötz Valley; The rock contains mainly feldspar, biotite and hornblende; bulky (upper picture) as well as schistose (lower picture); fragments of the Cambrian, surfaced through the Variscan Orogenesis; pictures taken by the author on June 7 th , 2013	11
Figure 10: Paragneiss found near Längenfeld Ötz Valley, containing muscovite, biotite, feldspar and quartz; the texture shows layering which is a hint towards a sedimentary origin; pictures taken by the author on June 7 th , 2013	12
Figure 11: Typical orthogneiss found at the Engelswand near Tumpfen in the Ötz Valley; surface is reddish due to weathering; a fresh cut is grey; heavily schistose texture; minerals are quartz, feldspar (anorthite) and biotite with traces of muscovite; formed from acidic magmatic rock through metamorphosis; pictures taken by the author on June 7 th , 2013	13
Figure 12: Partly cemented terrace gravel/ moraine material with a few larger boulders; Outcrop 11 (upper picture) Outcrop 12 (lower picture); both referenced in the large map at the end of the thesis	14

Figure 13: Estimated total precipitation amount in l/m^2 over 12 hours on June 7 th , 2015 (alpen.wetter, 2015); © ZAMG-INCA; The maximum amounts are located at Sellrain and Gries in Sellrain	16
Figure 14: Pictures of the aftermath in Sellrain; the destruction and the amount of deposits are easily visible (alpen.wetter, 2015) © zeitungsfoto.at	17
Figure 15: Illustration of an infinite slope model with the parameters involved; taken from Deb & El-Kadi (2009) as it can be seen in Equation 1; θ = slope angle, C_r = root cohesion, C_s = soil cohesion, φ (in this case ϕ) = internal friction angle, D = vertical soil height, h = soil depth perpendicular to the slope surface; h_w = water height perpendicular to slope surface; D_w = vertical water height, ρ_s = soil density, ρ_w = water density and S = slope length (Deb & El-Kadi, 2009)	22
Figure 16: Above: Illustration of a specific catchment area Below: The rainfall calibration for different regions that leads to R (=Steady state recharge); taken from Deb & El-Kadi (2009) as it can be seen in Equation 2 (Deb & El-Kadi, 2009)	23
Figure 17: Results of the SINMAP-model for region 1 of Deb & El-Kadi (2009)	24
Figure 18: Subbasin model according to Beven & Kirkby (1979); with S_x = Subbasin stores, A_c being the upslope contributing area, m = a constant factor, q_b = flow reaching the channel, q_0 = flow when $S_3=0$ and m is a constant (Beven & Kirkby, 1979)	26
Figure 19: An example for calculated results of the TOPMODEL for basin outflow/discharge, namely the Lanshaw sub-basin in the winter; Beven & Kirkby (1979)	27
Figure 20: Variation of the different equations above; z_{c0} (dry soil) and z_{c1} (saturated soil) are from Lida (1999) (Equations 6 and 7) and z_c (any degree of soil saturation) are derived from MEMPS for similar conditions (Michel & Kobiyama, 2016)	30
Figure 21: Graphic of MEMPS used in this thesis/study; created by the QGIS-graphic modeler; (QGIS, 2018 - 2019)	35
Figure 22: Drunken trees in the municipal forest of Neder on 2019/07/17; the crooked growth is clearly visible; Outcrop 143 (referenced in the large map at the end of the thesis)	40
Figure 23: very small landslide; mostly contains fine grained material with few larger blocks; outcrop approx. 5m wide and 0.5 m high. Found in the municipal forest of on 2019/07/17; Outcrop 144 (referenced in the large map at the end of the thesis)	41
Figure 24: A larger landslide, its headscarp is approximately 5 to 10 m above; found at the Seigesbach; different kinds of blocky material going from fine grained sand to block in cm - to m- range; part of Outcrop 86 (referenced in the large map at the end of the thesis);	41
Figure 25: left: Landslide near Perfall; right: Landslide up close (Outcrop 54), with a new wooden bridge; picture below: Possible landslide continues beneath the trail; fine grained soil with blocks up to a 0.5 m. ; Outcrop 149 (referenced in the large map at the end of the thesis)	42

Figure 26: Picture of possible landslides on the slopes of the Tiefen Valley between Oberperfuss and Sellrain; Outcrop 28 (referenced in the large map at the end of the thesis)	43
Figure 27:Left: Outcrop 12: Moraine material made of partly cemented terrace gravel with blocks of several sizes in between; right: Outcrop 4: Big blocks of unknown size ; no schistosity or layers visible (outcrops referenced in the large map at the end of the thesis)	43
Figure 28: Composition: Sand and gravel; Outcrop 26 (referenced in the large map at the end of the thesis).....	44
Figure 29: Above: Seigesbach as it can be seen from St. Quirin, Outcrop 121; below: Seigesbach up close: possible bedrock (?), Outcrop 88; (outcrops referenced in the large map at the end of the thesis)	45
Figure 30: Several examples for cracks in the roads; Outcrop 123 (Left) and Outcrop 132 (Right) are located in Taugert, Sellrain; Outcrop 155 (Below) is located in Durögg, Sellrain (outcrops referenced in the large map at the end of the thesis)	46
Figure 31: Examples for hummocky topography; Above: St. Quirin, Sellrain (Outcrop 126); Below: Neder, Grinzens (Outcrop 27) (outcrops referenced in the large map at the end of the thesis)	47
Figure 32:The outcrop map of the study area, which is marked red; The categories' colors and symbols are as described: Landslide (yellow): on the same side as outcrop point(circle) and remote observation (star); Hummocky topography (pink): on the same side as outcrop point (circle) and remote observation (star);Multi-Part outcrop (White): Different categories (diamond), different scales of hummocky topography (circle) and different scales of landslide(star); Drunken trees (green); Cracks in road (blue); Others (turquoise); base map: © Google Earth;	48
Figure 33: Category III (potential instability): The results for the calculations of the critical soil depth z_c of the 2007- 5-m resolution (DEM); Period 1 is blue, Period 2 is orange and Period 3 is grey	51
Figure 34: The results for the calculations of the critical soil depths z_c of the 2007, 5-m resolution (DEM); Upper Left: The histogram of all Precipitation - Periods containing the absolute count (green) and its percentage (blue) for three categories: Category I (no risk), Category II (onset of shallow landslides) and Category III (potential instability) Upper Left: Period 1, upper right: Period 2 and lower left: Period 3.....	52
Figure 35: Category III (potential instability): The results for the calculations of the critical soil depths z_c of the 2007,10-m resolution (DEM); Period 1 is blue, Period 2 is orange and Period 3 is grey.....	53
Figure 36: The results for the calculations of the critical soil depths z_c of the 2007, 10m-resolution (DEM); Upper Left: The histogram of all Precipitation - Periods containing the	

absolute count (green) and its percentage (blue) for three categories: Category I (no risk), Category II (onset of shallow landslides) and Category III (potential instability) Upper Left: Period 1, upper right: Period 2 and lower left: Period 3.....	54
Figure 37: Category III (potential instability): The results for the calculations of z_c of the 2013-5-m resolution (DEM); Period 1 is blue, Period 2 is orange and Period 3 is grey	55
Figure 38: The results for the calculations of the critical soil depths z_c of the 2013, 5-m resolution (DEM);Upper Left: The histogram of all Precipitation - Periods containing the absolute count (green) and its percentage (blue) for three categories: Category I (no risk), Category II (onset of shallow landslides) and Category III (potential instability) Upper Left: Period 1, upper right: Period 2 and lower left: Period 3.....	56
Figure 39: Category III (potential instability): The results for the calculations of the critical soil depths z_c of the 2013-10-m resolution (DEM); Period 1 is blue, Period 2 is orange and Period 3 is grey.....	57
Figure 40: The results for the calculations of the critical soil depths z_c of the 2013, 10-m-resolution (DEM); Upper Left: The histogram of all Precipitation - Periods containing the absolute count (green) and its percentage (blue) for three categories: Category I (no risk), Category II (onset of shallow landslides) and Category III (potential instability) Upper Left: Period 1, upper right: Period 2 and lower left: Period 3.....	58
Figure 41: Map of the critical soil depth z_c for the average annual precipitation between 1980 and 2010 (2007 - DEM, 1m); raw data: © (Land Tirol - data.tirol.gv.at, 2018), orthophoto: © (Land Tirol - data.tirol.gv.at, 2019).....	59
Figure 42: Map of the critical soil depth z_c for the average annual precipitation between 2010 and 2016 (2007 - DEM, 1m); raw data: © (Land Tirol - data.tirol.gv.at, 2018), orthophoto: © (Land Tirol - data.tirol.gv.at, 2019).....	60
Figure 43: Map of the critical soil depth z_c for the extreme precipitation of June 2015 (2007 - DEM, 1m); raw Data: © (Land Tirol - data.tirol.gv.at, 2018), orthophoto: © (Land Tirol - data.tirol.gv.at, 2019).....	61
Figure 44 Map of the critical soil depth z_c for the average annual precipitation between 1980 and 2010 (2013 - DEM, 1m); raw data: © (Land Tirol - data.tirol.gv.at, 2018), orthophoto: © (Land Tirol - data.tirol.gv.at, 2019).....	62
Figure 45: Map of the critical soil depth z_c for the average annual precipitation between 2010 and 2016 (2013 - DEM, 1m); raw Data: © (Land Tirol - data.tirol.gv.at, 2018), orthophoto: © (Land Tirol - data.tirol.gv.at, 2019).....	63
Figure 46: Map of the critical soil depth z_c for the extreme precipitation of June 2015 (2013 - DEM, 1m); raw Data: © (Land Tirol - data.tirol.gv.at, 2018), orthophoto: © (Land Tirol - data.tirol.gv.at, 2019).....	64

Figure 47: Category III (potential instability): The results for the calculations of the critical soil depths z_c of the 2007, 5-m resolution (DTM); Period 1 is blue, Period 2 is orange and Period 3 is grey	65
Figure 48: The results for the calculations of the critical soil depths z_c of the 2007, 5-m resolution (DTM);Upper Left: The histogram of all Precipitation - Periods containing the absolute count (green) and its percentage (blue) for three categories: Category I (no risk), Category II (onset of shallow landslides) and Category III (potential instability) Upper Left: Period 1, upper right: Period 2 and lower left: Period 3.....	66
Figure 49: Category III (potential instability): The results for the calculations of the critical soil depths z_c of the 2007, 10-m resolution (DTM); Period 1 is blue, Period 2 is orange and Period 3 is grey.....	67
Figure 50: The results for the calculations of the critical soil depths z_c of the 2007, 10-m resolution (DTM);Upper Left: The histogram of all Precipitation - Periods containing the absolute count (green) and its percentage (blue) for three categories: Category I (no risk), Category II (onset of shallow landslides) and Category III (potential instability) Upper Left: Period 1, upper right: Period 2 and lower left: Period 3.....	68
Figure 51: Category III (potential instability): The results for the calculations of the critical soil depths z_c of the 2013, 5-m resolution (DTM); Period 1 is blue, Period 2 is orange and Period 3 is grey	69
Figure 52: The results for the calculations of the critical soil depths z_c of the 2013, 5-m resolution (DTM);Upper Left: The histogram of all Precipitation-Periods containing the absolute count (green) and its percentage (blue) for three categories: Category I (no risk), Category II (onset of shallow landslides) and Category III (potential instability) Upper Left: Period 1, upper right: Period 2 and lower left: Period 3.....	70
Figure 53: Map of the critical soil depth z_c for the average annual precipitation between 1980 and 2010 (2007 - DTM, 1m); raw data: © (Land Tirol - data.tirol.gv.at, 2018), orthophoto: © (Land Tirol - data.tirol.gv.at, 2019).....	71
Figure 54: Map of the critical soil depth z_c for the average annual precipitation between 2010 and 2016 (2007 - DTM, 1m); raw data: © (Land Tirol - data.tirol.gv.at, 2018), orthophoto: © (Land Tirol - data.tirol.gv.at, 2019).....	72
Figure 55: Map of the critical soil depth z_c for the extreme precipitation of June 2015 (2007 - DTM, 1m); raw data: © (Land Tirol - data.tirol.gv.at, 2018), orthophoto: © (Land Tirol - data.tirol.gv.at, 2019).....	73
Figure 56: Map of the critical soil depth z_c for the average annual precipitation between 1980 and 2010 (2013 - DTM, 1m); raw data: © (Land Tirol - data.tirol.gv.at, 2018), orthophoto: © (Land Tirol - data.tirol.gv.at, 2019).....	74

Figure 57: Map of the critical soil depth z_c for the average annual precipitation between 2010 and 2016 (2013 - DTM, 1m); raw data: © (Land Tirol - data.tirol.gv.at, 2018), orthophoto: © (Land Tirol - data.tirol.gv.at, 2019).....	75
Figure 58: Map of the critical soil depth z_c for the extreme precipitation of June 2015 (2013 - DTM, 1m); raw data: © (Land Tirol - data.tirol.gv.at, 2018), orthophoto: © (Land Tirol - data.tirol.gv.at, 2019).....	76
Figure 59: Pictures of outcrops westward of St. Quirin; namely the pictures above are from Outcrop 19 (first two upper pictures from the left) and Outcrop 110 (last upper picture from the left) and Outcrop 24 (picture below); the upper pictures describe drunken trees and the bottom picture shows a small slide along the road, approximately 4 to 5 meters high and approx. 7 to 8 meters wide	83
Figure 60: Outtake of outcrop 141; upper picture: Drunken trees in the background as well as hummocky topography with several boulders in between; bottom picture landslide from below -> hummocky topography; unfortunately, a full size picture was not possible	85
Figure 61: Outcrop 152: Drunken tree(s) visible in the background (bottom pictures) plus possible headscarp in the upper and lower left picture	86
Figure 62: Both pictures are taken from Outcrop 80; several smaller landslides along the Seigesbach; varying sizes (from 5 to 10 meters high and 10 to 20 meters wide)	87
Figure 63: Smaller slide along Seigesbach (Outcrop 79); boulder of 1- 2 meters to fine grained material (sand) possible headscarp visible in the picture; varying height (5 – 15 m) and wide up to 20 meters)	88
Figure 64: Map of the critical soil depth z_c for the average annual precipitation between 1980 and 2010 (2007 - DEM, 5m); raw data: © (Land Tirol - data.tirol.gv.at, 2018), orthophoto: © (Land Tirol - data.tirol.gv.at, 2019).....	102
Figure 65: Map of the critical soil depth z_c for the average annual precipitation between 2010 and 2016 (2007 - DEM, 5m); raw data: © (Land Tirol - data.tirol.gv.at, 2018), orthophoto: © (Land Tirol - data.tirol.gv.at, 2019).....	103
Figure 66: Map of the critical soil depth z_c for the Extreme Precipitation of June 2015 (2007 - DEM, 5m); raw data: © (Land Tirol - data.tirol.gv.at, 2018), orthophoto: © (Land Tirol - data.tirol.gv.at, 2019).....	104
Figure 67: Map of the critical soil depth z_c for the average annual precipitation between 1980 and 2010 (2013 - DEM, 5m); raw data: © (Land Tirol - data.tirol.gv.at, 2018), orthophoto: © (Land Tirol - data.tirol.gv.at, 2019).....	105
Figure 68: Map of the critical soil depth z_c for the average annual precipitation between 2010 and 2016 (2013 - DEM, 5m); raw data: © (Land Tirol - data.tirol.gv.at, 2018), orthophoto: © (Land Tirol - data.tirol.gv.at, 2019).....	106

Figure 69: Map of the critical soil depth z_c for the extreme precipitation of June 2015 (2013 - DEM, 5m); raw data: © (Land Tirol - data.tirol.gv.at, 2018), orthophoto: © (Land Tirol - data.tirol.gv.at, 2019).....	107
Figure 70: Map of the critical soil depth z_c for the average annual precipitation between 1980 and 2010 (2007 - DEM, 10m); raw data: © (Land Tirol - data.tirol.gv.at, 2018), orthophoto: © (Land Tirol - data.tirol.gv.at, 2019).....	108
Figure 71: Map of the critical soil depth z_c for the average annual precipitation between 2010 and 2016 (2007 - DEM, 10m); raw data: © (Land Tirol - data.tirol.gv.at, 2018), orthophoto: © (Land Tirol - data.tirol.gv.at, 2019).....	109
Figure 72: Map of the critical soil depth z_c for the extreme precipitation of June 2015 (2007 - DEM, 10m); raw data: © (Land Tirol - data.tirol.gv.at, 2018), orthophoto: © (Land Tirol - data.tirol.gv.at, 2019).....	110
Figure 73 Map of the critical soil depth z_c for the average annual precipitation between 1980 and 2010 (2013 - DEM, 10m); raw data: © (Land Tirol - data.tirol.gv.at, 2018), orthophoto: © (Land Tirol - data.tirol.gv.at, 2019).....	111
Figure 74: Map of the critical soil depth z_c for the average annual precipitation between 2010 and 2016 (2013 - DEM, 10m); raw data: © (Land Tirol - data.tirol.gv.at, 2018), orthophoto: © (Land Tirol - data.tirol.gv.at, 2019).....	112
Figure 75: Map of the critical soil depth z_c for the Extreme Precipitation of June 2015 (2013 - DEM, 10m); raw data: © (Land Tirol - data.tirol.gv.at, 2018), orthophoto: © (Land Tirol - data.tirol.gv.at, 2019).....	113
Figure 76: Map of the critical soil depth z_c for the average annual precipitation between 1980 and 2010 (2007 - DTM, 5m); raw data: © (Land Tirol - data.tirol.gv.at, 2018), orthophoto: © (Land Tirol - data.tirol.gv.at, 2019).....	114
Figure 77: Map of the critical soil depth z_c for the average annual precipitation between 2010 and 2016 (2007 - DTM, 5m); raw data: © (Land Tirol - data.tirol.gv.at, 2018), orthophoto: © (Land Tirol - data.tirol.gv.at, 2019).....	115
Figure 78: Map of the critical soil depth z_c for the extreme precipitation of June 2015 (2007 - DTM, 5m); raw data: © (Land Tirol - data.tirol.gv.at, 2018), orthophoto: © (Land Tirol - data.tirol.gv.at, 2019).....	116
Figure 79: Map of the critical soil depth z_c for the average annual precipitation between 1980 and 2010 (2013 - DTM, 5m); raw data: © (Land Tirol - data.tirol.gv.at, 2018), orthophoto: © (Land Tirol - data.tirol.gv.at, 2019).....	117
Figure 80: Map of the critical soil depth z_c for the average annual precipitation between 2010 and 2016 (2013 - DTM, 5m); raw data: © (Land Tirol - data.tirol.gv.at, 2018), orthophoto: © (Land Tirol - data.tirol.gv.at, 2019).....	118

Figure 81: Map of the critical soil depth z_c for the extreme precipitation of June 2015 (2013 - DTM, 5m); raw data: © (Land Tirol - data.tirol.gv.at, 2018), orthophoto: © (Land Tirol - data.tirol.gv.at, 2019).....	119
Figure 82: Map of the critical soil depth z_c for the average annual precipitation between 1980 and 2010 (2007 - DTM, 10m); raw data: © (Land Tirol - data.tirol.gv.at, 2018), orthophoto: © (Land Tirol - data.tirol.gv.at, 2019).....	120
Figure 83: Map of the critical soil depth z_c for the average annual precipitation between 2010 and 2016 (2007 - DTM, 10m); raw data: © (Land Tirol - data.tirol.gv.at, 2018), orthophoto: © (Land Tirol - data.tirol.gv.at, 2019).....	121
Figure 84: Map of the critical soil depth z_c for the extreme precipitation of June 2015 (2007 - DTM, 10m); raw data: © (Land Tirol - data.tirol.gv.at, 2018), orthophoto: © (Land Tirol - data.tirol.gv.at, 2019).....	122

0.2 Tables

Table 1: Constant Values for the Study Area along with their respective units and symbols.50

Table 2: Outcrop Protocol of the field work done by the author; It includes the number, the description and the coordinates of every outcrop (N/E/Height-> zero because not included); in German and English due to the fact that it was recorded that way.....95

0.3 Symbols and Variables

Symbol	Definition	Dimension	Unit
A_c	upslope (contributing) area (TOPMODEL)	L ²	m ²
a	upslope (contributing) area (TOPMODEL) specific catchment area (SINMAP) upstream area (MEMPS)	(M*L /T ²)/ L ²	kg/m ²
b	Contour length	L	[m]
c	Soil cohesion	(M*L /T ²)/ L ²	kg/m ²
C	Combined cohesion of soil and root	(M*L /T ²)/ L ²	kg/m ²
C₂	Cohesion	(M*L /T ²)/ L ²	kg/m ²
CHA	Channel constant	-	[-]
CHB	Channel constant	-	[-]
C_r	Root cohesion	(M*L /T ²)/ L ²	kg/m ²
C_s	Soil cohesion	(M*L /T ²)/ L ²	kg/m ²
D	Vertical soil height	L	[m]
D_w	Vertical water height	L	[m]
g	Gravitational Acceleration	L/T ²	m/s ²
h	Soil depth perpendicular to the slope surface (SINMAP) Height of water column (= water height) (MEMPS)	L	[m]
h_w	Water height perpendicular to slope surface	L	[m]
i	Rainfall rate = precipitation	(L ³ / L ²)/T	[mm/30 min]
K_s	Saturated Hydraulic Conductivity	L/T	m/day
m	Precipitation constant	L ³ /L ²	[mm]
OFV	Overland flow velocity	L/T	[m/30 min]
q	Uniform steady recharge/ Precipitation	(L ³ / L ²)/T	m/day
q₀	Flow reaching the channel	(L ³ / L ²)/T	[mm/30 min]
q_b	Flow when S ₃ = 0 and m constant	(L ³ / L ²)/T	[mm/30 min]
r	Water to soil density ratio	-	[-]
R	Steady state recharge	(L ³ / L ²)/T	m/day
S	Slope length	L	[m]
SF	Factor of safety	-	[-]
S_x (x= 1,2,3,D,C)	Subbasin stores	L ³ /L ²	[mm]
T	Soil transmissivity	L ² /T	m ² /day
T₀	Lateral transmissivity	L ² /T	m ² /day
w	Relative wetness	-	[%]
z	Soil depth	L	[m]
z_{c0}	Critical soil depth for dry soil	L	[m]
z_{c1}	Critical soil depth of saturated soil	L	[m]
θ, β	Slope angle	L/L = 1	[°]
ρ_s	Soil density	M/L ³	kg/m ³

<u>Symbol</u>	<u>Definition</u>	<u>Dimension</u>	<u>Unit</u>
ρ_w	Water density	M/L^3	kg/m^3
φ	(Internal) friction angle	$L/L = 1$	$[\circ]$

1 Acknowledgments

I would like to express my thanks to the following persons and institutions for their invaluable help in writing this thesis:

- My Advisor Ao.Univ.-Prof. Dr. Liu, Qian of the Technical University of Graz for his precious support.
- The Geo-Services of Tyrol operated by the Tyrolean Government for the DTM/DEM data (Amt der Tiroler Landesregierung - Abteilung Geoinformation - Geobasisdaten)
- The Bridge and Tunnel department of the Tyrolean Government (Amt der Tiroler Landesregierung Sachgebiet Brücken- und Tunnelbau) for providing a geotechnical survey
- My father Mag. Erwin Abfalterer, MSc for proofreading this thesis

2 Abstract

For the assessment of shallow landslides Michel & Kobiyama (2016) developed a new model called MEMPS (Modelo de Estimativa da Maxima Profundidade do Solo), which can calculate the critical soil depth for varying saturation. It was tested for the first time in the Sellrain Valley near the Village of Sellrain, Tyrol in 2019, by applying the model to an area known to be prone to shallow landslides. The first recorded event dates back to the 18th century, the most recent took place on June 7th 2015.

At the same time the model calculations were accompanied by a field study and were done primarily with a formula developed from QGIS's own graphic modeler for three separate precipitation periods (\emptyset 1980 - 2010, \emptyset 2010 - 2016 and the extreme precipitation of June 7th, 2015) on two different basemodels (DEM/DTM) with three different resolutions (1 m/5 m/10 m).

The calculations showed plausible results as they were corroborated by the findings of the field study. MEMPS identified areas of possible shallow landslides. Before using MEMPS on a larger scale, however, we have to evaluate errors within a data set, more soil measurements, hardware restrictions and above all the reproducibility of the results. But for the time being a positive feedback outweighs.

3 Problem Statement

In June 2015 Sellrain in Tyrol experienced a natural disaster which was caused by an extreme precipitation event. Although comparable catastrophes occurred in the past in this region, there was no model in place that could have predicted such an event. Several mudslides and (shallow) landslides covered the village and roads leading into the valley (Figure 2, Figure 3 & Figure 4).



Figure 2: Aerial photograph of the precipitation event June 7th, 2015 (Rauth, 2015) © Witting



Figure 3: View to the south, in the direction of the Fotscher Valley (alpen.wetter, 2015) © zeitungsfoto.at



Figure 4: Map of study area (red); satellite picture taken on July 31st 2015, about a month and a half after the event; the result of the precipitation is visible (e.g. west of the Sellrain map marker); base map: © Google Earth

There is an increasing risk of such events not only in the study area (Figure 4) but also elsewhere due to the increasing effects of climate change which is held responsible for more extreme precipitation events and extreme temperatures. Therefore, it should be imperative to have models in place that can identify problematic areas that are vulnerable for such events. So far, however, models have used either fully saturated soil or dry soil as a basis for soil saturation (Iida, 1999) but there are huge differences between these two scenarios which hardly occur in nature that way (Michel & Kobiyama, 2016).

In this thesis, therefore, the previously untested MEMPS (Modelo de Estimativa da Maxima Profundidade do Solo) by Michel & Kobiyama (2016) has been implemented for the first time to calculate the critical soil depth (the soil depth that can be moved in the event of a specific precipitation event resulting in a shallow landslide) for varying degrees of soil saturation.

This thesis is introduced by a short description of the study area that will be followed by an overview of previous approaches. Then, the objective of the case study and the origin and collection of relevant data are explained. Also, the methodology and the results of the investigation will be presented. This chapter is then followed by a discussion of the findings and the conclusions to be drawn.

4 The Study Area

4.1 General Information

The Sellrain Valley, also known as “Sellraintal”, is located approximately 15 kilometers west of Innsbruck, the capital of Tyrol, Austria. The valley runs parallel to the Inn valley and it starts in the West at the ski resort Kühtai which is part of the municipality of Silz and runs eastward to Kematen in Tyrol where it reaches the Inn valley. From Kühtai westward you reach the Ötz Valley, which is also known as “Ötztal”.

The lowest point of the valley is at 594 meters above sea level (m.a.s.l.) at the Melach mouth, the highest point is the “Hintere Brunnenkogel” with an elevation of 3.325 m.a.s.l. Thus, there is an elevation difference of around 2700 meters for the whole Sellrain Valley.

Sellrain, Gries, St. Sigmund are the villages in the valley. Several small hamlets included, the valley has a population of approximately 2,100 (Jäger, 2015) and covers an area of 187 km² (Jäger, 2015).

The main river through the valley is the “Melach” with the “Zirnbach” and the “Fotscher Bach” as its most notable tributaries. (Figure 5).

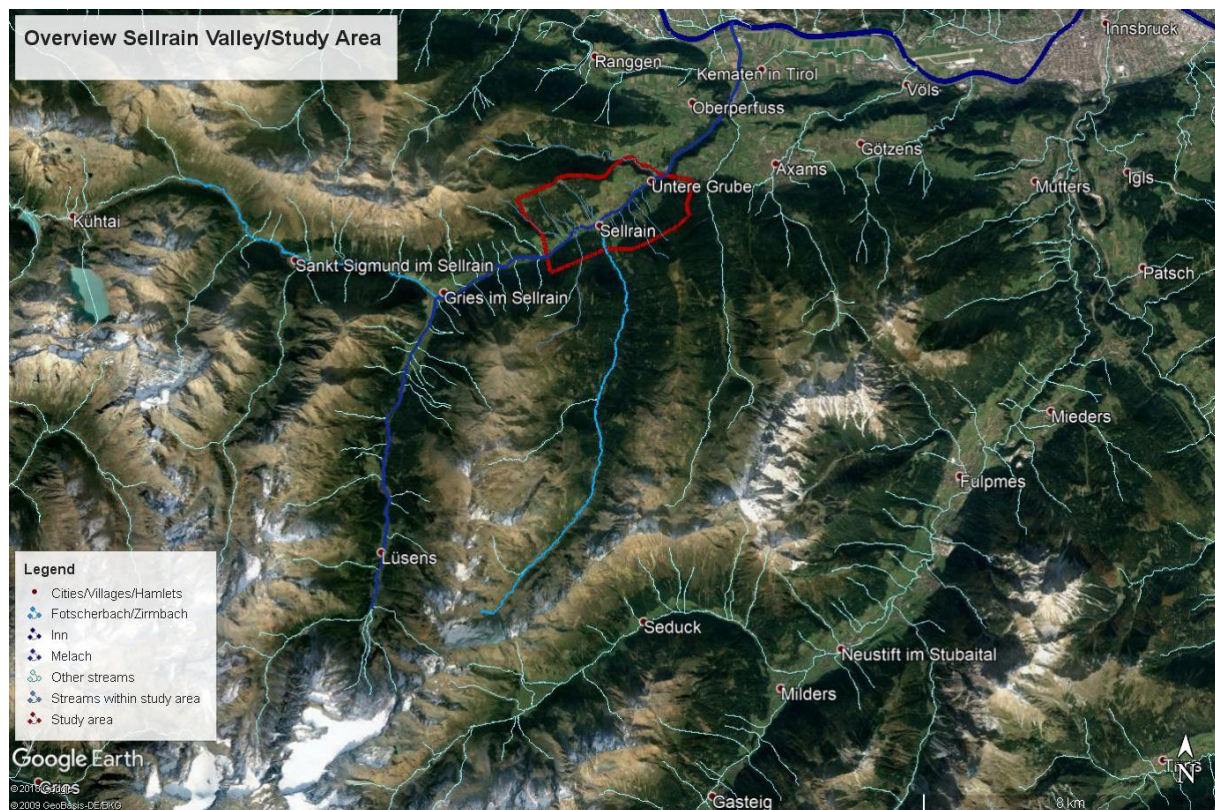


Figure 5: Overview of the study area (red) with the water network – selected rivers and streams are named – that is part of the study area and the river Inn outside of it; base map: © Google Earth; water network: © (Land Tirol - data.tirol.gv.at, 2019)

The “Zirnbach” runs through the upper Sellrain Valley eastward and is fed mainly from two other streams, the “Kraspesbach”, which originates from the Kraspes Valley and the “Gleirschbach”, which itself has its source in the Gleirsch Valley (Jäger, 2015). At Gries in Sellrain the “Zirnbach” merges with the Melach, which is the main outflow of the valley. This river springs from the glacier “Lüsener Ferner” located in the Lüsens Valley (Jäger, 2015), flows then through the Sellrain Valley to the Inn Valley and finally into the river Inn at Kematen in Tirol (Figure 5). Lastly, there is the “Fotscher Bach” that originates from the Fotscher Valley, a side valley of the Sellrain Valley, merging with Melach at the Village of Sellrain. Other smaller streams lead into those three rivers as the map below shows (Figure 6).

The main characteristic of the valley besides the rivers/streams is its steep flanks and the lack of visible bare rock, which can only be found in the back of the Lüsens Valley and the Fotscher Valley. Therefore, the main dangers for the people are avalanches in winter and flooding and landslides/mudslides in summer due to extreme precipitation and steep slopes (Jäger, 2015).

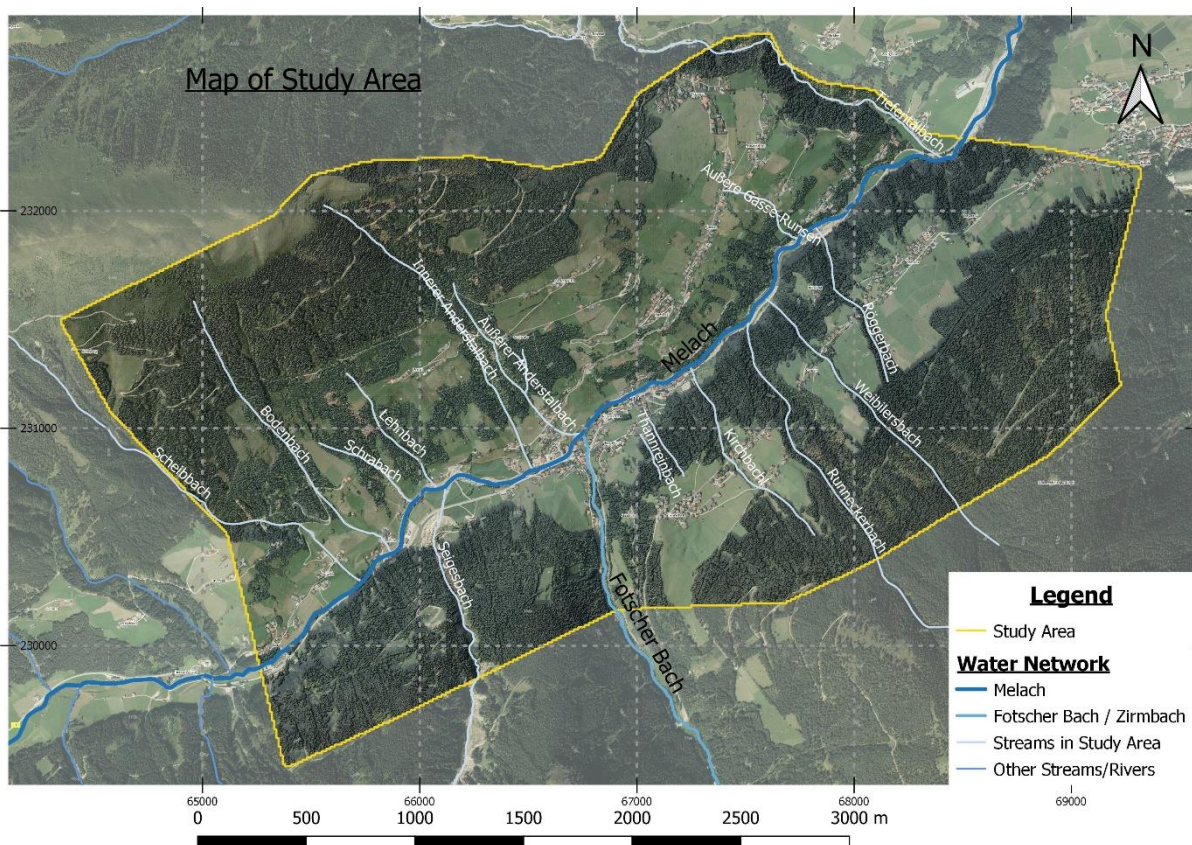


Figure 6: Map of the study area with the corresponding water network, which includes Melach, Fotscher Bach additional streams located in the study area and other streams located outside the study area; raw data: © (Land Tirol - data.tirol.gv.at, 2018), orthophoto and water network: © (Land Tirol - data.tirol.gv.at, 2019)

The study area itself is located around the village of Sellrain containing also the hamlets St. Quirin, Perfall, Tauegert, Tanneben and Neder (Grinzens). The main river flowing through the area is the Melach, then comes the Fotscher Bach followed by smaller streams that lead directly into the Melach, namely the "Scheibbach", the "Bodenbach", "Schrabach", Inner and Outer "Anderstalbach", "Äußere Gasse-Runsen and the "Tiefentalbach" north of the Melach and the "Seigesbach", the "Kirchbach" , the "Runneckerbach", the "Weibilersbach" and the "Röggerbach" south of the Melach.

4.2 Geology

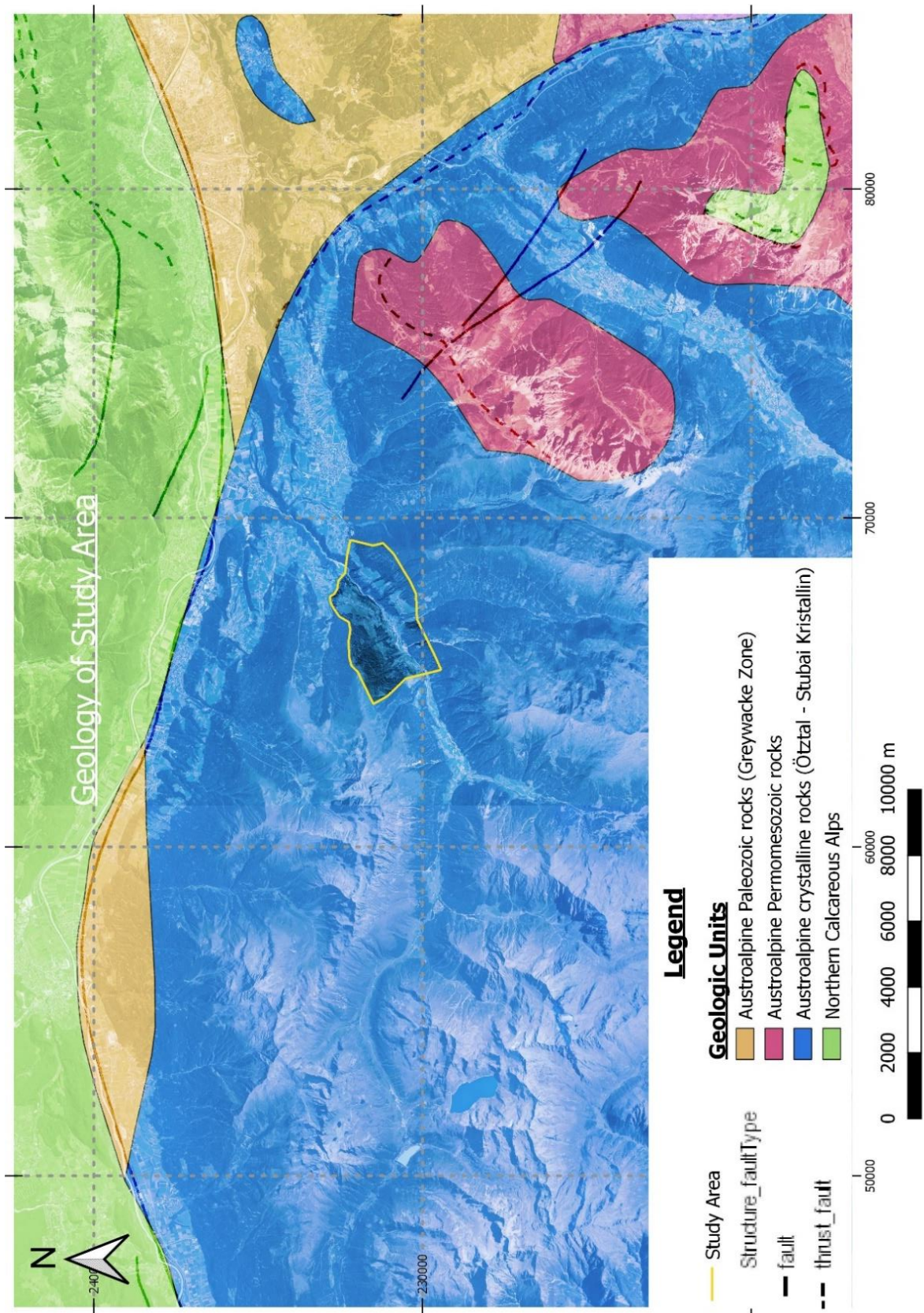


Figure 7: Geologic map of the study area (yellow) and of its surroundings; Greywacke zone is orange, the Permomesozoic rocks are red, the Ötztal - Stubai Kristallin is blue, the Northern Calcareous Alps are green, faults and thrust faults are marked black; raw data: © (Land Tirol - data.tirol.gv.at, 2018), orthophoto: © (Land Tirol - data.tirol.gv.at, 2019), geology: © (Geologische Bundesanstalt - geologie.ac.at, 2019)

As Figure 7 shows, the geology of the Sellrain Valley is made up entirely of the crystalline basement "Ötztal-Stubai Kristallin" (ÖSK) and no geologic features such as faults have been found in the Sellrain Valley. The present shape is a result of glacial activity during the Quaternary. Therefore, in this chapter, a short overview will be given of the ÖSK and the Quaternary of the area since there are no other geologic units in this area.

4.2.1 Basement geology

The Eastern Alps consist of the Helvetic and Penninic units (e.g.: the Tauern Window), the Lower Eastern Nappe and the Upper Eastern Nappe (also known as the Lower and Upper Austroalpine Nappe (Neubauer et al., 1999)). The ÖSK was originally part of the Middle Austroalpine (Geologische Bundesanstalt, 1980) but since restructuring it is now part of the Upper Austroalpine Nappe.

The ÖSK borders the Northern Limestone Alps (Geologische Bundesanstalt, 1980) to the north, the Brenner Mesozoic to the east (Geologische Bundesanstalt, 1980), a not so clear cut border to the Schneeberg complex (Geologische Bundesanstalt, 1980) to the south and the Silvretta Crystalline and the Lower -Engadin Tauern Window (Geologische Bundesanstalt, 1980) to the West (Figure 8).

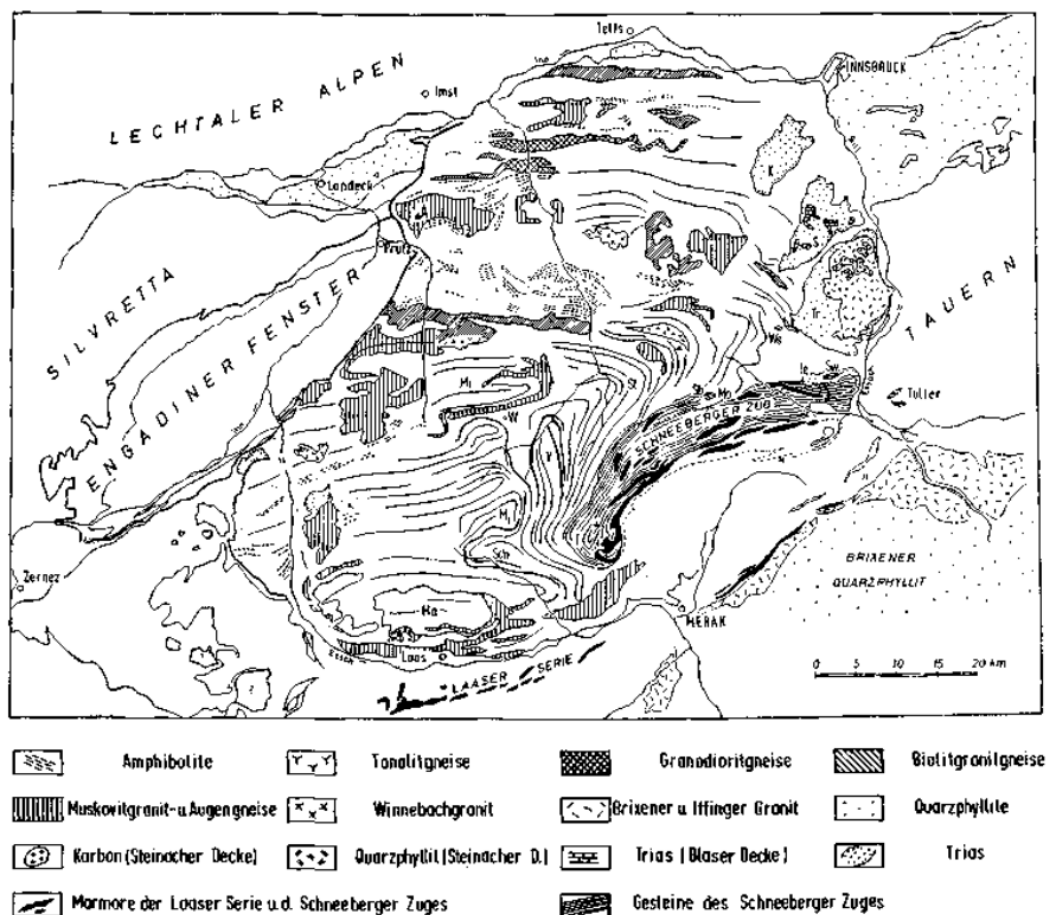


Figure 8: Overview map of the ÖSK (Schmidt, 1965)

The Unit itself is made of schist gneiss variations which are mainly a result of the Variscan Orogenesis with an alpidic overprint (Upper Cretaceous Period) in the South (Geologische Bundesanstalt, 1980). That includes metapelites and quartz-feldspathic rocks of the amphibolite facies (Figure 9) and metacarbonates which can be found in the South as a result of the Schneeberg Crystallization (von Raumer & Neubauer, 1993).



Figure 9: Amphibolite found near Längenfeld , Ötz Valley; The rock contains mainly feldspar, biotite and hornblende; bulky (upper picture) as well as schistose (lower picture); fragments of the Cambrian, surfaced through the Variscan Orogenesis; pictures taken by the author on June 7th , 2013

Large open folds, also known as “Schlingen” (Schmidt, 1965) are described by their steep folding style (Schmidt, 1965) and are a characteristic for the ÖSK. They consist of

amphibolite-gneiss and mica-schist bands and are the result of the already mentioned Variscan Orogenesis (Schmidt, 1965; Vavtar, 1988). In the northern and the middle part paragneiss-series can be found which are a result of the Caledonian Orogenesis (Vavtar, 1988), which makes them the oldest rocks found in the ÖSK (Figure 10).



Figure 10: Paragneiss found near Längenfeld Ötz Valley, containing muscovite, biotite, feldspar and quartz; the texture shows layering which is a hint towards a sedimentary origin; pictures taken by the author on June 7th, 2013

The study area in the Sellrain Valley mainly consists of metapelites, such as orthogneiss (Figure 11) with an East-West oriented foliation (Jenner, 2015), and is covered by terrace gravel which was deposited during the Quaternary (von Raumer & Neubauer, 1993; Heuberger, 1966). Therefore, the ÖSK is the gravel source for the terraces since it is not visible in the study area.



Figure 11: Typical orthogneiss found at the Engelswand near Tumpen in the Ötz Valley; surface is reddish due to weathering; a fresh cut is grey; heavily schistose texture; minerals are quartz, feldspar (anorthite) and biotite with traces of muscovite; formed from acidic magmatic rock through metamorphism; pictures taken by the author on June 7th, 2013

4.2.2 Quaternary geology

The overall Quaternary geology of the Sellrain Valley is characterized by the glacial activity of the past (Heuberger, 1966). The only glacier left today is the “Lüsener Ferner” but for the shape of the valley today several others are responsible. Namely among others the glacier of the Fotscher Valley, the glacier of the Tiefen Valley and the glacier of the Sellrain Valley, which was big enough to reach the Inn Valley glacier at some point as the terraces around Oberperfuss and Grinzens show (Heuberger, 1966).

Several big moraine complexes can be found near Lüsens (Heuberger, 1966). One complex contains the relicts of a block glacier that fills the whole “Längental” and an another complex that is the result of a younger glacier which had three tongues as had its counterpart during the Little Ice Age (Heuberger, 1966). The second glacier at some point coexisted with the block glacier as several sites in the valley show (Heuberger, 1966).



Figure 12: Partly cemented terrace gravel/ moraine material with a few larger boulders; Outcrop 11 (upper picture) Outcrop 12 (lower picture); both referenced in the large map at the end of the thesis

The Quaternary geology in the study area is characterized by so called “Terrassenschotter” or terrace gravel which was left behind by the glaciers (Figure 12). Around Oberperfuss the base moraines are clearly visible (Bobek, 1935) and covered by gravel and in some areas by sand (Bobek, 1935), which are the result of fluvial deposition in the area “Mayrhof” (Bobek, 1935). Around the village of Sellrain the steep slopes, which are probably the result of glacial retreat (Heuberger, 1966), contain moraine material that changes very rapidly and make up the unruly formed moraine terrace in the steeper areas (Heuberger, 1966).

On the plateaus the moraine nappe is less visible (Heuberger, 1966). In the village of Sellrain the moraine reaches the valley floor as it does at the Tiefen Valley estuary to the east (Heuberger, 1966). The terrace between the “Fotschertal” and Grinzens is also made up of moraine material with the addition of dead ice kettles which lead to the topography of hilltops and crescent ridges (Bobek, 1935; Heuberger, 1966).

4.3 Historical Overview of Landslides/Mudslides in the Sellrain Valley

First documented floodings in the vicinity of the study area go back to 1748, but it is unclear whether mudslides or landslides occurred (Jäger, 2015). It is only documented that the area was covered with sand and stone on a scale of several meters (Jäger, 2015). Since then there were several documented events in 1885, 1893, 1910, 1928, 2003 (Jenner, 2015) and most recent on June 7th, 2015.

In 1910 it was documented that the event even reached the village Unterperfuss and the railway in the Inn Valley (Der Bote für Tirol, 1910; Jäger, 2015), but no sources were found detailing the following events besides the most recent in 2015. Therefore, the focus lies upon the most recent event, its history, the magnitude and the aftermath.

The most recent event which took place on June 7th 2015 was the result of several moist months before the catastrophe, the onset of the snowmelt at the beginning of June, whereupon the soil was already saturated (Lagger, 2015). Then a high intensity precipitation event occurred over a couple of days (June 6th to June 8th) (Lagger, 2015). On June 7th, 2015, over a period of 12 hours up to 150 l/m² rain fell (Lagger, 2015) and triggered mudslides from the Seigesbach into an already swollen Melach (Figure 13), making it the highest precipitation event ever measured in the area (Lagger, 2015).

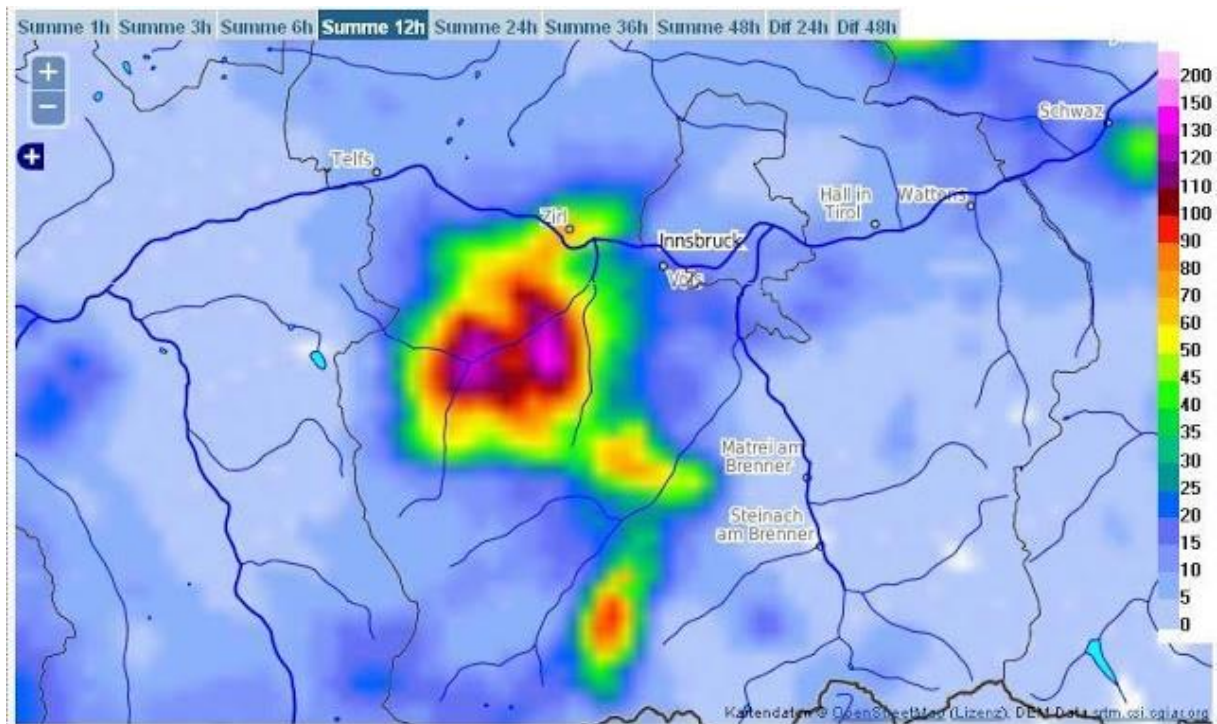


Figure 13: Estimated total precipitation amount in l/m^2 over 12 hours on June 7th, 2015 (alpen.wetter, 2015); © ZAMG-INCA; The maximum amounts are located at Sellrain and Gries in Sellrain

The high precipitation event above (Figure 13) and the already high soil saturation led to mudslides into the already high tide Melach which then led to the flooding of Sellrain (Lagger, 2015; Figure 14). Even days after the events mudslides and landslides occurred due to the over saturated soil, most of them happened without warning (Lagger, 2015). The steep slopes also contributed to the occurrence of more than a hundred smaller and bigger slope bursts and landslides (Lagger, 2015). The two main similarities between the burst and the landslides were the shallow depth of them, which only affected the vegetation cover and the loose-packed materials, and the location of where they occurred, mainly in the woods and meadows with steep slopes (Lagger, 2015).



Figure 14: Pictures of the aftermath in Sellrain; the destruction and the amount of deposits are easily visible (alpen.wetter, 2015) © zeitungsfoto.at

To summarize, the extreme events of June 7th, 2015, lead to shallow landslides, mudslides and slope bursts in varying sizes which then damaged and/or moved entire structures. Even though the occurrence of landslides etc. had several factors (already saturated soil, snowmelt) the focus of this thesis' assessment of shallow landslides will lie on the extreme precipitation event that occurred on June 7th, 2015.

5 Review of Previous Approaches

In this chapter a short overview will be given on shallow landslides, slope stability and its influencing factors as well as how models handled and implemented them.

5.1 Slope Stability and Shallow Landslides

5.1.1 Definition of shallow landslides

In a constantly changing landscape shallow landslides play a key role because of their fast mobilization and the then following destruction of anything that gets in their way (Montgomery & Dietrich, 1994). Therefore, disaster prevention has to be the research directive in the case of such events (Iida, 1999).

A key factor for prevention of (shallow) landslides is the understanding of slope stability and how it is influenced by the topography (Montgomery & Dietrich, 1994). Said stability is itself dependent on the slope angles, which are usually between 20 – 82° (Deb & El-Kadi, 2009) and on soil properties such as the clay content (Deb & El-Kadi, 2009), soil strength, soil conductivity and soil thickness (Montgomery & Dietrich, 1994). The latter one is especially susceptible to rainfall (Iida, 1999) and the topography (Montgomery & Dietrich, 1994). The typical depth of shallow landslides is between two to three meters. This points at another characteristic feature of shallow landslides, the slope length, since they (the landslides) are normally longer than deep (Zhuang et al., 2016). That leads to the conclusion that each model should consist of a hydrological part and a part to estimate soil depth as postulated by Iida (1999).

The difficulty of such models is that they must balance their complexity with the reality of a landscape in order to deliver credible results. Possible solutions include field inspection and projection of future patterns of instability (Montgomery & Dietrich, 1994), but the most suitable option might as well be the usage of digital elevation data (DED) in combination with hydrologic, vegetation and lithologic data (Montgomery & Dietrich, 1994). This means that every model depends on the resolution of the available digital data whereas coarser data should be used on smaller scales and finer data on larger scales (Montgomery & Dietrich, 1994) in order to identify (future) landslides (Lan et al., 2004).

5.1.2 Slope stability

In order to model shallow landslides, one must look at what influences slope stability and how it works first. Stability's general principle rests on the equilibrium of driving forces such as gravity and resisting forces such as shear resistance (van Beek et al., 2008). As long as the shear resistance is bigger than the driving forces, the slope is stable, but as soon as this correlation changes the slope will move as it is characterized by the Mohr Coulomb Criterion (van Beek et al., 2008). The shear stress is influenced by the slope material (e.g.: less shear strength if weathering occurred), geology, human impact etc. (van Beek et al., 2008). So the most important influencing factors will be described in detail in the paragraphs below.

5.1.2.1 Geology – slope material

The basis for every slope is its material which of course is dependent on the geology of the area (van Beek et al., 2008). Therefore, areas with rock that are subject to weathering and faulting are more prone to cause a landslide (van Beek et al., 2008). The same is true for plastic soils (van Beek et al., 2008). So, an analysis of the geologic situation of an area is essential.

5.1.2.2 Soil saturation

With the basis of a slope known through the geology, the exact knowledge of the composition is required (Lin & Zhong, 2018). This helps to determine the primary influence on slope stability, soil saturation and by extent the precipitation (Lin & Zhong, 2018). The reasoning behind this is that more rain leads to an increase of pore pressure (Delmonaco & Margottini, 2004) and reduces the slope stability (Lin & Zhong, 2018).

This pore pressure is governed by two main properties: the intensity and the duration of precipitation (Lin & Zhong, 2018) with the first one being dependent on the ratio of saturated permeability to the intensity (Lin & Zhong, 2018). If intensity is now smaller than the permeability, slope stability is reduced even more than vice versa. That is even more true the longer the rainfall lasts, which increases the chance that the soil is already saturated (Lin & Zhong, 2018). The effects of the duration of precipitation lowers the slope stability only to a certain degree if the intensity remains constant (Lin & Zhong, 2018).

A third factor is the snowmelt, because the faster it takes place the more likely it is that oversaturation is caused by a subsequent rainfall since the soil is already saturated (Lagger, 2015).

Concerning shallow landslides, it is now clear, that they are heavily dependable on the precipitation intensity that influences the soil's pore pressure and its duration, especially for homogeneous slopes (Delmonaco & Margottini, 2004).

5.1.2.3 Soil depth and other soil parameters

Even though precipitation is the primary influence on slope stability soil thickness and other soil parameters have also a considerable influence on it (Dietrich et al., 1995). It should be clear that sharp ridges have only a small amount of soil on it whereas the soil depth in the center of a slope can be considerably thick (Dietrich et al., 1995). So every model has to take the spatial variation of soil depth into account due to the effects of root cohesion or soil moisture (Dietrich et al., 1995). Therefore, this parameter is highly dependent on the chosen method, especially since often soil depth classes are used (Segoni et al., 2012), which can be quite inaccurate because of the sensibility of slope stability concerning soil depth (Segoni et al., 2012).

To make matters even more complex, a high degree of bias can be introduced in a model as each model treats soil thickness differently (Segoni et al., 2012), going from linear correlation with elevation to a more complex approach using a mixture of slope gradient and curvature along with geomorphological and geological factors (Segoni et al., 2012).

Other soil parameters such as cohesion and density are dependent on the source material of the slope and its size and shape. This aspect has already been discussed above (Chapter 5.1.2.1).

5.1.2.4 Slope angle

The slope angle in itself can influence slope stability indirectly through a change in vegetation and/or human impact (van Beek et al., 2008), which can lead to landslides occurring on slopes that have an angle lower than 10 degrees with the slope's material having also an impact (van Beek et al., 2008).

5.1.2.5 Vegetation

Another factor influencing soil parameters is vegetation or so-called root strength (Dietrich et al., 1995). A considerable human impact can be detected through deforestation, farming and ski slopes etc. (van Beek et al., 2008). That can lead to an underdeveloped vegetation which in itself leads then to a decreased slope stability. An increase of slope stability can be reached by reforestation with a mix of shallow- rooted and deep-rooted trees.

5.1.2.6 Human impact

The human impact on slope stability is manifold (Jong et al., 2015). They reach from the changes in vegetation and soil cover to an increased surface runoff (Jong et al., 2015). Ski slopes, for example, show higher levels of pH and a reduced permeability (Jong et al., 2015) along with a change in vegetation (deforestation for ski slopes etc.) and reduced recovery time due to longer skiing seasons (Jong et al., 2015). These properties can have dramatic consequences when strong precipitation events occur (Jong et al., 2015).

Although the above paragraph highlights the human impact on ski slopes, the overall human impact is undeniable because of deforestation, construction activities of any kind, building of roads and railways and climate change. Not a human impact per se, but the burning of fossil fuels for example leads to an increased occurrence in extreme weather conditions (van Beek et al., 2008) and higher temperatures (Jong et al., 2015). So, in conclusion, slope stability is decreased as a result e.g. for an increased erosion rate due to the lack of vegetation through the effects of climate change (van Beek et al., 2008).

5.1.3 Modelling shallow landslides

The following paragraphs give an overview both on the different concepts of assessing shallow landslides or slope stability and the evolvement of models over time and on the importance of their influencing factors.

5.1.3.1 The importance of data acquisition on the example of the SINMAP-model

To highlight the importance of data acquisition the deterministic SINMAP-model was used, which includes an infinite-slope stability model (Figure 15) and a hydrological model (Deb & El-Kadi, 2009).

It includes an infinite slope model, that weighs destabilizing against stabilizing components in order to calculate the factor of safety (dimensionless):

$$SF = \frac{C + \cos \theta * (1 - w * r) * \tan \varphi}{\sin \theta} \quad (\text{Deb \& El-Kadi, 2009}) \quad (1)$$

With SF = factor of safety, w = relative wetness, C = combined cohesion of soil and root, φ = angle of internal friction, r = water to soil density ratio and θ = slope angle

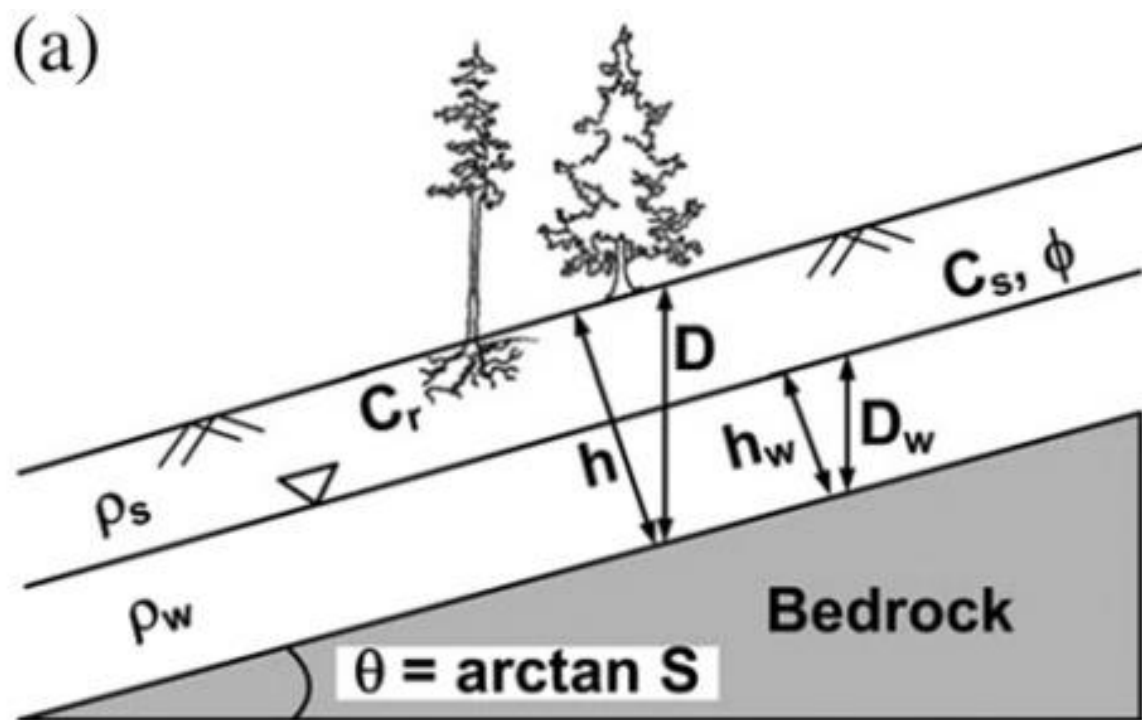


Figure 15: Illustration of an infinite slope model with the parameters involved; taken from Deb & El-Kadi (2009) as it can be seen in Equation 1; θ = slope angle, C_r = root cohesion, C_s = soil cohesion, φ (in this case ϕ) = internal friction angle, D = vertical soil height, h = soil depth perpendicular to the slope surface; h_w = water height perpendicular to slope surface; D_w = vertical water height, ρ_s = soil density, ρ_w = water density and S = slope length (Deb & El-Kadi, 2009)

Also, a topographic wetness index is the hydrologic part of the SINMAP-model, which is based on three assumptions. First the discharge is in equilibrium at each point with steady state recharge R , secondly subsurface flow advances along topographic gradients and lastly the capacity of flux is defined by $T * \sin \theta$ with T being the soil transmissivity. With that in mind the relative wetness is defined (Deb & El-Kadi, 2009; Figure 16).

$$w = \min\left(\frac{Ra}{T * \sin \theta}, 1\right) \quad (\text{Deb \& El-Kadi, 2009}) \quad (2)$$

With w = relative wetness, R = steady state recharge, T = soil transmissivity, θ = slope angle and a = upslope contributing area

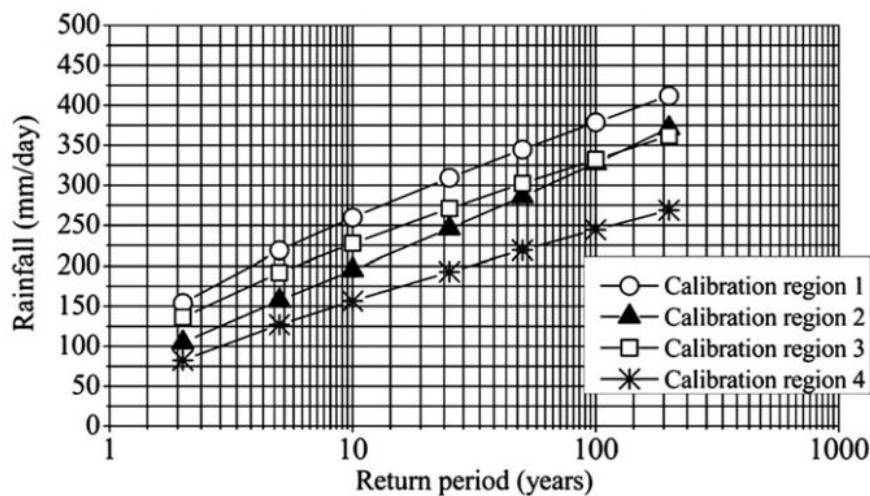
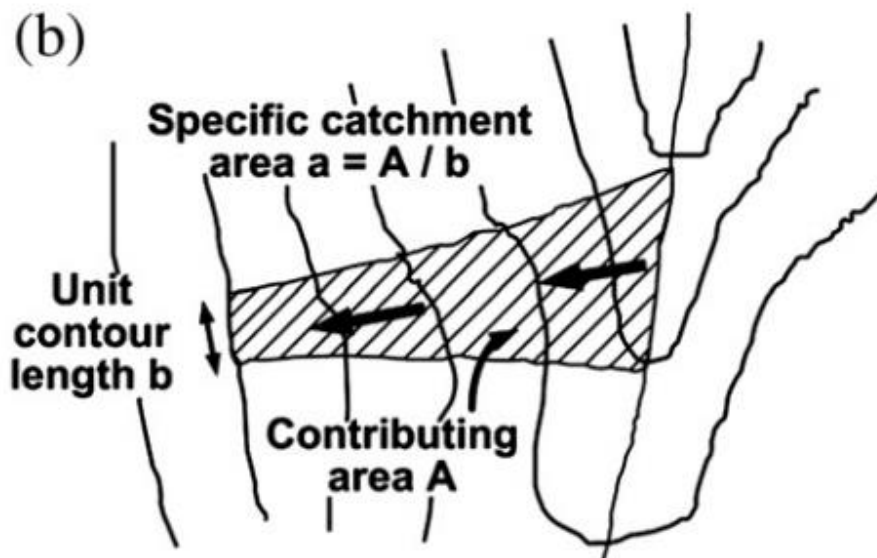


Figure 16: Above: Illustration of a specific catchment area Below: The rainfall calibration for different regions that leads to R (=Steady state recharge); taken from Deb & El-Kadi (2009) as it can be seen in Equation 2 (Deb & El-Kadi, 2009)

Both combined result in the SINMAP-model:

$$SF = \frac{C_2 + \cos \theta * \left(1 - \min\left(\frac{Ra}{T * \sin \theta}, 1\right) * r\right) * \tan \varphi}{\sin \theta} \quad (\text{Deb \& El-Kadi, 2009}) \quad (3)$$

With w = relative wetness, R = steady state recharge, T = soil transmissivity, θ = slope angle, a = upslope contributing area, φ = friction angle and C_2 = cohesion

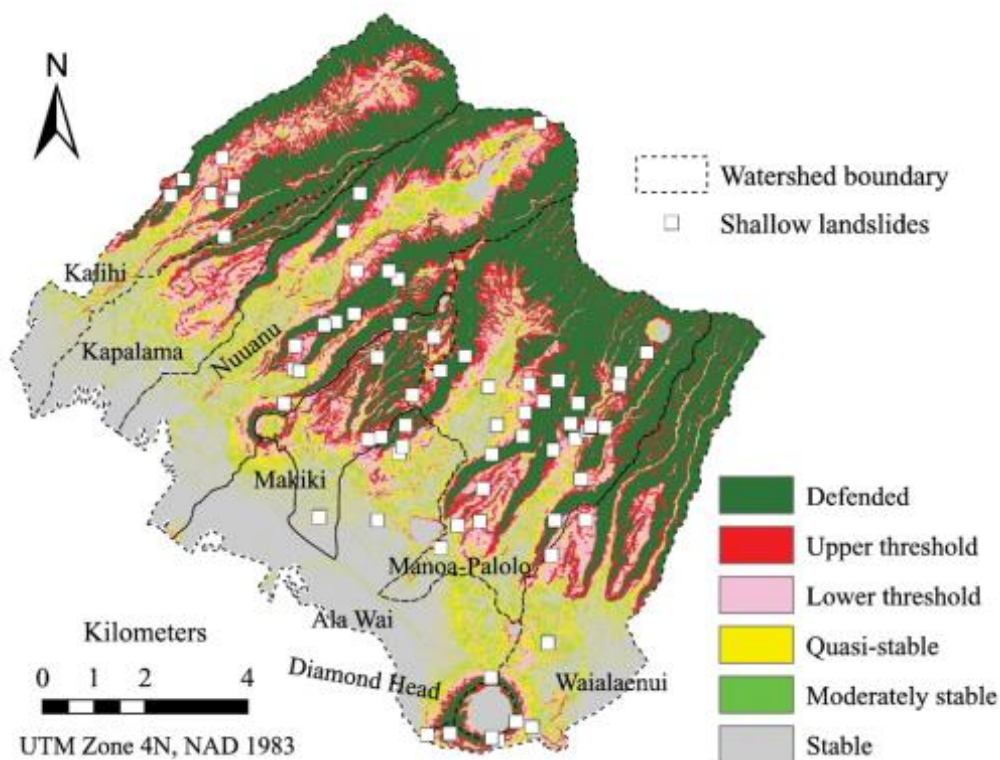


Figure 17: Results of the SINMAP-model for region 1 of Deb & El-Kadi (2009)

For modelling, SINMAP uses the surface topography to map downslope flow leading to a model that can be used to assess slope stability (Michel & Kobiyama, 2016; Figure 17). The data required are derived from digital elevation models, a map of observed landslides and the values for the calibration parameters (Michel & Kobiyama, 2016).

Then, it is imperative to gather data on surveyed areas to lighten the workload and to make correct calibrations and assumptions in your model when it is necessary to find representative parameters (Michel & Kobiyama, 2016). The gathered data should include a historic catalog of landslide events and inventory maps that include the most recent shallow landslide events and the geomorphological data (Deb & El-Kadi, 2009), such as aerial photographs and other data obtained through field investigation (Lan et al., 2004) in order to identify their scars (Deb & El-Kadi, 2009).

5.1.3.2 *The importance of modelling hydrology - TOPMODEL*

After the discussion of the importance of data acquisition, the next essential step to a sufficient model is the assessment of hydrology. To have a viable slope stability model, it is necessary to map the basin outflow, that includes the overland flow (flow on the surface) as well as other outflow paths (e.g. groundwater). As an easy solution for a complex parameter, Beven & Kirkby (1979) came up with an easy model to assess exactly that parameter. Their model is called TOPMODEL and is represented in the simplified Equation 4 below.

$$\ln(a/\tan\beta) \text{ or } \ln\left(\frac{a}{T_0} * \tan\beta\right) \quad (4)$$

With a = the upslope contributing area, tan β = the local slope acting on a cell, T₀ = the lateral transmissivity

5.1.3.2.1 The modelling concept itself

The major paths for a runoff occurrence must not be forgotten (Beven & Kirkby, 1979) since the runoff's extent is highly dependent on the drainage flow (O'Loughlin, 1986). The first concept covers low vegetation areas with high rainfall that results in an overland flow, hence the low infiltration capability (Beven & Kirkby, 1979). Secondly, the rainfall falls on variably saturated soil, which leads to either an overland flow or infiltration (Beven & Kirkby, 1979). Next to consider is the rainfall on stream channels and saturated soils that contributes to the storm hydrograph (Beven & Kirkby, 1979). The last way is the behavior of downslope lateral flow of saturated or unsaturated soil that mainly occurs subsurface, hence subsurface flow (Beven & Kirkby, 1979). It is often the case that overland flow is faster than its subsurface counterpart (Beven & Kirkby, 1979).

It should be made clear that there are several different ways to model basin flow, firstly, the infiltration approach (Beven & Kirkby, 1979) and secondly, the soil storage approach (Beven & Kirkby, 1979), which accounts for moisture more reliably than the first (Beven & Kirkby, 1979).

The simplicity of a model and its usefulness relies on two key assumptions (O'Loughlin, 1986). First, there is the subsurface water flow, which is dominated by the topographic elevation (O'Loughlin, 1986) and second, the steady state conditions that prevail in a draining hillslope (O'Loughlin, 1986). That makes it possible to assess a basin faster and in a more economical way.

Furthermore, it is critical to reflect at least some key hydrological characteristics, such as different basin stores S₁ (maximum = S_D) called the interception store, S₂ (maximum = S_c) called the infiltration store and S₃ at the bottom as the saturated zone store. Along with that comes the rainfall rate *i* and the upslope contributing area *a*. These factors lead to a sub basin model that can be seen in Figure 18 below.

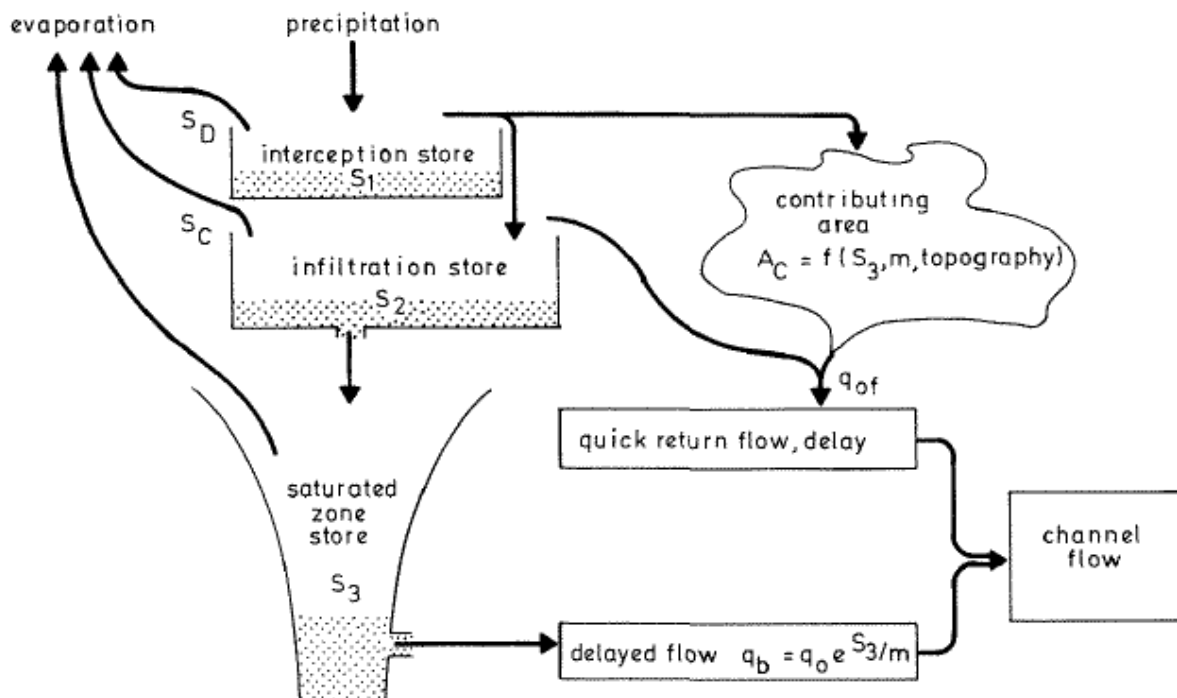


Figure 18: Subbasin model according to Beven & Kirkby (1979); with S_x = Subbasin stores, A_c being the upslope contributing area, m = a constant factor, q_b = flow reaching the channel, q_o = flow when $S_3=0$ and m is a constant (Beven & Kirkby, 1979)

To account for overland flow the OFV (Overland flow velocity) parameter was introduced along with the sub basin model and CHA and CHB (both constants that are based on the channel type) in order to account for channel velocity (Beven & Kirkby, 1979). Note that the runoff between a storm event to the pre-storm discharge is non-linear (O'Loughlin, 1980) since a rapid stormflow hardly infiltrates the ground (O'Loughlin, 1980).

5.1.3.2.2 The application of TOPMODEL

Before modelling it is necessary to measure several field parameters for vegetation, hydrology, geology etc. , but one should be aware that some parameters are not as trustworthy as they seem, since some of them are done in a laboratory (Beven & Kirkby, 1979).

The modelling itself can be done in one of two possible ways (Beven & Kirkby, 1979). The first possibility is to calculate the contributing area by hand, which is rather difficult since it is impossible to know all parameters. The second possibility is to use a computer to divide the surveyed area into several slope and channel network elements (Beven & Kirkby, 1979). The only thing left to do is to account for enough elements in order to represent the area as accurately as possible (Beven & Kirkby, 1979) and evaluate the results (Figure 19).

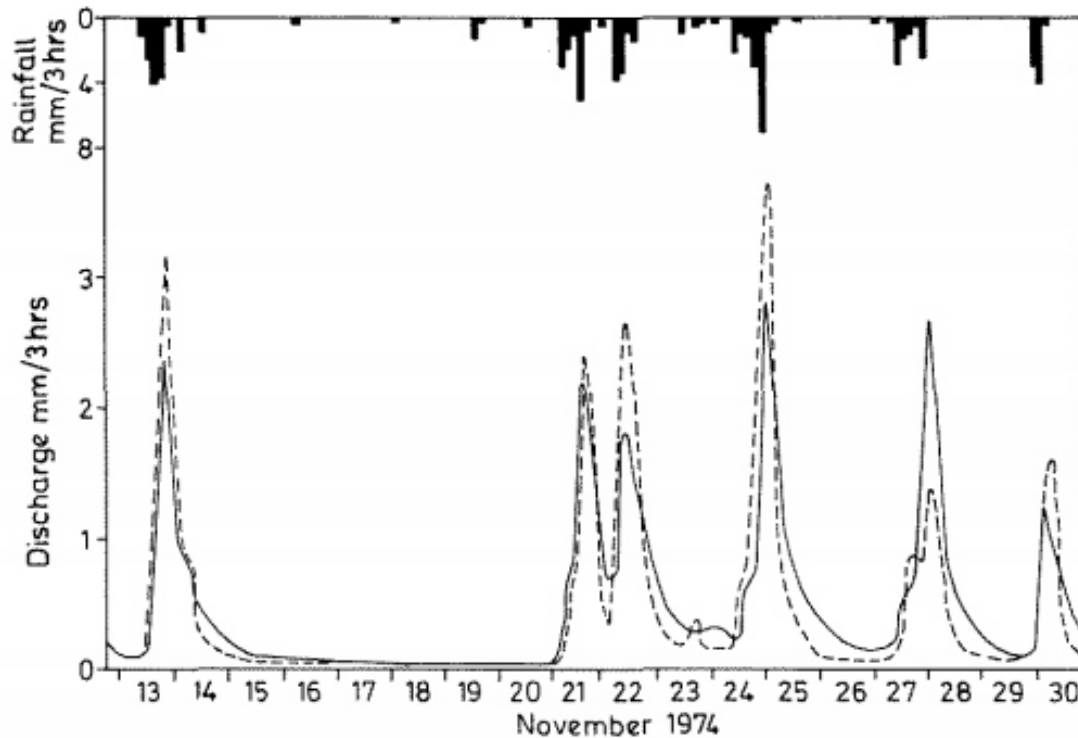


Figure 19: An example for calculated results of the TOPMODEL for basin outflow/discharge, namely the Lanshaw sub-basin in the winter; Beven & Kirkby (1979)

5.1.3.3 Influence of grid size/resolution

The impact of the resolution or grid size of Digital Terrain Analyses (DTA) on a hydrologic model is inevitable, since large pixel resolutions give bias to large $\ln(a/\tan\beta)$ - values (also known as TOPMODEL) (Quinn et al., 1995). So, they should not be used for detailed surveys, but it is still possible to use them on macroscale interpretations (Quinn et al., 1995) as it has already been stated above.

5.1.3.4 Model for topographic control – a more complex model for soil estimation

A new approach was used by Dietrich et al. (1995) by deducing a definition for the soil production rate and then developing on that ground an equation (based on Selby's 1993) that combined the slope stability with an hydrologic model in order to predict soil depth (Dietrich et al., 1995).

If applied to a specific problem, this model reveals that it is more applicable for larger watersheds than simpler ones (Dietrich et al., 1995) since its nine input parameters are harder to derive for local and thus smaller topographies. Therefore, it is hardly applicable to predict soil depth here and a simpler model should be used (Dietrich et al., 1995).

Dietrich et al. (1995) further concluded that the soil depth cannot be thinner than its maximum production rate and that soil depth is influenced by the topographic curvature. Furthermore, the authors (Dietrich et al., 1995) came to the conclusion that root strength, which influences the soil strength, is one of the most volatile parameters over time since it is highly influenced by climate, land use and other factors (Dietrich et al., 1995).

5.1.4 A new modelling approach - MEMPS

One of the newest equations to properly investigate the maximum soil depth, that can settle on a hill slope which then can lead to shallow landslides, is MEMPS (Modelo de Estimativa da Maxima Profundidade do Solo) (Michel & Kobiyama, 2016). Unlike other methods it does not require any assumptions of the saturation (Michel & Kobiyama, 2016).

MEMPS is based on the following formula of Selby (1993) for the factor of safety and a limit equilibrium analysis is done by Lida (1999).

$$FS = \frac{c + (\rho_s * g * z * \cos^2 \theta - \rho_w * g * h * \cos^2 \theta) * \tan \varphi}{\rho_s * g * z * \cos \theta * \sin \theta} \quad (5)$$

With FS = factor of safety, c = soil cohesion, ρ_s = soil density, ρ_w = density of water, z = soil depth, h = height of the water column of the soil layer, g = gravitational acceleration, φ = internal friction angle and θ = slope angle

Working of equation 5 leads to equations of Lida (1999), which are able to calculate only the critical soil depth for two extreme situations (Equation 6 & 7; Figure 20), i.e. complete saturation and complete dryness (Michel & Kobiyama, 2016).

$$z_{c0} = \frac{c}{\rho_s * g * \cos^2 \theta * (\tan \theta - \tan \varphi)} \quad (6)$$

With z_{c0} = critical soil depth for dry soil, c = soil cohesion, ρ_s = soil density, g = gravitational acceleration, φ = internal friction angle and θ = slope angle

$$z_{c1} = \frac{c}{\cos^2 \theta * [\rho_s * g * (\tan \theta - \tan \varphi) + \rho_w * g * \tan \varphi]} \quad (7)$$

With z_{c1} = critical soil depth of saturated soil, c = soil cohesion, ρ_s = soil density, ρ_w = density of water, g = gravitational acceleration, φ = internal friction angle and θ = slope angle

Therefore, Michel & Kobiyama (2016) came up with a uniform hydrological model that is based on Selby's equation (Equation 5) and several substitutions in order to quantify the saturation level of a soil, because soils are normally not fully saturated or fully dry.

The final formula (= MEMPS) of Michel & Kobiyama (2016), i.e. Equation 10 and Figure 20, incorporates said hydrological model by comparing the water height (Equation 8) to the critical soil depth of saturated soil (Equation 7) and taking only the minimum of those two values into account (Equation 9; Michel & Kobiyama, 2016).

$$h = \frac{q \cdot a}{b \cdot K_s \cdot \sin \theta \cdot \cos \theta} \quad (8)$$

With h = water height, θ = slope angle, a = upstream area at one point, b = contour length, q = uniform steady state recharge and K_s = saturated hydraulic conductivity

$$\min(z_{c1}, h) \quad (9)$$

With h = water height and z_{c1} = critical depth of saturated soil

The complete formula is (Michel & Kobiyama, 2016):

$$z_c = \frac{c}{\rho_s \cdot g \cdot \cos^2 \theta} - \frac{\tan \varphi \cdot \rho_w \cdot \min\left(z_{c1}, \frac{q \cdot a}{b \cdot K_s \cdot \sin \theta \cdot \cos \theta}\right)}{\tan \vartheta \cdot \tan \varphi} \quad (10)$$

With z_c = critical soil depth for any degree of saturation (further called critical soil depth), z_{c1} = critical depth of saturated soil, c = soil cohesion, ρ_s = soil density, ρ_w = density of water, g = gravitational acceleration, φ = soil internal friction angle, θ = slope angle, a = upstream area at one point, b = contour length, q = uniform steady state recharge and K_s = saturated hydraulic conductivity

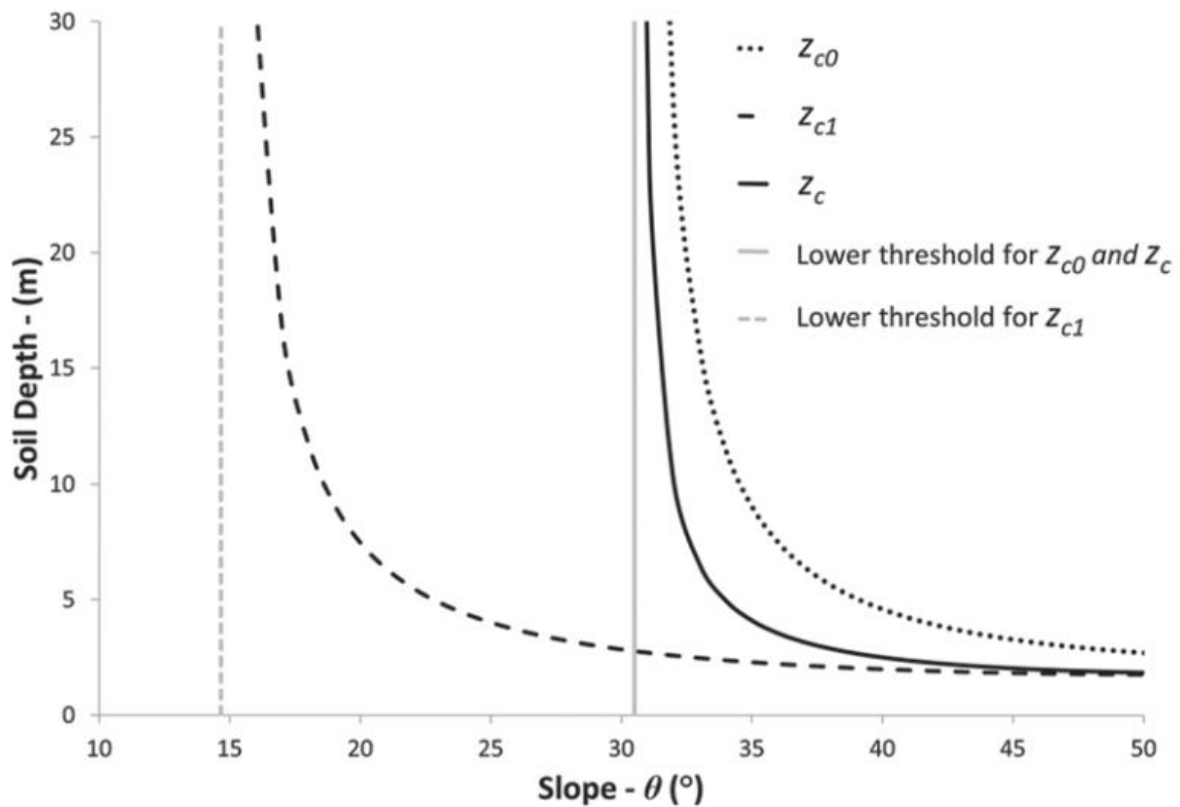


Figure 20: Variation of the different equations above; z_{c0} (dry soil) and z_{c1} (saturated soil) are from Iida (1999) (Equations 6 and 7) and z_c (any degree of soil saturation) are derived from MEMPS for similar conditions (Michel & Kobiyama, 2016)

In their paper Michel and Kobiyama (2016) revealed that for small soil depths MEMPS mirrored a high saturation and for large soil depths a low saturation. That being said, Michel and Kobiyama (2016) only took the interface between soil and bedrock into account because of its susceptibility to failure.

6 Objective of Thesis

It is now clear that the area around Sellrain is susceptible to landslides as recent history suggests. MEMPS which has not been field tested yet, nevertheless presents an opportunity to put Michel and Kobiyama's (2016) theory to a practical test and to find out if it results in reasonable models for different resolutions and precipitation periods.

Unfortunately, an error assessment was not possible due to restrictions in available data since no error was given for any parameter, and in PC - hardware.

Therefore, the resulting models will only be compared with each other and with the field work, which was done to corroborate the results in order to account for the missing error assessment.

7 Integrated Data

The integrated data used in this thesis were provided by several agencies and collected through field work. The origin of the digital data is divided into open source data and non-public data that were provided for this thesis by Tyrolean governmental agencies.

7.1 Field Data

The field data contain mainly observations done by the author during the summer of 2019 in order to corroborate the results of the calculations done with MEMPS and to find an estimate for the soil parameters.

7.2 Open Source Data

Open source data was downloaded from “ehyd”, a website operated by the Austrian ministry for sustainability and tourism (Bundesministerium Nachhaltigkeit und Tourismus, 2018) in order to have precipitation data for the time periods from 1980 to 2010 and from 2010 to 2016.

More data were implemented from the open data portal of Austria (Open Data Österreich) branches of Tyrol (Land Tirol - data.tirol.gv.at, 2019) and the “Geologische Bundesanstalt Österreich” (Geological Survey of Austria). The data includes orthophotos, geologic maps and the water network that can be seen above.

7.3 Non-Public Data Provided by Tyrolean Governmental Agencies

Non-Public data were provided by the Geo-Services of Tyrol and the department of Bridge and Tunnel Construction of Tyrol.

The digital terrain models (DTMs), digital elevation models (DEMs) and shapefiles of the study area in the Sellrain Valley were provided by the Geo-Services of Tyrol for two different measurement epochs (Land Tirol - data.tirol.gv.at, 2018), namely the data of the year 2007 with a 1 meter resolution and the data of 2013 with a 0.5 meter resolution, although the latter period only covered a smaller area. The difference between a DEM and a DTM is the fact that the first one includes the earth’s surface as it is, including such things as structures and forests whereas the DTM only contains the height information of the surface without any further information of the surface.

In order to corroborate the soil data mentioned above with the field work, a geotechnical survey was provided by the Department of Bridge and Tunnel Construction of Tyrol (Abteilung für Brücken-und Tunnelbau des Landes Tirol). It was compiled by Dr. techn. Dipl.-Ing. Jörg Henzinger from the “Ingenieurbüro Henzinger” in the area of the L233, also known as “Sellrain Gasse” (Henzinger, 2008).

8 Methodology

8.1 Calculation of MEMPS

The calculation of MEMPS includes two separate formulae to calculate the critical soil depth. The first one is for calculating the critical soil depth for fully saturated soil and called z_{c1} (Equation 7) and the second one for any degree of soil saturation called z_c (Equation 8).

As it can be seen in the previous chapter 5.1.4, MEMPS uses a wide array of parameters, both constant and non-constant. For the sake of a better understanding these parameters will be described separately below.

8.1.1 Input parameters

8.1.1.1 Constant values

For the purpose of this thesis the constant parameters are split into two groups. One contains the physical constants and the other measurements that are supposed to be applicable and relatively constant for the whole study area around Sellrain.

The physical constants used are the gravitational acceleration g the water density ρ_w , which both are well defined and established and will not be explained further.

The second group includes the following parameters, which were derived/collected through field work and literature studies. These include the uniform steady recharge q (a.k.a. precipitation) for two different time periods, which were collected from the “ehyd” - website (Bundesministerium Nachhaltigkeit und Tourismus, 2018), and the maximum precipitation ever recorded in the study area. This parameter can be found in the paper of Lagger (2015).

Field work and literature studies were used to gather the soil data such as soil cohesion, soil density and its friction angle, all derived from the geotechnical report of Henzinger (2008) and checked against the data collected beforehand in the field. Those parameters stay the same through all precipitation periods and are supposed to be relatively constant in the study area. More extensive measurements were not possible and would go beyond the scope of this thesis. Since the soil structure remains relatively unchanged through the area this set of soil parameters are considered valid for the whole area.

The saturated hydraulic conductivity K_s is not given specifically in the report of Henzinger (2008) or in the paper of Lagger (2015), so a value was taken that is applicable for soils that consist of gravel and sand of varying grain sizes (Wikipedia.org, 2019). This is an accurate estimate for a soil that mostly consists of terrace gravel and moraine material.

The last constant parameter is the contour length b which is directly connected to the pixel size and therefore they both share the same value.

8.1.1.2 Non-constant parameters

Two parameters can be considered non-constant for the study area. The first one is the slope angle θ and the second one the flow accumulation, which is needed for calculating the source area. Both parameters are based on the DEM/DTM provided by Land Tirol – data.tirol.gv.at (2018) for three different resolutions for each time period.

8.1.2 MEMPS calculation

After the collection of data, the MEMPS formulae are implemented into QGIS (2018 - 2019) with the help of its own graphic modeler in order to connect the different calculation steps as it can be seen in Figure 21 below. As base model here a mosaic raster created from the data provided is used in three different resolutions, which were created by using QGIS (2018 - 2019).

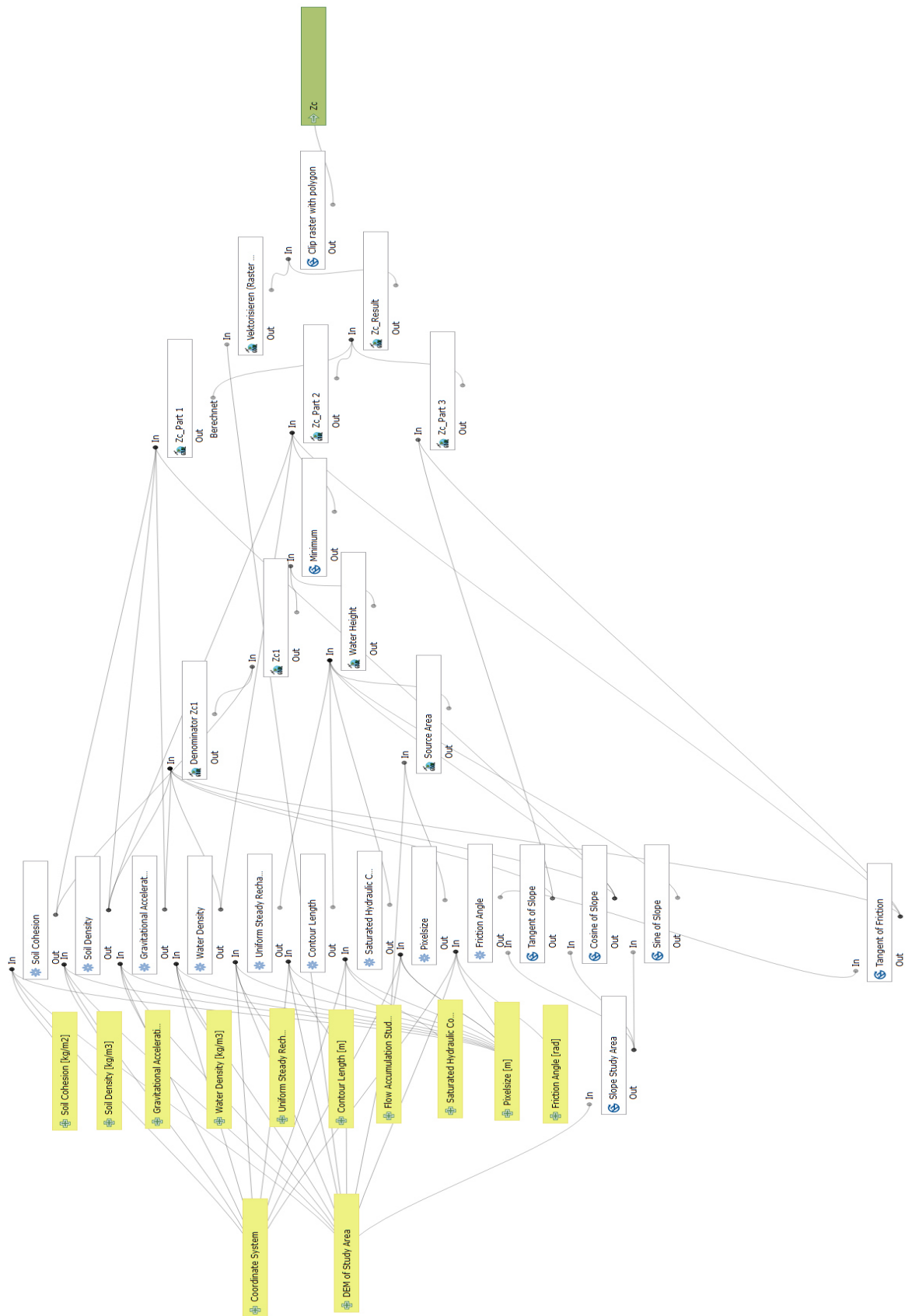


Figure 21: Graphic of MEMPS used in this thesis/study; created by the QGIS-graphic modeler; (QGIS, 2018 - 2019)

Before running the model (Figure 21), a flow accumulation is created by using the Whitebox-GAT Project - GIS application (Lindsay, 2009) because the built-in version of QGIS crashed the program (QGIS, 2018 - 2019). In that application a DEM with filled sinks is made to correct the hydrology followed by the calculation of a flow accumulation raster containing the number of upslope cells that flow through each given cell of a given resolution. The source or upstream area was then calculated by multiplying the value of each with the area of each pixel (Figure 21).

Next to the flow accumulation, the original DEM/DTM (a mosaic raster created from the data provided) is then selected as second input parameter followed by the constant values, of which for each one of them a constant-value raster is created with the same resolution as both raster inputs.

All of the calculations described above are included in the model of MEMPS built with the QGIS-graphic modeler (QGIS, 2018 - 2019; Figure 21) as mentioned in the beginning of the section. As a check for the model a step by step calculation was done for one resolution/precipitation period outside the graphic modeler.

In order to gain comparable results and to facilitate the procedure all values are transferred into their respective SI-Units with the exception of the uniform steady recharge and saturated hydraulic conductivity whereas the unit m/day is used to have larger values to be calculated with.

The checked model was then used to calculate the critical soil depth for any degree of soil saturation z_c for each resolution and each precipitation period.

To improve visualization of the resulting raster datasets histograms were created from it.

Here now are three examples of MEMPS calculations with the data of Table 1 and an upstream area of 7000 m², one for a slope angle smaller than the friction angle, another for a slope angle the same as the friction angle and one larger.

First to calculate is the critical soil depth for a saturated soil (z_{c1} = Equation 7), then calculate the water height (h = Equation 8), followed by the comparison of those two (Equation 9). Then at last the critical soil depth for any degree of saturation (z_c) can be calculated (Equation 10).

8.1.2.1 Example 1: Friction angle larger than slope angle

$$\theta \text{ (slope angle)} = 25^\circ \text{ and } \varphi \text{ (friction angle)} = 35^\circ$$

$$z_{c1} = \frac{510}{\cos^2(25) * [2141 * 9.81 * (\tan(25) - \tan(35)) + 1000 * 9.81 * \tan(35)]} = 0.317369 \text{ m}$$

$$h = \frac{0.0026 * 7000}{1 * 8.64 * \sin(25) * \cos(25)} = 5.49963 \text{ m}$$

$$\min(0.317369, 5.49963) = 0.317369 \text{ m}$$

$$z_c = \frac{\frac{510}{2141 * 9.81 * \cos^2(25)} - \tan(35) * \frac{1000}{2141} * \min(0.317369, 5.49963)}{\tan(25) * \tan(35)} = -0.227350 \text{ m}$$

8.1.2.2 Example 2: Friction angle smaller than slope angle

$$\theta \text{ (slope angle)} = 45^\circ \text{ and } \varphi \text{ (friction angle)} = 35^\circ$$

$$z_{c1} = \frac{510}{\cos^2(45) * [2141 * 9.81 * (\tan(45) - \tan(35)) + 1000 * 9.81 * \tan(35)]} = 0.0774744 \text{ m}$$

$$h = \frac{0.0026 * 7000}{1 * 8.64 * \sin(45) * \cos(45)} = 5.49963 \text{ m}$$

$$\min(0.317369, 5.49963) = 0.317369 \text{ m}$$

$$z_c = \frac{\frac{510}{2141 * 9.81 * \cos^2(45)} - \tan(35) * \frac{1000}{2141} * \min(0.317369, 5.49963)}{\tan(45) * \tan(35)} = 0.0331705 \text{ m}$$

8.1.2.3 Example 3: Friction angle the same as the slope angle

$$\theta \text{ (slope angle)} = \varphi \text{ (friction angle)} = 35^\circ$$

$$z_{c1} = \frac{510}{\cos^2(35) * [2141 * 9.81 * (\tan(35) - \tan(35)) + 1000 * 9.81 * \tan(35)]} = 0.110648 \text{ m}$$

$$h = \frac{0.0026 * 7000}{1 * 8.64 * \sin(35) * \cos(35)} = 4.212963 \text{ m}$$

$$\min(0.317369, 5.49963) = 0.110648 \text{ m}$$

$$\begin{aligned} z_c &= \frac{\frac{510}{2141 * 9.81 * \cos^2(35)} - \tan(35) * \frac{1000}{2141} * \min(0.317369, 5.49963)}{\tan(35) * \tan(35)} \\ &= 3.02444 * 10^{-7} \text{ m} \sim 0 \text{ m} \end{aligned}$$

Those examples illustrate that usable results can come solely for slope angles that are larger than the friction angle (Chapter 8.1.2.2), otherwise the results are practically zero (Chapter 8.1.2.3) or smaller than zero (Chapter 8.1.2.1). This then leads to the following categorization for the results in Chapter 9.2.2 defined by their susceptibility to shallow landslides. All results below zero meters are found in Category I, dubbed “no risk”, as the friction angle is larger than the slope angle, which prevents any movement in connection to landslides. All results between zero and three meters are found in Category II, dubbed “onset of shallow landslides”, because shallow landslides are bound to happen in these areas. All results for three meters and above are found in Category III, dubbed “potential instability”, because shallow landslides might occur in these areas.

8.1.3 Error assessment of MEMPS

In the light of missing error parameters (e.g. soil parameters), the decision was taken that the comparison of the model to the field work should suffice as proof for the applicability of MEMPS.

8.2 Field Work

Field work was done in order to validate the geology and the soil parameters postulated in the literature (Bobek, 1935; Henzinger, 2008; Heuberger, 1966) since most of them are more than 50 years old.

But field work was not only limited to the geology itself, it also included the search for landslide indicators such as headscarps, drunken trees, cracks in the road and hummocky topography in order to check and validate the critical soil depths of the QGIS-model.

Field work was mostly done along streets, forest roads and hiking trails since the study area is very steep and therefore not reachable on foot. It also included a remote sensing part to get a better overview. This was done by looking at each valley side from its counterpart. All outcrops were marked with GPS and are included in the map, the description of them can be found in the appendix (Chapter 13.1). The outcrops were then categorized in Landslides, Hummocky Topography, Drunken Trees, Cracks in the roads, Others and multi-part outcrops, which contain at least two of the above categories.

8.2.1 Drunken trees

Plenty of Drunken trees were found in the study area as Figure 32 shows. Each outcrop normally contains trees of similar thickness and size. Single trees were mostly ignored due to the fact that a single tree could have grown crooked because of other reasons (e.g. snow deposits etc.). Furthermore, landslide - outcrops containing drunken trees were categorized as landslides.

8.2.2 Possible landslides

This category contains two “possible landslide” subcategories. Landslides on the same valley side as the outcrop point are in the first subcategory. The second subcategory consists of probable landslides that were only possible to be observed from a distance, for example from the opposite valley side of the outcrop point (Figure 32).

8.2.3 Cracks in the road and hummocky topography

The “Hummocky Topography”-outcrops were similarly categorized to the landslides. As to the cracks in the road, the result shows cracks that run parallel to the slope with the hammer perpendicular to the slope (Figure 32). Furthermore, where possible, landslides that contained signs of a hummocky topography were categorized as landslides.

8.2.4 Multi-Part outcrops and others

The “Others”-category contains outcrops where changes in vegetation were witnessed and outcrops where the composition of the soil was visible, for example through construction sites (Figure 32).

Multi-Part Outcrops contain outcrops of different scale (small scale vs. remote observations) and different kind of different kind of outcrops within one (landslide vs. composition outcrops only)

9 Results

The results are divided into the calculations done with QGIS and the field work done in the study area.

9.1 Field Work

The field work was done in the summers of 2018 and 2019 on seven different tours. Findings include, as described before, possible landslides, drunken trees, cracks in the road and hummocky topography, which can all indicate a moving slope, as well as the remote observation from opposite valley sides. A map of all 156 outcrops can be found at the end of the section (Figure 32). The full description of each outcrop can be found in the appendix (Chapter 13.1). Among the largest categories are the Drunken trees (Figure 22 & Figure 32) and the landslide category. The smallest are the “Others” and the Multi-Part Outcrops.



Figure 22: Drunken trees in the municipal forest of Neder on 2019/07/17; the crooked growth is clearly visible; Outcrop 143 (referenced in the large map at the end of the thesis)

Smaller-scale (a maximum of few meters in size) landslides were found in several places all over the study area (Figure 23).



Figure 23: very small landslide; mostly contains fine grained material with few larger blocks; outcrop approx. 5m wide and 0.5 m high. Found in the municipal forest of on 2019/07/17; Outcrop 144 (referenced in the large map at the end of the thesis)

Larger landslides (several meters and bigger) were also found (Figure 24 & Figure 25) partly because they were first observed from a remote location. An example for that is a landslide near Perfall, which was viewed more thoroughly (Figure 25).



Figure 24: A larger landslide, its headscarp is approximately 5 to 10 m above; found at the Seigesbach; different kinds of blocky material going from fine grained sand to block in cm - to m- range; part of Outcrop 86 (referenced in the large map at the end of the thesis);



Figure 25: left: Landslide near Perfall; right: Landslide up close (Outcrop 54), with a new wooden bridge; picture below: Possible landslide continues beneath the trail; fine grained soil with blocks up to a 0.5 m. ; Outcrop 149 (referenced in the large map at the end of the thesis)

Other probable landslides were not possible to reach because of terrain restraints or lack of trails. E.g. Figure 26 shows a landslide at the Eastern slope of the “Tiefental” or Tiefen Valley with the picture taken from Grinzens, the opposite valley side.



Figure 26: Picture of possible landslides on the slopes of the Tiefen Valley between Oberperfuss and Sellrain; Outcrop 28 (referenced in the large map at the end of the thesis)

But as different as they might look all landslides have a common denominator, their composition. They are mostly made up of moraine material containing rocks of the ÖSK left behind by the Sellrain glacier during the ice age(s) (Figure 27 & Figure 28).



Figure 27: Left: Outcrop 12: Moraine material made of partly cemented terrace gravel with blocks of several sizes in between; right: Outcrop 4: Big blocks of unknown size ; no schistosity or layers visible (outcrops referenced in the large map at the end of the thesis)

The components are for a great part subangular to very angular and blocks vary in sizes from several centimeters to possible 10 meters and larger. It was not possible to determine the actual size because these blocks were not fully visible (Figure 27). The fine-grained material is partly cemented and of sand grain size (Figure 27 & Figure 28).



Figure 28: Composition: Sand and gravel; Outcrop 26 (referenced in the large map at the end of the thesis)

The only areas where a possible bedrock was visible were the riverbeds, e.g. the Seigesbach (Figure 29).

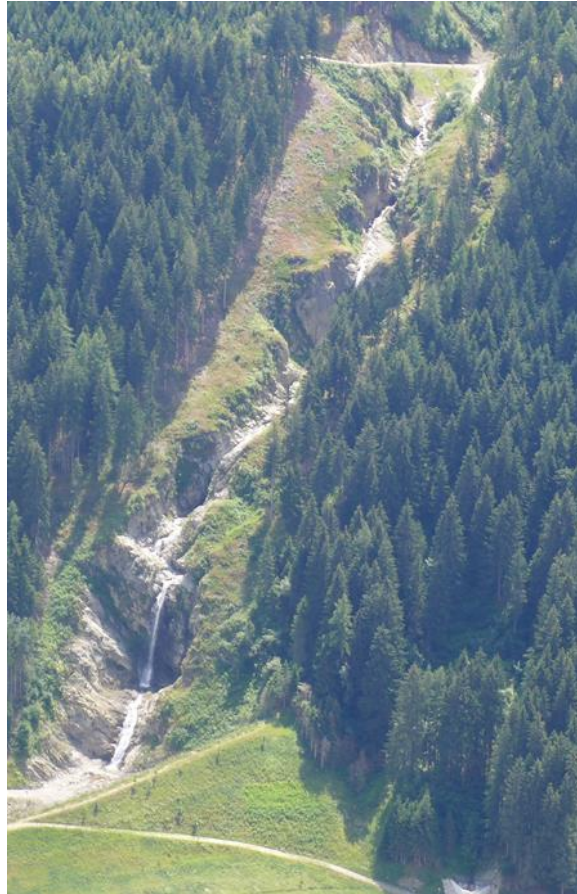


Figure 29: Above: Seigesbach as it can be seen from St. Quirin, Outcrop 121; below: Seigesbach up close: possible bedrock (?), Outcrop 88; (outcrops referenced in the large map at the end of the thesis)

Two other indications for possible landslides are the hummocky topography and cracks in the road. For the latter the cracks have to run parallel to the slope as Figure 30 illustrates.



Figure 30: Several examples for cracks in the roads; Outcrop 123 (Left) and Outcrop 132 (Right) are located in Tauogert, Sellrain; Outcrop 155 (Below) is located in Durögg, Sellrain (outcrops referenced in the large map at the end of the thesis)

The hummocky topography is best viewed from a distance and is therefore divided into two categories for the case of this thesis similar to the subdivision for possible landslides (Figure 31).



Figure 31: Examples for hummocky topography; Above: St. Quirin, Sellrain (Outcrop 126); Below: Neder, Grinzens (Outcrop 27) (outcrops referenced in the large map at the end of the thesis)

9.1.1 Outcrop Map

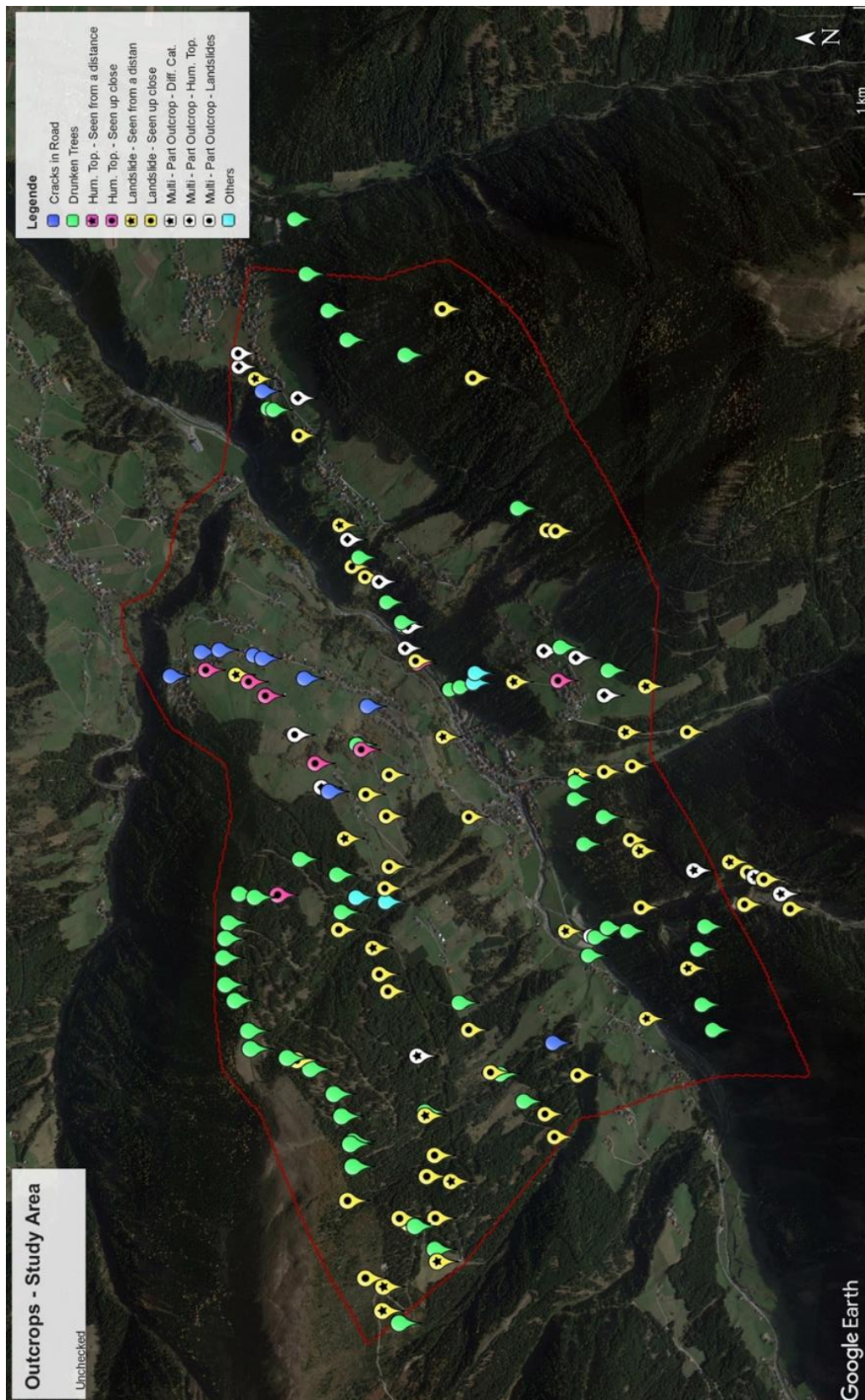


Figure 32: The outcrop map of the study area, which is marked red; The categories' colors and symbols are as described: Landslide (yellow): on the same side as outcrop point (circle) and remote observation (star); Hummocky topography (pink): on the same side as outcrop point (circle) and remote observation (star); Multi-Part outcrop (White): Different categories (diamond), different scales of hummocky topography (circle) and different scales of landslide (star); Drunken trees (green); Cracks in road (blue); Others (turquoise); base map: © Google Earth;

9.2 MEMPS

9.2.1 Input parameters

As mentioned before the values for the constant parameters came from different sources. The soil cohesion, the soil density and the friction angle are taken from the geotechnical report of Henzinger (2008) and are as follows: the soil cohesion = 510 kg/m², the soil density = 2141 kg/m³ and the friction angle = 35° (Table 1). The soil density was calculated from the specific weight because the density itself was not given. The friction angle was chosen because of the geotechnical report by Henzinger (2008), which was also corroborated by literature studies (Bobek, 1935; Heuberger, 1966; Stiftung Umwelt-Einsatz Schweiz, 2016) and the field work above. This led to a sandy gravel, that has a friction angle between 32° and 37° (Wikipedia.org, 2019). All units were transformed to their respective SI-Units with the exception of the uniform steady recharge as it has been mentioned above.

The value/parameter a.k.a. precipitation was calculated for the following time periods: The daily average from 1980 to 2010 (Bundesministerium Nachhaltigkeit und Tourismus, 2018), the daily average from 2010 to 2016 (Bundesministerium Nachhaltigkeit und Tourismus, 2018) and the maximum precipitation ever measured (Lagger, 2015). Here the SI-Unit for time was not taken since the precipitation per second would be too small for calculating with QGIS (2018 - 2019) and converted into m/day (Table 1).

The saturated hydraulic conductivity was set at 8.64 m/day (Wikipedia.org, 2019), which is the typical value for a soil containing mostly gravel and sand, the water density at 1000 kg/m³ and the gravitational acceleration at 9.81 m/s² (Table 1).

Next the contour length was set according to the resolution with the values of 1m, 5m and 10m (Table 1).

Finally, the flow accumulation raster was calculated with Whitebox GIS (Lindsay, 2009) and then imported into QGIS (2018 – 2019). With all the values now known and all necessary raster datasets available the model can be run for each period/resolution.

9.2.1.1 Calculation of the precipitation

In order to compare the soil depth later three time periods for the precipitation rates were created. The first period covers the years from 1980 to 2010, the second from 2010 to 2016 and the extreme precipitation that occurred in June 2015. The precipitation rates can be found in Table 1 and were calculated from the mean annual precipitation (1980 – 2010) and the average of the total sum of precipitation (2010 – 2016). The extreme precipitation was taken directly from the paper of Lagger (2015). The resulting values are 0.0026 m/day (1980 – 2010), dubbed Period 1, 0.0030 m/day (2010 – 2016), dubbed Period 2, and 0.28 m/day (June 2015), dubbed Period 3 (Table 1).

9.2.2 The calculation of MEMPS

Table 1: Constant Values for the Study Area along with their respective units and symbols

Parameter	Symbol	Value
Soil cohesion	c	510 kg/m ²
Soil density	ρ_s	2141 kg/m ³
Water density	ρ_w	1000 kg/m ³
Gravitational Acceleration	g	9.81 m/s ²
Friction Angle	φ	35 °
Uniform Steady Recharge/Precipitation	q	0.0026 / 0.0030 / 0.28 m/day
Contour Length/Pixel Size	b	1/5/10 m
Saturated Hydraulic Conductivity	K_s	8.64 m/day

The following section includes histograms of all calculated raster datasets with the following categories: Category I (no risk), Category II (onset of shallow landslides) and Category III (potential instability). Due to their number of data points the 1-m resolution datasets are represented here as maps because they exceed cell limit of an Excel-Datasheet. This was done both for the DEM and DTM for both raster measurement epochs of 2007 and 2013. Unfortunately, a result for 2013, 10-meter DTM was impossible to calculate because the model would give back an error message regardless of the number of tries to calculate it.

Furthermore, separate column diagrams with a column for each precipitation period were created for Category III to illustrate it better. It was further subdivided into the following groups: 3 – 5 meters, smaller 10 meters, smaller 50 meters, smaller 100 meters and bigger 100 meters.

Before beginning with the in-detail description of the results one remark should be made to the Category I results: They are negative soil depths (e.g. Chapter 8.1.2.3), that do not exist. They are just the result of small slope angles and will therefore not discussed any further.

9.2.2.1 DEM – results

The DEM-Results include 12 histograms and 12 column diagrams for the 5- and 10-meter resolutions and 6 maps for the 1-meter resolution.

For the critical soil depth z_c of the DEM of the 2007, 5-m-resolution-histogram of Period 1 (Figure 34) the results are 170801 data points (45.23% of all points) for Category I, 203140 data points (53.79%) for Category II and 3708 data points (0.98%) for Category III. For the Period-2-histogram (Figure 34) the numbers are 168540 data points (44.63%) for Category I, 205471 data points (54.41%) for Category II and 3638 (0.98%) for Category III. For the Period-3-histogram (Figure 34) the following results were calculated: 103071 data points (27.29%) for Category I, 270765 data points (71.70%) for Category II and 3813 (1.01%) for Category III.

Figure 33 visualizes the results for z_c larger than 3 meters. The figures are as follows: Period 1 results: For 3 – 5 meters 38.70%, for smaller than 10 meters 29.40%, for smaller than 50 meters 25.27%, for smaller than 100 meters 3.56% and bigger than 100 meters 3.07%. Period 2 results are the following: For 3 – 5 meters 38.07%, for smaller than 10 meters 29.80%, for smaller than 50 meters 25.48%, for smaller than 100 meters 3.55% and bigger than 100 meters 3.11%. The calculation results for Period 3 are: For 3 – 5 meters 43.33%, for smaller than 10 meters 30.03%, for smaller than 50 meters 21.64%, for smaller than 100 meters 2.57% and bigger than 100 meters 2.44%.

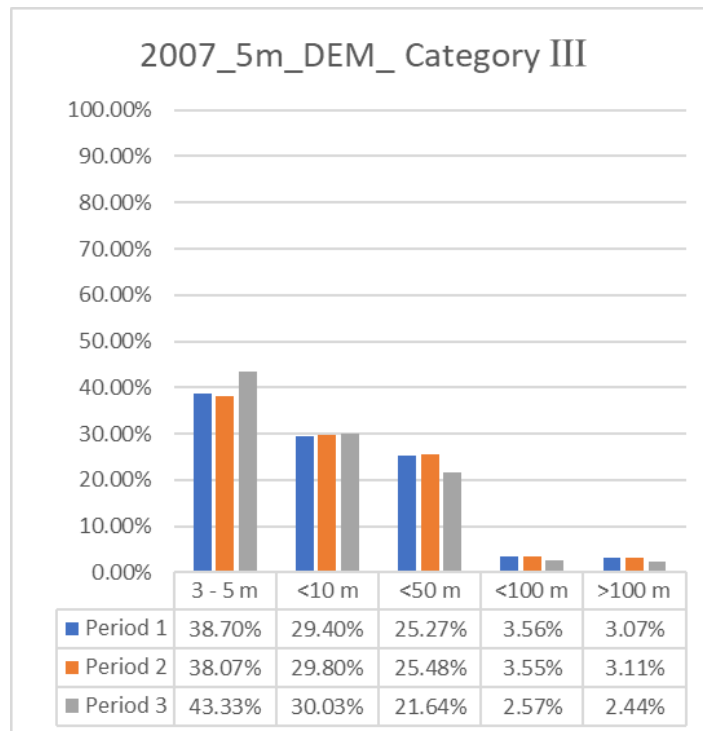


Figure 33: Category III (potential instability): The results for the calculations of the critical soil depth z_c of the 2007-5-m resolution (DEM); Period 1 is blue, Period 2 is orange and Period 3 is grey



Figure 34: The results for the calculations of the critical soil depths z_c of the 2007, 5-m resolution (DEM); Upper Left: The histogram of all Precipitation - Periods containing the absolute count (green) and its percentage (blue) for three categories: Category I (no risk), Category II (onset of shallow landslides) and Category III (potential instability) Upper Left: Period 1, upper right: Period 2 and lower left: Period 3

For z_c of the DEM of the 2007,10-m-resolution of Period-1-histogram (Figure 36) the results are 51730 data points (54.55%) for Category I, 41980 data points (44.27%) for Category II and 1125 (1.19%) for Category III. For the Period 2-histogram (Figure 36) the numbers are 50882 data points (53.65%) for Category I, 42848 data points (45.18%) for Category II and 1105 (1.17%) for Category III. For the Period-3-histogram (Figure 36) the following results were calculated: 31788 data points (33.52%) for Category I, 61595 data points (64.95%) for Category II and 1452 (1.53%) for Category III.

Figure 35 visualizes the results for the z_c larger than 3 meters. The figures are as follows, Period 1 results are the following: For 3 – 5 meters 39.64%, for smaller than 10 meters 32.00%, for smaller than 50 meters 21.69%, for smaller than 100 meters 3.29% and bigger than 100 meters 3.38%. Period 2 results are the following: For 3 – 5 meters 39.91%, for smaller than 10 meters 31.31%, for smaller than 50 meters 22.08%, for smaller than 100 meters 3.35% and bigger than 100 meters 3.35%. Period 3 results are the following: For 3 – 5 meters 42.84%, for smaller than 10 meters 29.34%, for smaller than 50 meters 23.35%, for smaller than 100 meters 2.55% and bigger than 100 meters 1.93%.

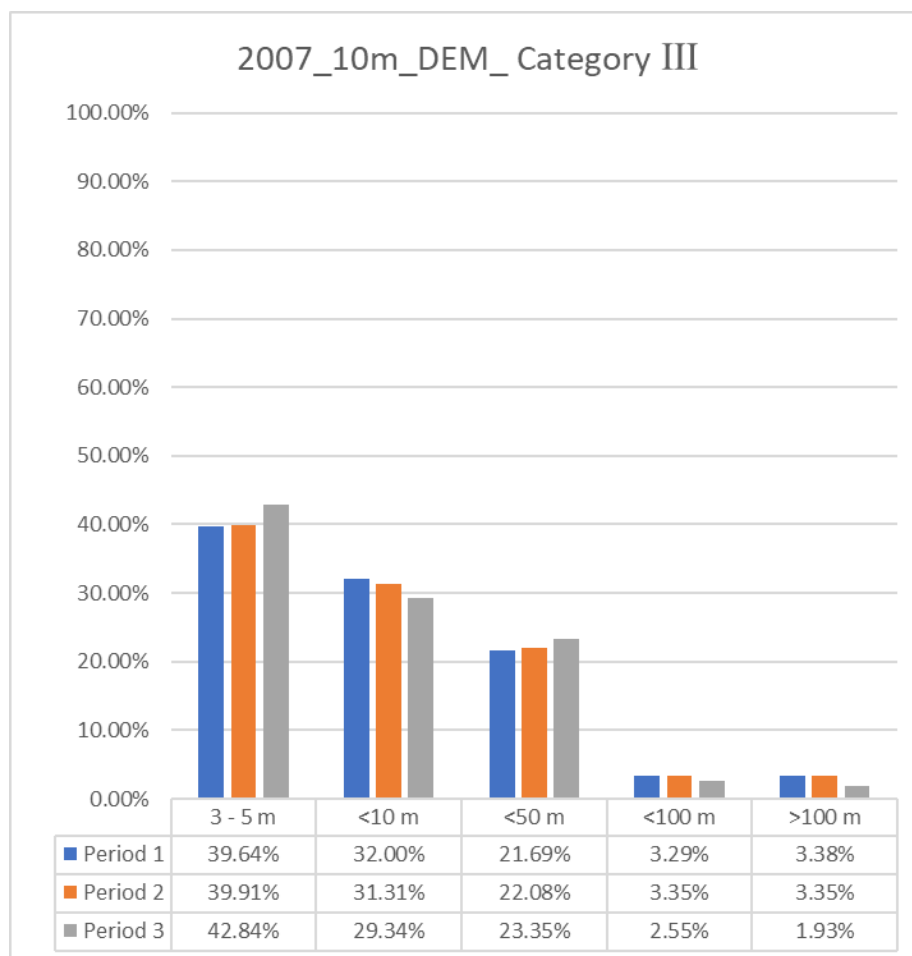


Figure 35: Category III (potential instability): The results for the calculations of the critical soil depths z_c of the 2007,10-m resolution (DEM); Period 1 is blue, Period 2 is orange and Period 3 is grey



Figure 36: The results for the calculations of the critical soil depths z_c of the 2007, 10m-resolution (DEM); Upper Left: The histogram of all Precipitation - Periods containing the absolute count (green) and its percentage (blue) for three categories: Category I (no risk), Category II (onset of shallow landslides) and Category III (potential instability) Upper Left: Period 1, upper right: Period 2 and lower left: Period 3

For the z_c of the DEM of the 2013, 5-m-resolution-histogram of Period 1 (Figure 38) the results are 114995 data points (44.91%) for Category I, 139062 data points (54.31%) for Category II and 1982 (0.77%) for Category III. For the Period-2-histogram (Figure 38) the numbers are: 113549 data points (44.35%) for Category I, 140537 data points (54.89%) for Category II and 1953 (0.76%) for Category III. For the Period-3-histogram (Figure 38) the following results were calculated: 66834 data points (26.10%) for Category I, 186941 data points (73.01%) for Category II and 2264 (0.88%) for Category III.

Figure 37 visualizes the results for the z_c larger than 3 meters. The numbers look as follows: Period 1 results are the following: For 3 – 5 meters 39.40%, for smaller than 10 meters 29.57%, for smaller than 50 meters 24.17%, for smaller than 100 meters 3.33% and bigger than 100 meters 3.53%. Period 2 results are the following: For 3 – 5 meters 39.17%, for smaller than 10 meters 29.75%, for smaller than 50 meters 24.22%, for smaller than 100 meters 3.33% and bigger than 100 meters 3.53%. The calculation results for Period 3 are: For 3 – 5 meters 45.67%, for smaller than 10 meters 30.70%, for smaller than 50 meters 18.82%, for smaller than 100 meters 2.47% and bigger than 100 meters 2.34%.

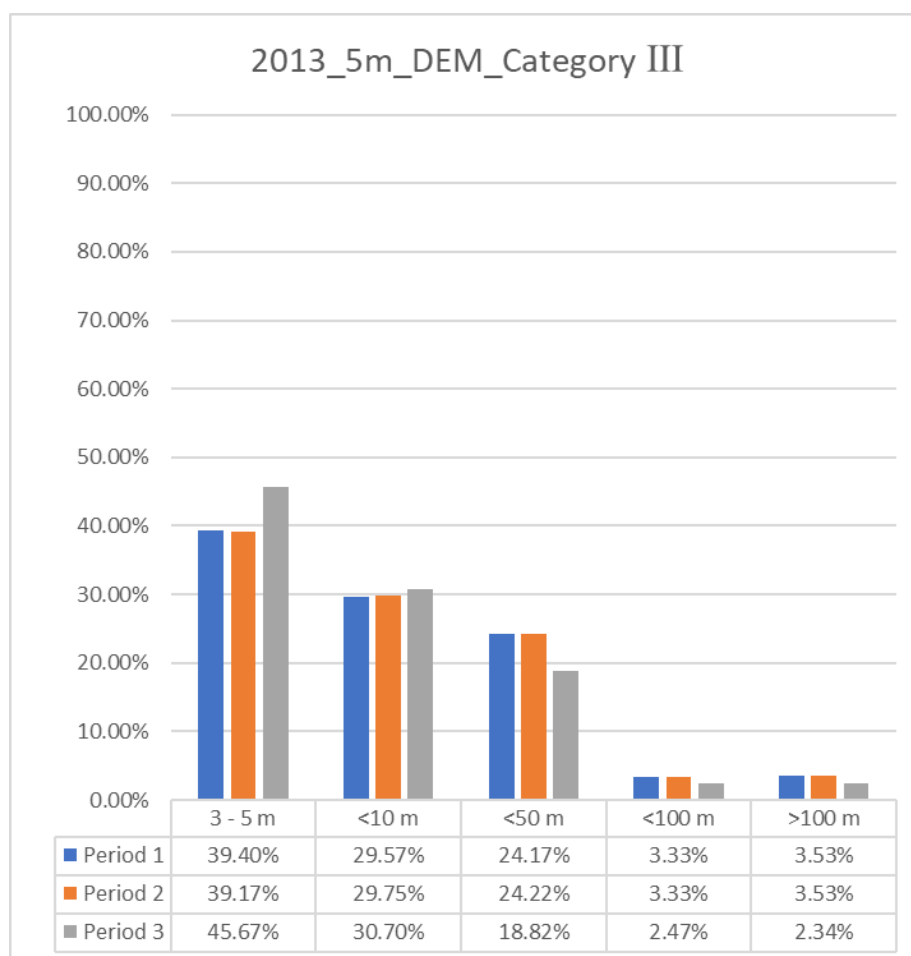


Figure 37: Category III (potential instability): The results for the calculations of z_c of the 2013-5-m resolution (DEM); Period 1 is blue, Period 2 is orange and Period 3 is grey



Figure 38: The results for the calculations of the critical soil depths z_c of the 2013, 5-m resolution (DEM); Upper Left: The histogram of all Precipitation - Periods containing the absolute count (green) and its percentage (blue) for three categories: Category I (no risk), Category II (onset of shallow landslides) and Category III (potential instability) Upper Left: Period 1, upper right: Period 2 and lower left: Period 3

For z_c of the DEM of the 2013, 10-m resolution-histogram of Period 1 (Figure 40) the results are 32779 data points (51.21%) for Category I, 30640 data points (47.86%) for Category II and 595 (0.93%) for Category III. For the Period-2-histogram (Figure 40) the numbers are 32266 data points (50.40%) for Category I, 31159 data points (48.68%) for Category II and 589 (0.92%) for Category III. For the Period 3-histogram (Figure 40) the following results were calculated: 21095 data points (32.95%) for Category I, 42098 data points (65.76%) for Category II and 821 (1.28%) for Category III.

Figure 39 visualizes the results for z_c larger than 3 meters. The figures are as follows: Period 1 results are the following: For 3 – 5 meters 39.66%, for smaller than 10 meters 32.44%, for smaller than 50 meters 21.01%, for smaller than 100 meters 3.36% and bigger than 100 meters 3.53%. Period 2 results are the following: For 3 – 5 meters 39.22%, for smaller than 10 meters 32.09%, for smaller than 50 meters 21.73%, for smaller than 100 meters 3.23% and bigger than 100 meters 3.74%. The calculation results for Period 3 are: For 3 – 5 meters 44.95%, for smaller than 10 meters 29.60%, for smaller than 50 meters 20.95%, for smaller than 100 meters 2.31% and bigger than 100 meters 2.19%.

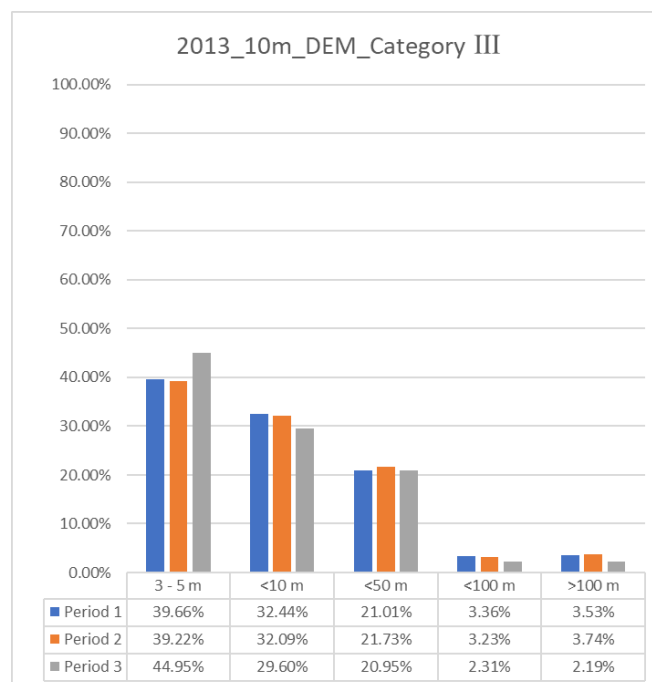


Figure 39: Category III (potential instability): The results for the calculations of the critical soil depths z_c of the 2013-10-m resolution (DEM); Period 1 is blue, Period 2 is orange and Period 3 is grey

Below, after the histograms of the 2013 DEM (10-m resolution), are the maps of 1-meter resolution (DEM). For the year 2007 the Period 1 map (Figure 41), the Period 2 map (Figure 42), the Period 3 map (Figure 43) and for the year 2013 the Period 1 map (Figure 44), the Period 2 map (Figure 45) and the Period 3 map (Figure 46). The maps for the other resolutions can be found in the appendix (Figure 64 to Figure 75).



Figure 40: The results for the calculations of the critical soil depths z_c of the 2013, 10-m-resolution (DEM); Upper Left: The histogram of all Precipitation - Periods containing the absolute count (green) and its percentage (blue) for three categories: Category I (no risk), Category II (onset of shallow landslides) and Category III (potential instability) Upper Left: Period 1, upper right: Period 2 and lower left: Period 3

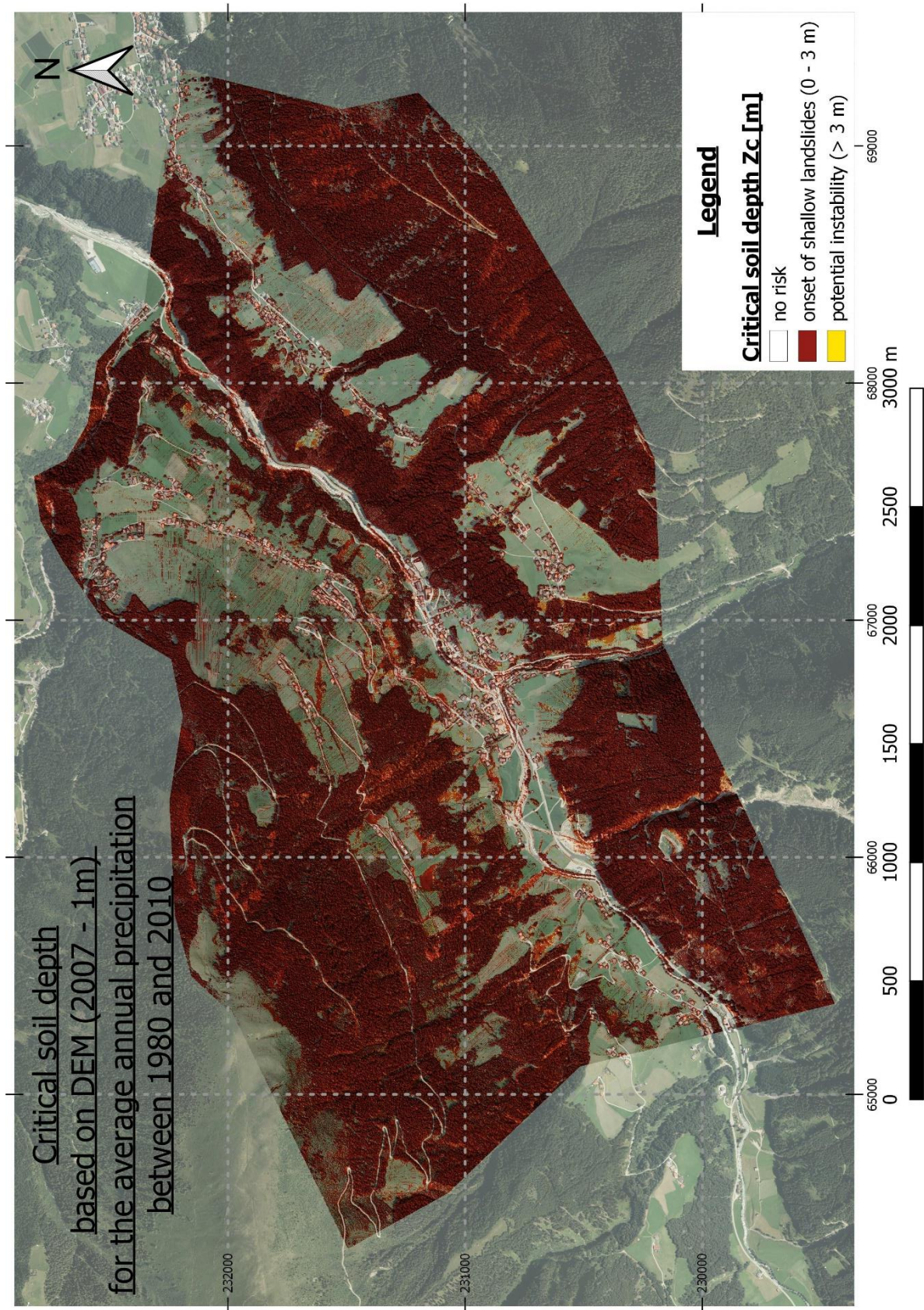


Figure 41: Map of the critical soil depth z_c for the average annual precipitation between 1980 and 2010 (2007 - DEM, 1m); raw data: © (Land Tirol - data.tirol.gv.at, 2018), orthophoto: © (Land Tirol - data.tirol.gv.at, 2019)

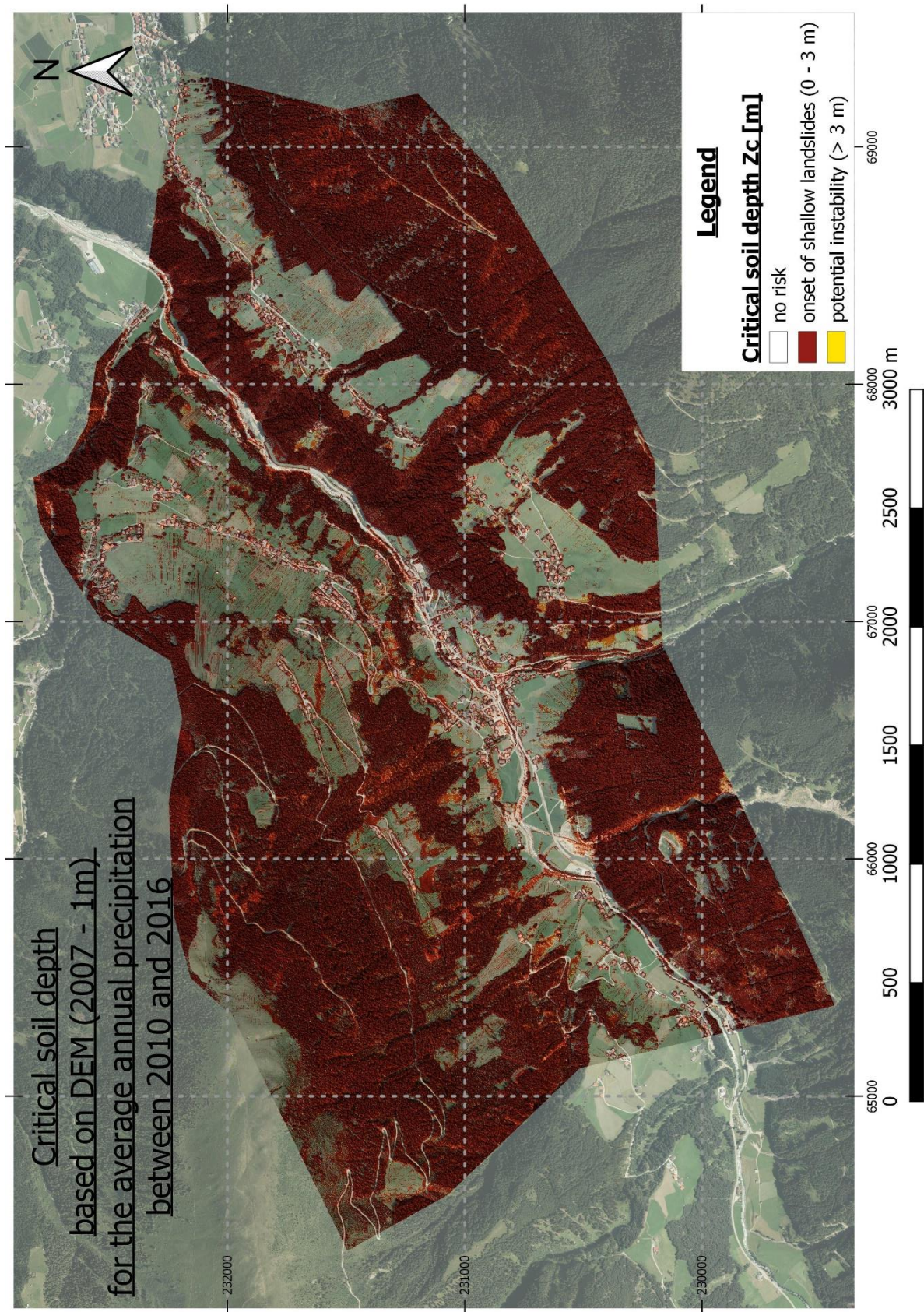


Figure 42: Map of the critical soil depth z_c for the average annual precipitation between 2010 and 2016 (2007 - DEM, 1m); raw data: © (Land Tirol - data.tirol.gv.at, 2018), orthophoto: © (Land Tirol - data.tirol.gv.at, 2019)

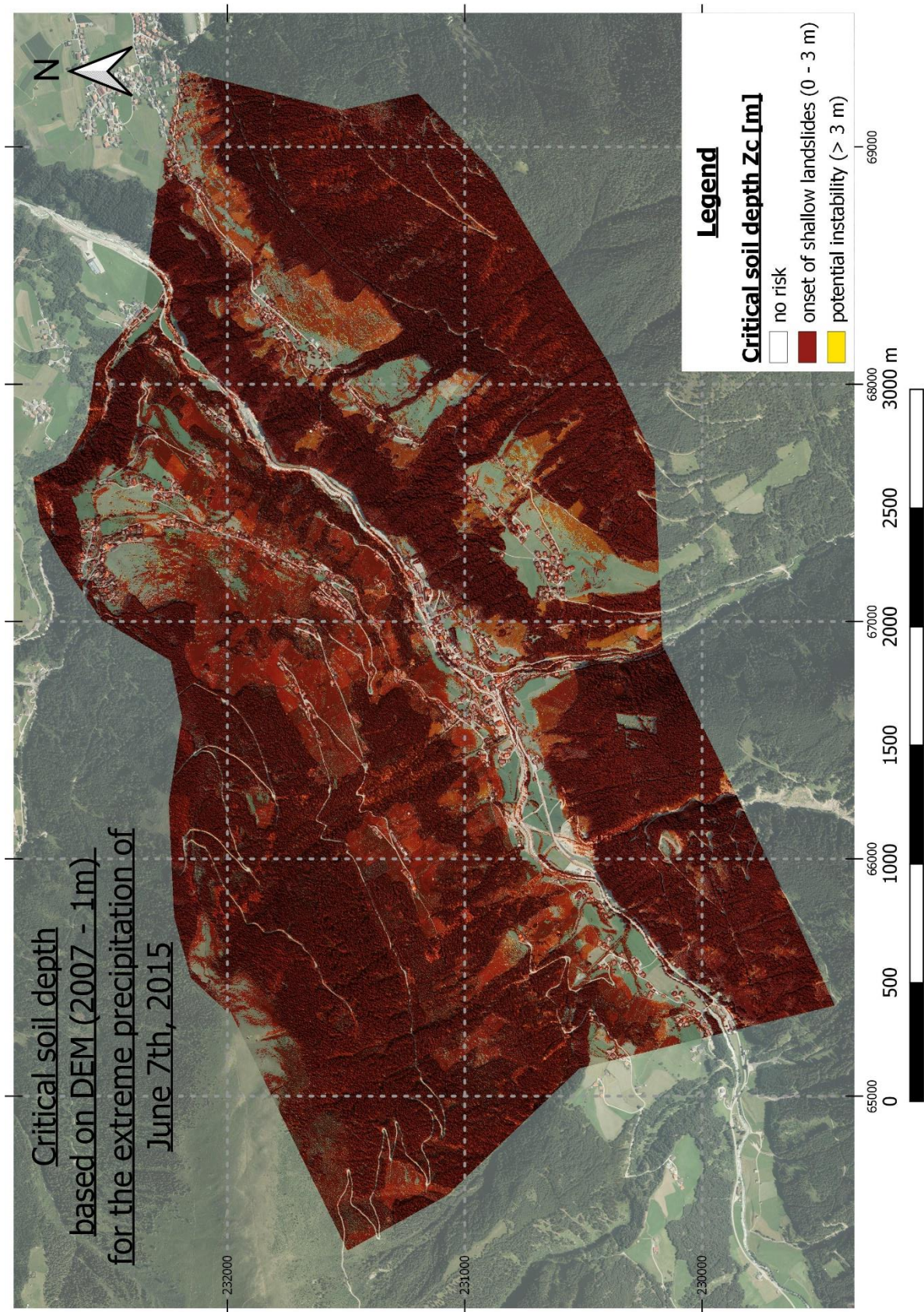


Figure 43: Map of the critical soil depth z_c for the extreme precipitation of June 2015 (2007 - DEM, 1m); raw Data: © (Land Tirol - data.tirol.gv.at, 2018), orthophoto: © (Land Tirol - data.tirol.gv.at, 2019)

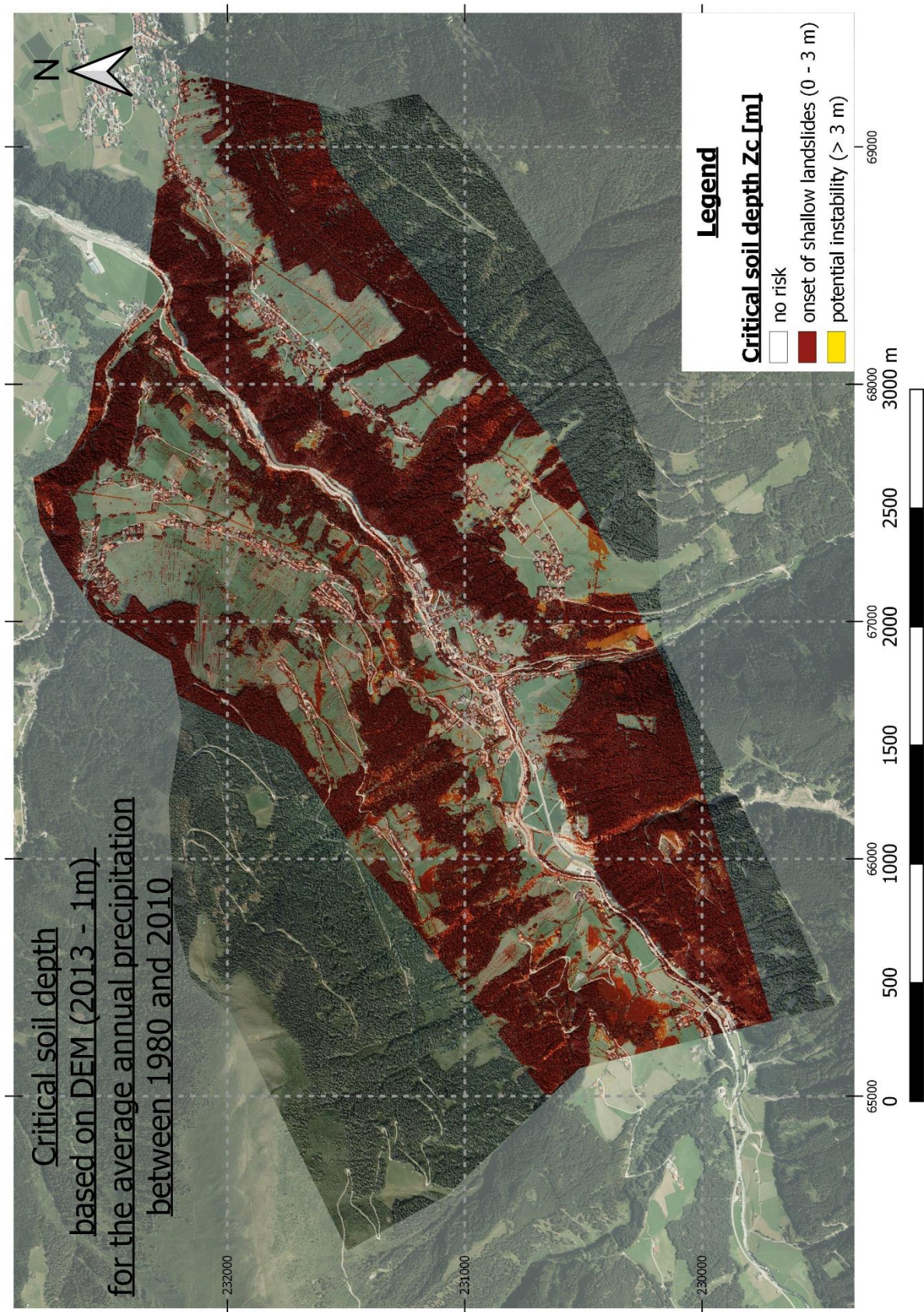


Figure 44 Map of the critical soil depth z_c for the average annual precipitation between 1980 and 2010 (2013 - DEM, 1m); raw data: © (Land Tirol - data.tirol.gv.at, 2018), orthophoto: © (Land Tirol - data.tirol.gv.at, 2019)

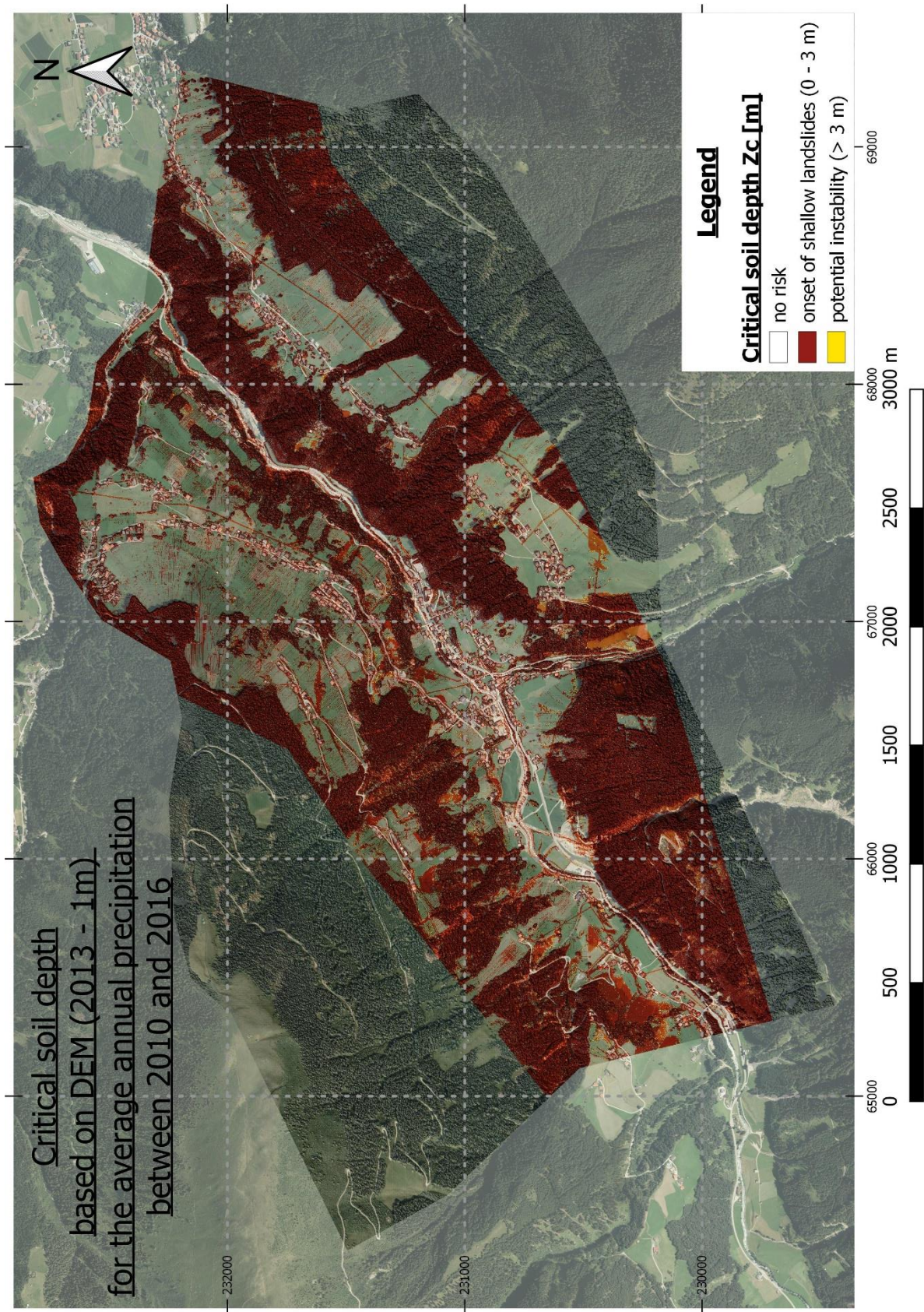


Figure 45: Map of the critical soil depth z_c for the average annual precipitation between 2010 and 2016 (2013 - DEM, 1m); raw Data: © (Land Tirol - data.tirol.gv.at, 2018), orthophoto: © (Land Tirol - data.tirol.gv.at, 2019)

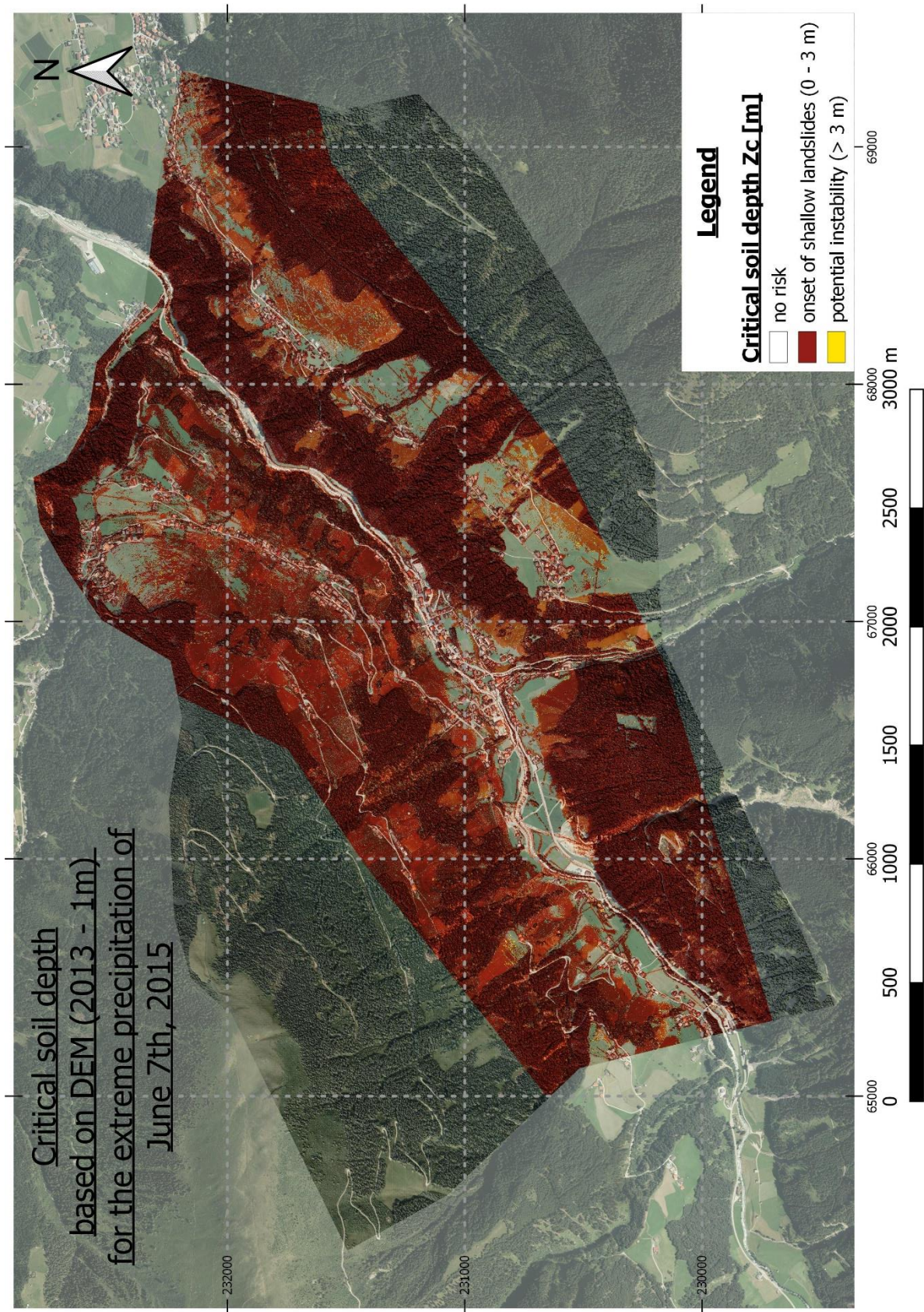


Figure 46: Map of the critical soil depth z_c for the extreme precipitation of June 2015 (2013 - DEM, 1m); raw Data: © (Land Tirol - data.tirol.gv.at, 2018), orthophoto: © (Land Tirol - data.tirol.gv.at, 2019)

9.2.2.2 DTM – results

The DTM-Results include 9 histograms and 9 column diagrams for the 5- and 10-meter resolutions and 6 maps for the 1-meter resolution.

For z_c of the DTM of the 2007, 5-m resolution histogram of Period 1 (Figure 48) the results are 224221 data points (59.42% of all points) for Category I (smaller than zero meters) , 148370 data points (39.32 %) for Category II (zero to three meters) and 4728 (1.25%) for Category III (potential instability). For the Period-2-histogram (Figure 48) the numbers are 218737 data points (57.97%) for Category I, 154051 data points (40.83%) for Category II and 4531 (1.20%) for Category III. For the Period-3-histogram (Figure 48) the following results were calculated: 87403 data points (23.16%) for Category I, 286604 data points (75.96%) for Category II and 3312 (0.88%) for Category III.

Figure 47 visualizes the results for z_c larger than 3 meters. The numbers look as followed, Period 1 results are the following: For 3 – 5 meters 40.84%, for smaller than 10 meters 29.67%, for smaller than 50 meters 23.39%, for smaller than 100 meters 2.90% and bigger than 100 meters 3.19%. Period 2 results are the following: For 3 – 5 meters 41.01%, for smaller than 10 meters 29.73%, for smaller than 50 meters 23.11%, for smaller than 100 meters 2.96% and bigger than 100 meters 3.20%. The calculation results for Period 3 are: For 3 – 5 meters 48.04%, for smaller than 10 meters 30.31%, for smaller than 50 meters 18.63%, for smaller than 100 meters 1.57% and bigger than 100 meters 1.45%.

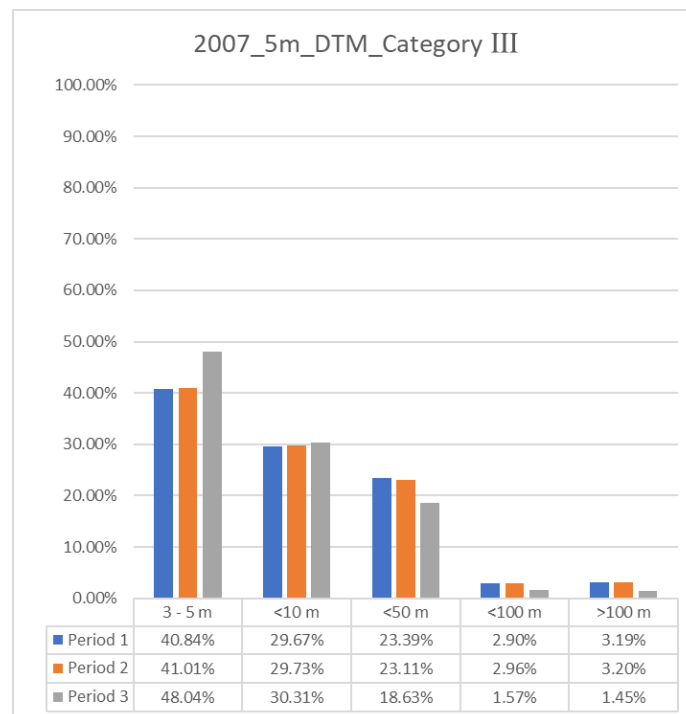


Figure 47: Category III (potential instability): The results for the calculations of the critical soil depths z_c of the 2007, 5-m resolution (DTM); Period 1 is blue, Period 2 is orange and Period 3 is grey



Figure 48: The results for the calculations of the critical soil depths z_c of the 2007, 5-m resolution (DTM); Upper Left: The histogram of all Precipitation - Periods containing the absolute count (green) and its percentage (blue) for three categories: Category I (no risk), Category II (onset of shallow landslides) and Category III (potential instability) Upper Left: Period 1, upper right: Period 2 and lower left: Period 3

For z_c of the DTM of the 2007, 10-m-resolution-histogram of Period 1 (Figure 50) the results are 53408 data points (56.62%) for Category I, 39857 data points (42.25%) for Category II and 1069 (1.13%) for Category III. For the Period-2-histogram (Figure 50) the numbers are 51660 data points (54.76%) for Category I, 41665 data points (44.17%) for Category II and 1009 (1.07%) for Category III. For the Period 3 – histogram (Figure 50) the following results were calculated: 22447 data points (23.80%) for Category I, 70935 data points (75.20%) for Category II and 952 (1.01%) for Category III.

Figure 49 visualizes the results for z_c larger than 3 meters. The numbers look as followed. Period 1 results are the following: For 3 – 5 meters 39.38%, for smaller than 10 meters 29.75%, for smaller than 50 meters 24.79%, for smaller than 100 meters 2.62% and bigger than 100 meters 3.46%. Period-2-results are the following: For 3 – 5 meters 40.04%, for smaller than 10 meters 29.04%, for smaller than 50 meters 24.68%, for smaller than 100 meters 2.97% and bigger than 100 meters 3.27%. The calculation results for Period 3 are: For 3 – 5 meters 46.11%, for smaller than 10 meters 30.15%, for smaller than 50 meters 20.48%, for smaller than 100 meters 1.58% and bigger than 100 meters 1.68%.

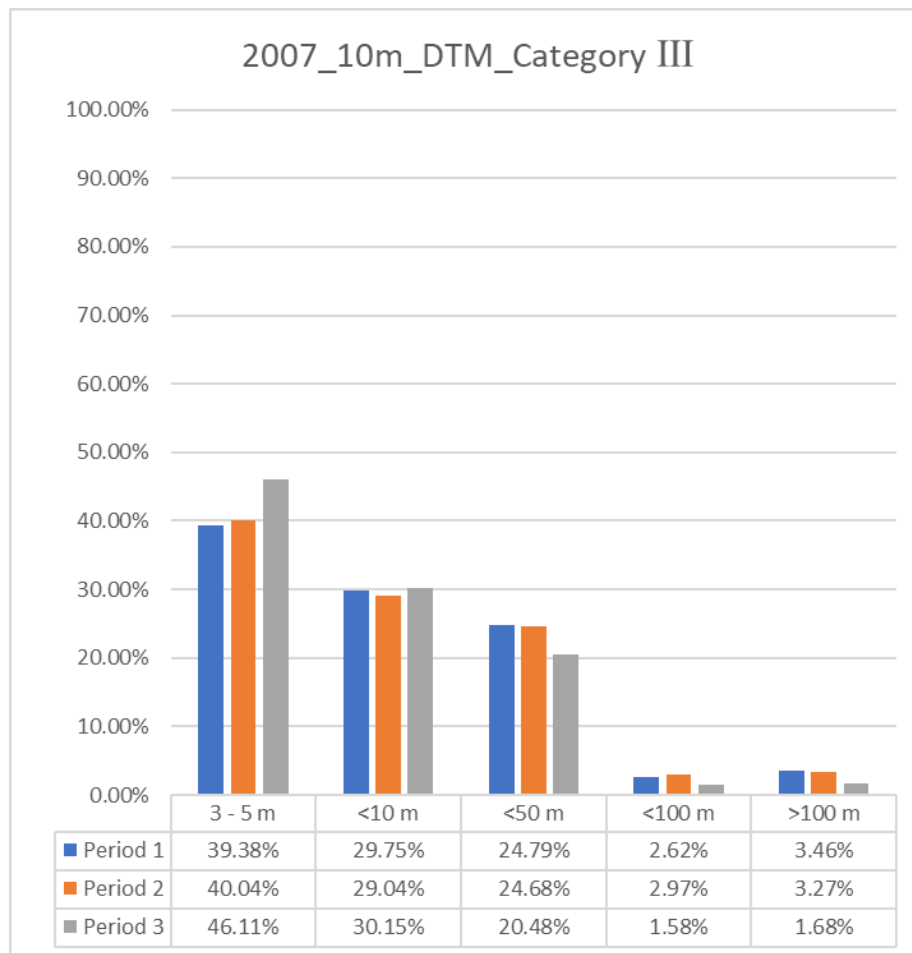


Figure 49: Category III (potential instability): The results for the calculations of the critical soil depths z_c of the 2007, 10-m resolution (DTM); Period 1 is blue, Period 2 is orange and Period 3 is grey



Figure 50: The results for the calculations of the critical soil depths z_c of the 2007, 10-m resolution (DTM); Upper Left: The histogram of all Precipitation - Periods containing the absolute count (green) and its percentage (blue) for three categories: Category I (no risk), Category II (onset of shallow landslides) and Category III (potential instability) Upper Left: Period 1, upper right: Period 2 and lower left: Period 3

For z_c of the DTM of the 2013, 5-m-resolution-histogram of Period 1 (Figure 52) the results are 164788 data points (64.10%) for Category I, 89327 data points (34.75%) for Category II and 2960 (1.15%) for Category III. For the Period-2-histogram (Figure 52) the numbers are 161649 data points (62.88%) for Category I, 92555 data points (36.00%) for Category II and 2871 (1.12%) for Category III. For the Period-3-histogram (Figure 52) the following results were calculated: 75280 data points (29.28%) for Category I, 179231 data points (69.72%) for Category II and 2564 (1.00%) for Category III.

Figure 51 visualizes the results for z_c larger than 3 meters. The numbers look as follows. Period 1 results are the following: For 3 – 5 meters 40.91%, for smaller than 10 meters 28.45%, for smaller than 50 meters 23.78%, for smaller than 100 meters 3.18% and bigger than 100 meters 3.68%. Period 2 results are the following: For 3 – 5 meters 40.54%, for smaller than 10 meters 28.81%, for smaller than 50 meters 23.93%, for smaller than 100 meters 3.03% and bigger than 100 meters 3.69%. The calculation results for Period 3 are: For 3 – 5 meters 49.30%, for smaller than 10 meters 27.73%, for smaller than 50 meters 19.89%, for smaller than 100 meters 1.68% and bigger than 100 meters 1.40%.

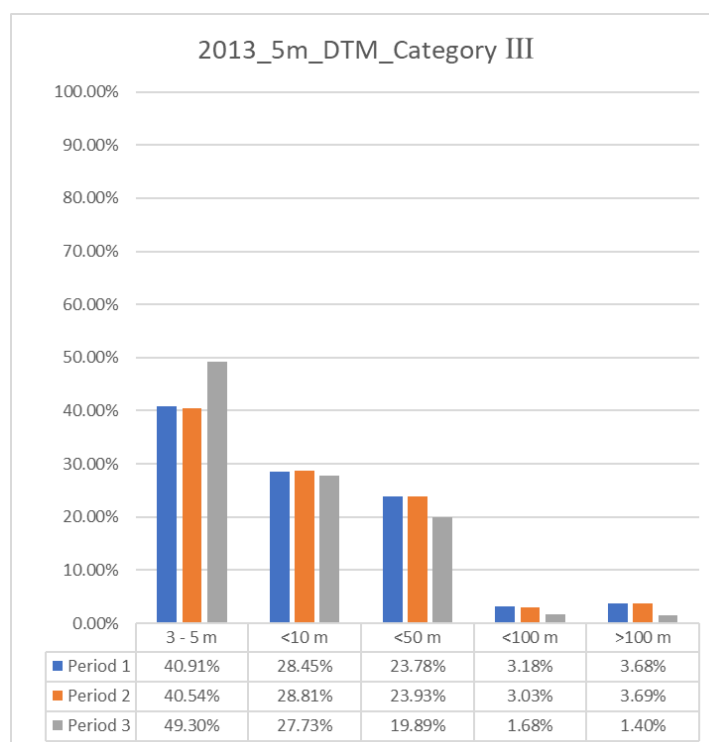


Figure 51: Category III (potential instability): The results for the calculations of the critical soil depths z_c of the 2013, 5-m resolution (DTM); Period 1 is blue, Period 2 is orange and Period 3 is grey

Below are the maps of 1-meter resolution (DTM). For the year 2007 the Period-1-map (Figure 53), the Period-2-map (Figure 54), the Period 3 map (Figure 55) and for the year 2013 the Period-1-map (Figure 56), the Period-2-map (Figure 57) and the Period-3-map (Figure 58). The maps for the other resolutions can be found in the appendix (Figure 76 to Figure 84).

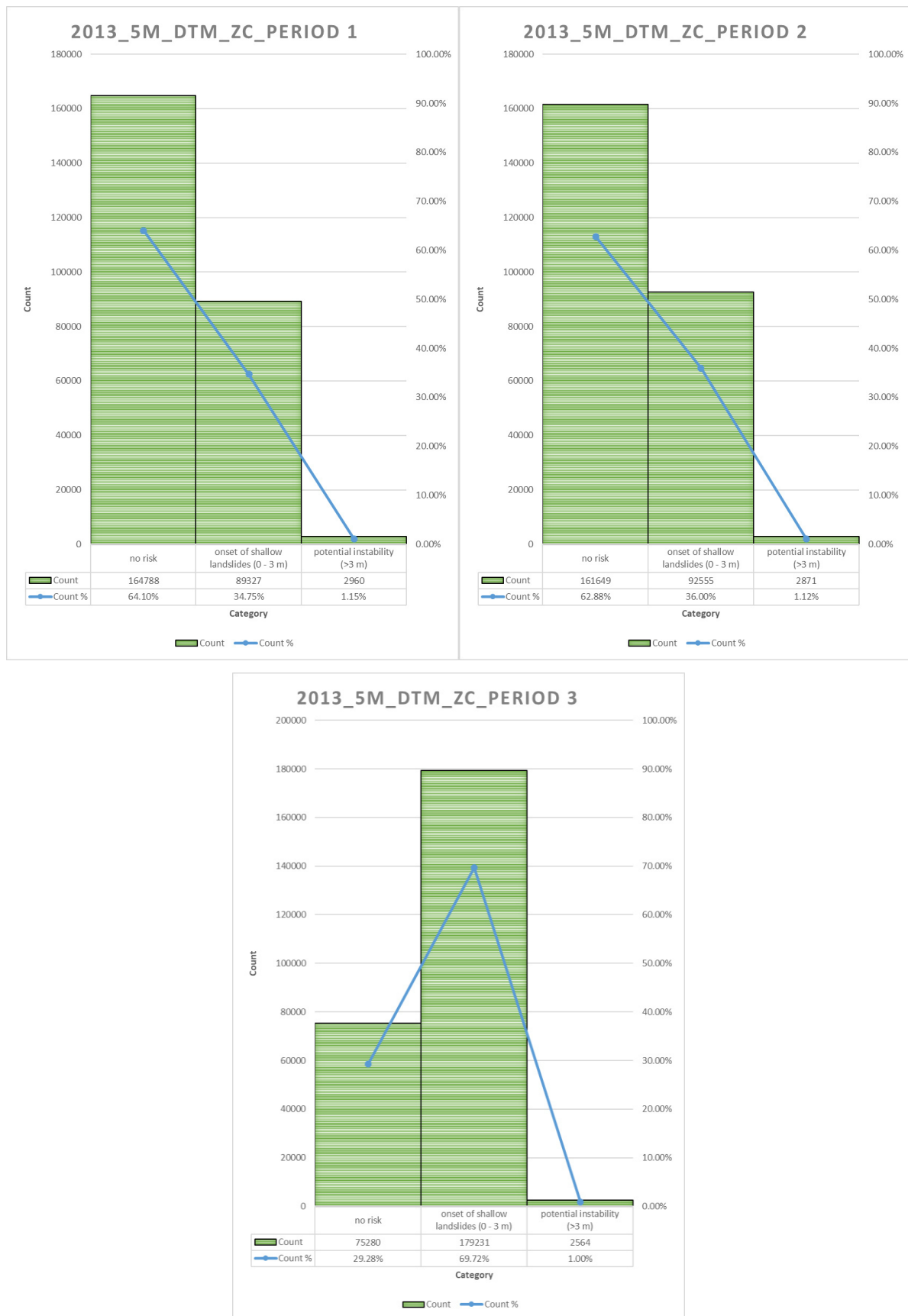


Figure 52: The results for the calculations of the critical soil depths z_c of the 2013, 5-m resolution (DTM); Upper Left: The histogram of all Precipitation-Periods containing the absolute count (green) and its percentage (blue) for three categories: Category I (no risk), Category II (onset of shallow landslides) and Category III (potential instability) Upper Left: Period 1, upper right: Period 2 and lower left: Period 3

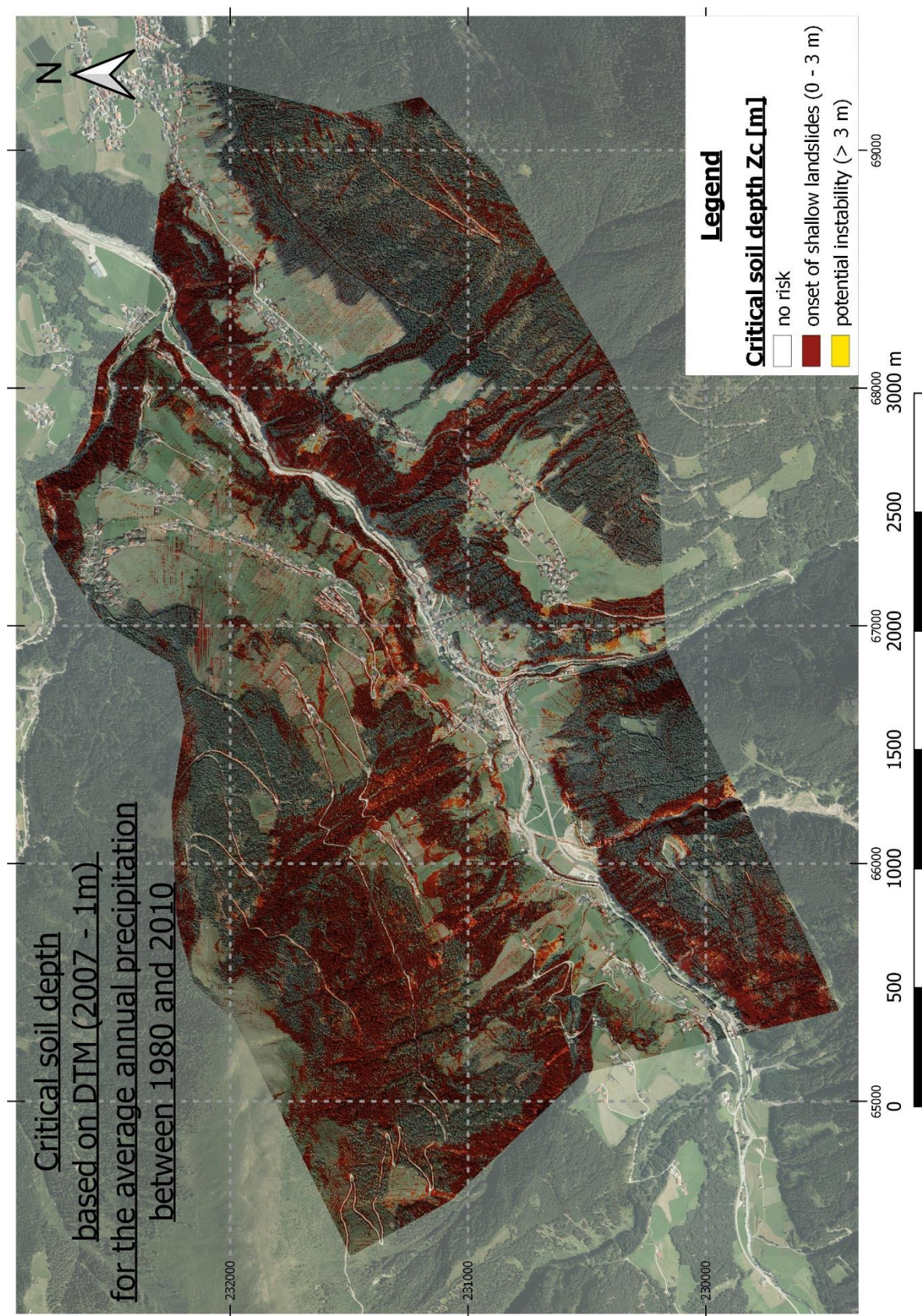


Figure 53: Map of the critical soil depth z_c for the average annual precipitation between 1980 and 2010 (2007 - DTM, 1m); raw data: © (Land Tirol - data.tirol.gv.at, 2018), orthophoto: © (Land Tirol - data.tirol.gv.at, 2019)

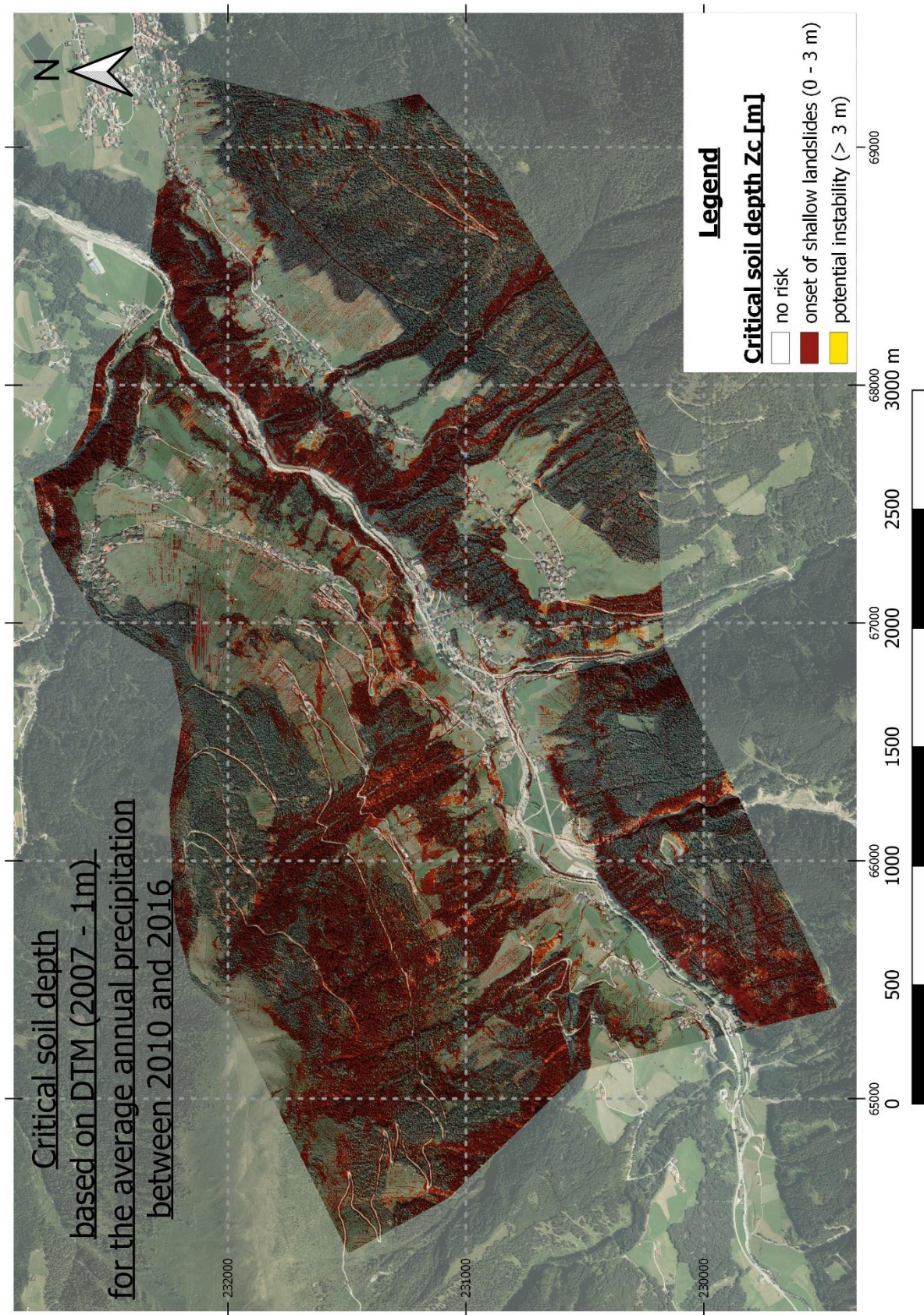


Figure 54: Map of the critical soil depth z_c for the average annual precipitation between 2010 and 2016 (2007 - DTM, 1m); raw data: © (Land Tirol - data.tirol.gv.at, 2018), orthophoto: © (Land Tirol - data.tirol.gv.at, 2019)

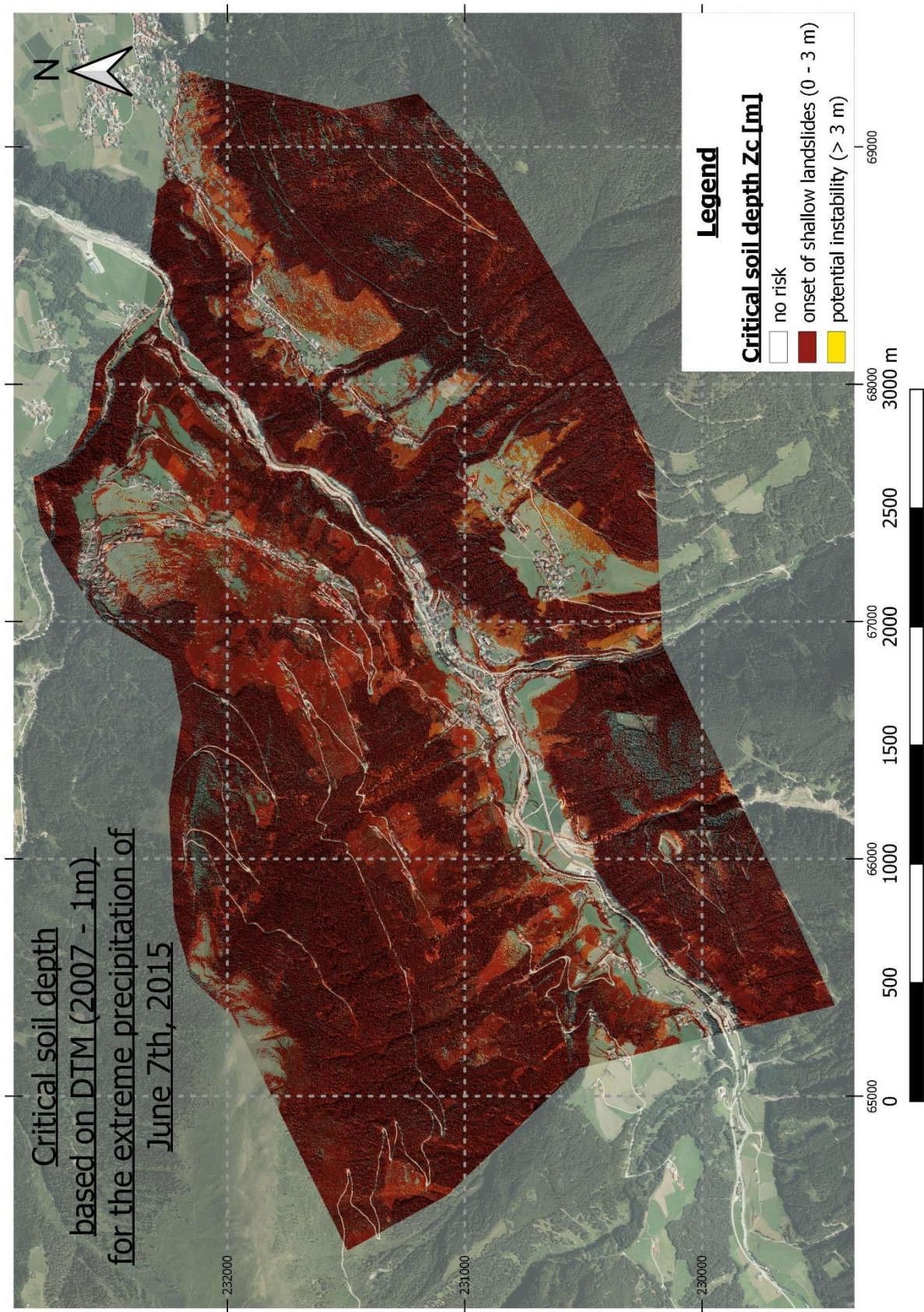


Figure 55: Map of the critical soil depth z_c for the extreme precipitation of June 2015 (2007 - DTM, 1m); raw data: © (Land Tirol - data.tirol.gv.at, 2018), orthophoto: © (Land Tirol - data.tirol.gv.at, 2019)

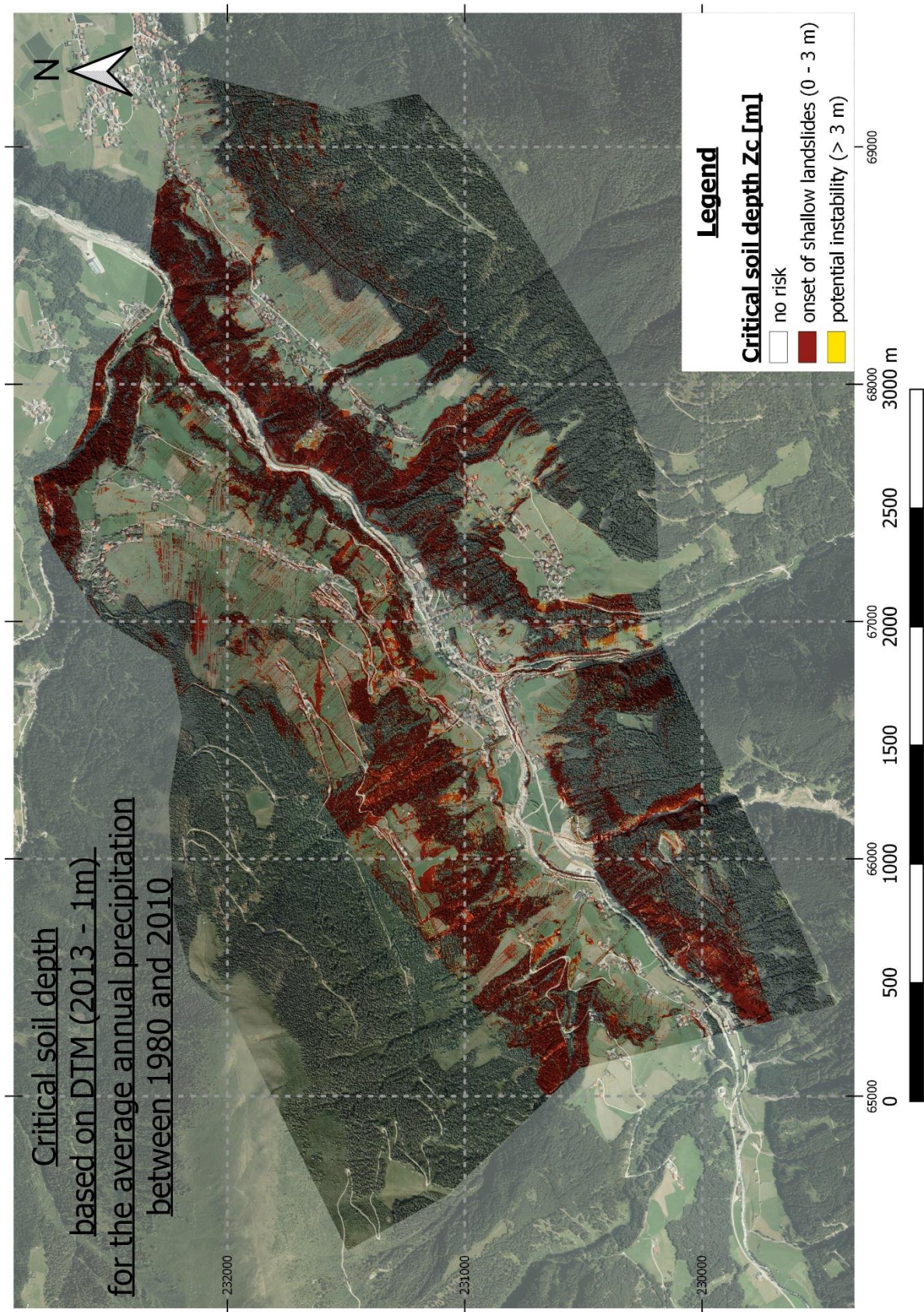


Figure 56: Map of the critical soil depth z_c for the average annual precipitation between 1980 and 2010 (2013 - DTM, 1m); raw data: © (Land Tirol - data.tirol.gv.at, 2018), orthophoto: © (Land Tirol - data.tirol.gv.at, 2019)

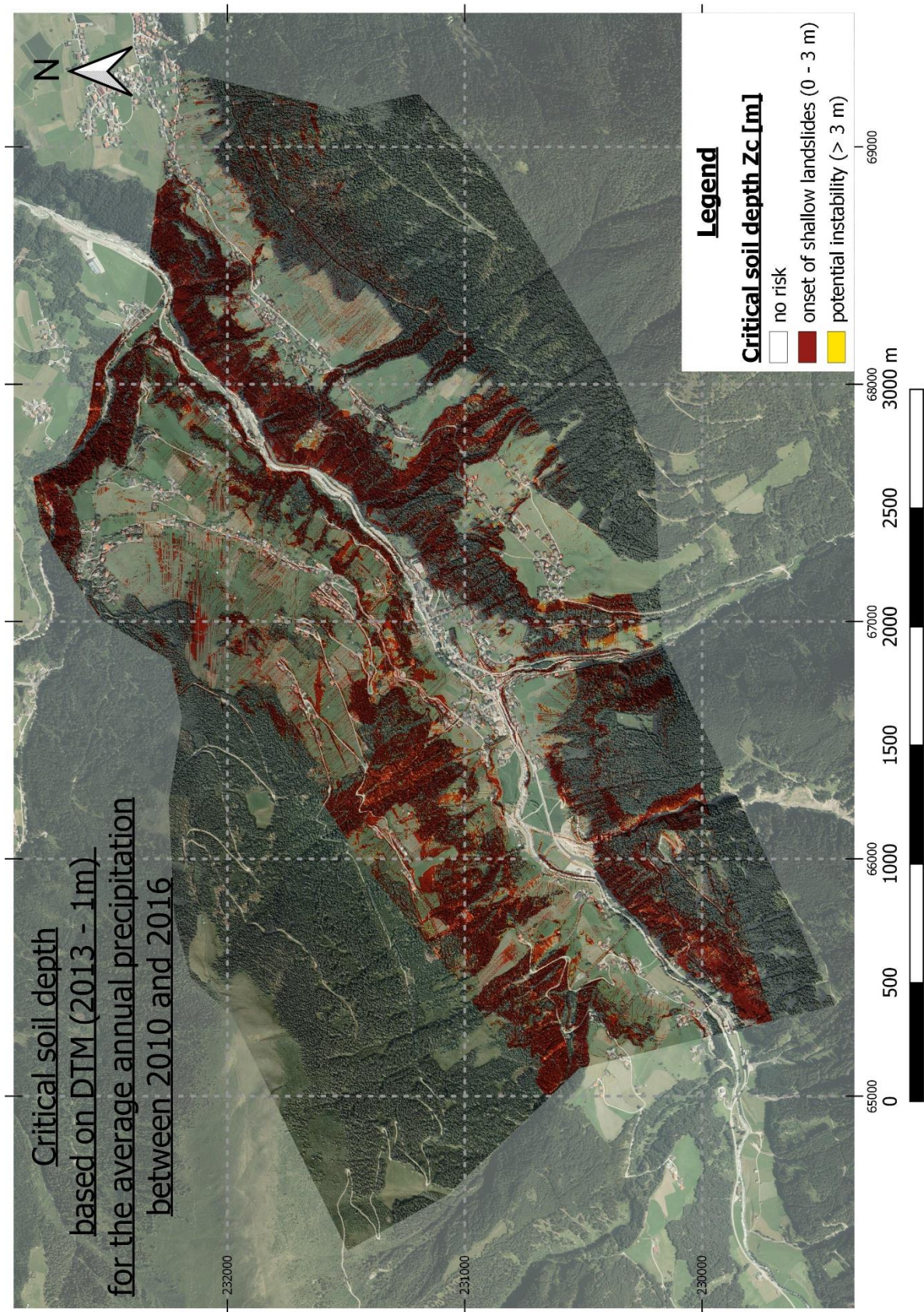


Figure 57: Map of the critical soil depth z_c for the average annual precipitation between 2010 and 2016 (2013 - DTM, 1m); raw data: © (Land Tirol - data.tirol.gv.at, 2018), orthophoto: © (Land Tirol - data.tirol.gv.at, 2019)

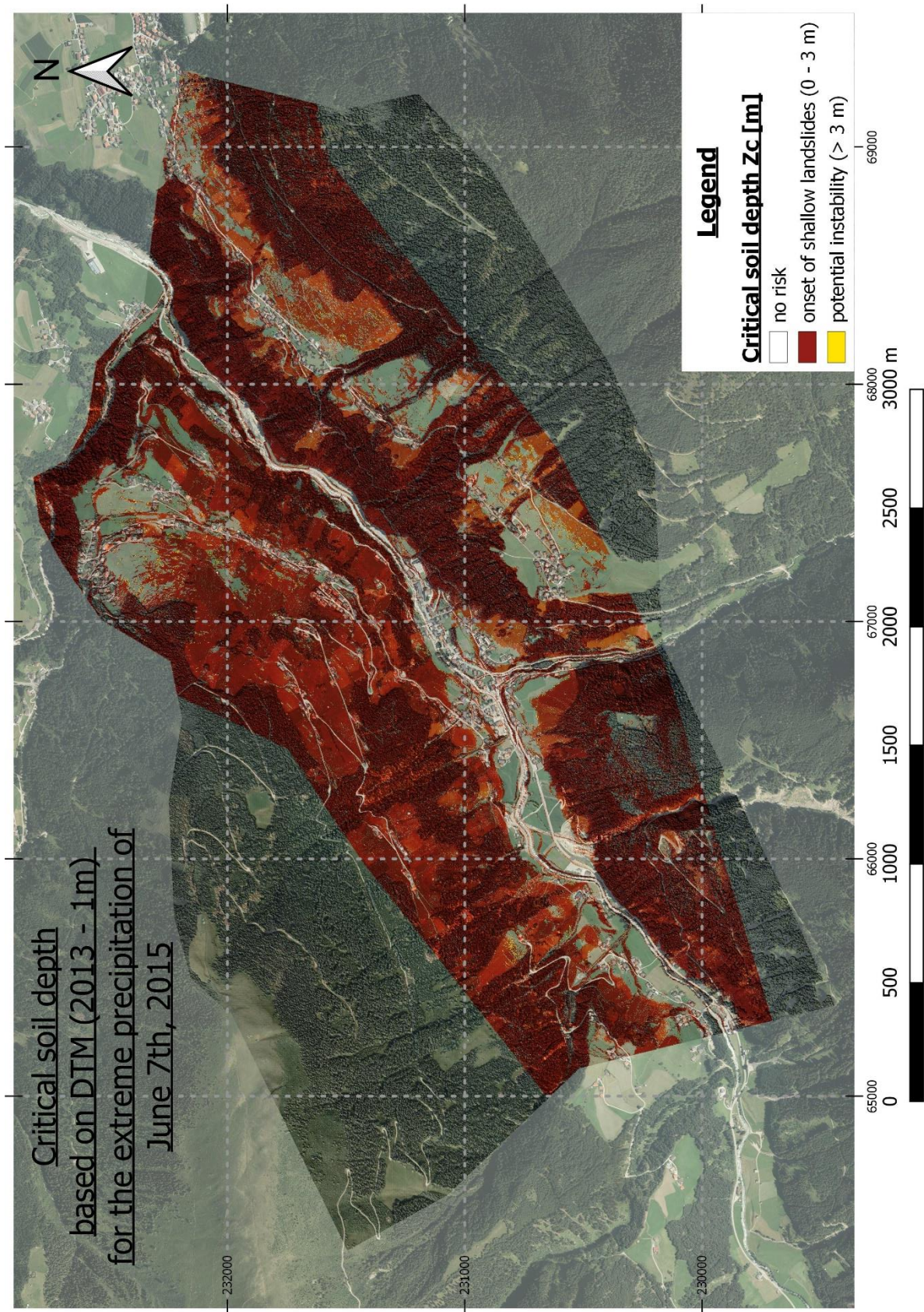


Figure 58: Map of the critical soil depth z_c for the extreme precipitation of June 2015 (2013 - DTM, 1m); raw data: © (Land Tirol - data.tirol.gv.at, 2018), orthophoto: © (Land Tirol - data.tirol.gv.at, 2019)

9.3 Remarks to the Large-Scale Map

The large map attached to this thesis contains as its title states the model based on the 2007 DTM with a resolution of 10 meters for two reasons.

Reason one being that shallow landslides are normally longer than deep and with a 10-meter resolution that is most certainly the case. Reason two concern the base model that was chosen. The DTM was chosen over the DEM because the former one is the better basis for a natural flow pattern due to the exclusion of e.g. structures and forests from its data.

Furthermore, for all three precipitation periods (1980 – 2010 / 2010 - 2016 / extreme precipitation) the critical soil depth z_c is included. Blue marks period 1, green period 2 and red period 3. Since they are stacked above each other only the differences are visible between the periods. Therefore, period 2 appears to be rather small, but in fact it covers the same area as period 1 plus the green areas visible. The same is true for period 3 with respect to period 1 and 2. These assumptions were made in order to place all three of them together into one map. Although not completely correct, this is done to such a degree where the minor differences can be ignored.

Also included in the map are the outcrop points, divided into the same categories as in the outcrop map (Figure 32).

10 Discussion

10.1 Concerning results of Category III (Potential instability)

Category III contains depths from 3 to over 100 meters, but only the results for less than 10 meters seem plausible. As for depths larger than ten meters the following reason may explain their occurrence.

Calculations in QGIS can lead to so called artifacts, which do not fit anywhere and are the result of e.g. corrupt data which can occur in using a GIS-software. This is especially the case for values bigger than 10 meters. Said values make up 25 to 30 % of the total values that are bigger than 3 meters. In this case the artifacts are mixed with results that were correctly calculated, however since the chosen soil parameters are not applicable for infinite soil depths, they are most likely false (Figure 33, Figure 35, Figure 37, Figure 39, Figure 47, Figure 49 and Figure 51). The shares here seem very balanced and for larger depths rather huge, but that is put into perspective by their share in the overall dataset (usually around 1%) This can be seen above in Figure 34, Figure 36, Figure 38, Figure 40, Figure 48, Figure 50 and Figure 52.

This is true for any given scanning epoch, precipitation period and any resolution and their respective results.

10.2 Concerning the Different MEMPS-Calculations

In this and the following sections the focus lies on the results for the critical soil depth z_c between zero and three meters. Here in this chapter the focus lies on comparing the results of the different calculations. First the focus lies on the differences between the DEM / DTM results, second on their respective recording periods and lastly on the different resolutions.

10.2.1 Precipitation Period 1 (1980 – 2010)

In the first precipitation period for the 5-meter resolution of the 2007 DEM recording period the critical soil depth z_c between zero and three meters (further known as Category II) make up 53.79% of all data points (Figure 34). In comparison with the respective DTM the percentage is 39.32% (Figure 48). That makes a difference of approximately 14% between the DEM and DTM. One or the main reason for this difference is that the DEM includes forests and structures that lead to such a stark difference in the two models.

For the same resolution remains in the recording year 2013 that the results look a little bit different but are largely in the same ballpark. The percentages changed for Category II to 54.31% for the DEM (nearly the same as 2007) (Figure 38) and to 34.75% for the DTM (a nearly 5% decrease to 2007) (Figure 52). These differences between recording periods should be neglected though, since the 2013 recording covered a smaller area than the 2007 recording and the possible differences in the years between are therefore only misleading. Nonetheless, the difference between the DTM and DEM of the 2013 recording becomes much more interesting, because it reaches now nearly 20% (Figure 38 & Figure 52). That of course is a slight increase from the year 2007 of 5 percentage points. The reason for this probably lies in the fact, that the 2013 recording mostly covered the more densely populated area, which is less steep, and therefore the share of the steep slopes is smaller in the model which affected the DTM-results much more than the DEM-results (contains structure etc.).

However, when the 10-meter resolutions are compared with each other, the results look very much different. The critical soil depth (z_c) in Category II based on the 10-meter DEM of 2007 is 44.27% compared to its DTM counterpart with 42.25% (Figure 36 & Figure 50), which is a decrease for the DEM-result and an increase for the DTM -result compared with its respective 5-meter resolution results. That being said, a difference of approximately 2 percent between DTM and DEM remains, which is 12 percentage points less than the 5-meter resolution difference.

For the 2013 recording it unfortunately was not possible to calculate the 2013 10-meter DTM result and therefore only the DEM results of the 2013 were compared with each other. Here Category II has a 6 percent decrease (to 47.86%) compared with the 2013 5-meter resolution result (Figure 40).

10.2.2 Precipitation Period 2 (2010 – 2016)

In the second precipitation period the values for Category II increase through all results but not much (the maximum is around 2%). The changes are the following:

For the 2007-5-meter-DEM Category II increases slightly to 54.41% (Period 1: 53.79%), for the DTM counterpart slightly to 40.83% (39.32%) (Figure 34 & Figure 50). Looking at Category II of the 2013-5-meter-DEM result, it nearly stays the same at 54.89% (54.31%), for the DTM version it increases to 36.00% (34.75%) (Figure 38 & Figure 52). With the 2007-10-meter results the DEM based model has an increase in Category II to 45.18% (44.27%) and the DTM version had an increase to 44.17% (42.25%) (Figure 36 & Figure 50). Finally, the 2013-10-meter resolution DEM result had an increase to 48.68% (47.86%) (Figure 36).

That means, only the 10-meter resolution saw somewhat of a change between the models, since the 5-meter resolution differences stayed more or less the same at approximately 14% (2007) and approximately 20% (2013). However, the change for the 10-meter resolution is also pretty small, nonetheless the difference between the DEM and DTM is now approximately 1% which was previously two percentage points.

10.2.3 Precipitation Period 3 (Maximum Precipitation)

In the third precipitation period, the share of Category II increased in all models above 60 percent, however, in varying degrees.

To begin again with the 2007- 5- meter resolution results the picture looks the following, the DEM based model has a Category II - percentage of 71.70 compared with the 75.96% of the DTM based model (Figure 34 & Figure 50). This means that the DTM version has now a higher percentage compared to DEM, by approximately 4 percentage points more. That is also the case for the 10-meter resolution results for the year 2007 with the DEM based Category II clocking in at 64.95 % and the DTM based Category II at 75.20 percent but compared to the 5-m versions there is now a 10 % gap in between those two (Figure 36 & Figure 50). The 2013 -5- meter resolution however shows a different outcome of 73.01 % for the DEM based model and 69.72 percent for the DTM based model, which leaves the DEM version of Category II four percent larger than the DTM Category II of the same resolution (Figure 38 & Figure 52). Nonetheless the difference decreased from nearly 20% in Period 1 by 16 percentage point to only 4 percent in Period 3. In order to show a comprehensive view, the 2013 10-meter resolution (DEM) is now at 65.76% (before: 48.68%) (Figure 40). Compared to the DEM's 5-meter version there is a difference of approximately 6 percent with the latter one being the larger one.

This means altogether that the higher the precipitation is, Category II for both the DEM and DTM versions increases significantly as it to be expected by a higher precipitation. The DTM based models react to such a change more perceptibly than the DEM based ones. The reason for this is again the fact that the DEM includes structures and forests, which of course make up a higher percentage of the critical soil depth z_c between zero and three meters but they also leave less room to increase, whereas the DTM versions have much more room for increase in this particular category. This also holds true for the 2013-5-meter resolution but since it is smaller than the 2007 recording the DEM still holds the maximum percentage for Category II in precipitation period 3.

As for the 10-meter resolution the differences between DEM and DTM based models seem to be less significant as the considerably smaller differences of said resolutions show, with exception of Period 3 (Figure 34, Figure 36, Figure 38, Figure 48, Figure 50 & Figure 52).

10.2.4 Comparison of the maps

Beginning with the 1-m resolution maps of the DEM (Figure 41 to Figure 46) and DTM (Figure 53 to Figure 58) is that where there is/are forest/buildings in a DEM the critical soil depths z_c is between zero and 3 meters for the most part, that is quite the opposite to the DTM 1-m resolution maps whereas the critical soil depths z_c follow more along the flow lines. But the difference gets less and less if the precipitation is increased as their respective maps and histograms show. When the resolution is decreased however these effects become also less and less visible as the maps in the appendix and the histograms above show.

Furthermore, all calculated models follow the flowlines, which are the result of their respective flow accumulations, which was expected and does not interfere with the overall results.

10.3 Reliability of the Field Work and its Comparison with the calculated Model(s) and Literature

After the detailed discussion of the different models, they are now compared with the data collected in the field as well as with the existing literature. In general, it was rather difficult to find “fresh” landslides because the area had experienced high temperatures throughout the field work periods with only a few days of rainfall in between and the last greater landslides happened in June 2015, about four years before this thesis was written and their indicator may have been covered by vegetation and/or human activity. Nevertheless, the data gained by field work show that it was not done in vain.

The drunken trees as indicated in the outcrop map above (Figure 32) and in the big map below are a strong sign that there is movement in the slope, but this evidence is not enough as their shape could also be the result of snow cover. Following that, observations of landslides of varying sizes and cracks on paved roads gave also indications towards a moving slope. If they overlap with hummocky topography, as it was indicated in the outcrop map, they are a strong hint towards landslides. But in the case of the absence of an overlap, they could be very well a result of the terrace-gravels of the ice ages, which again is not a conclusive indicator for possible landslides. The same holds true for possible landslide observations from a distance since an area affected by avalanches or by strong wind looks similar to landslide headscarp then and only on sight observation can sort that out.

This means, if all outcrops taken together, they reveal a plausible picture of the landslides in the Study Area. This also includes all outcrop - types. For the most part they seem to confirm what is stated by Heuberger (1966), that those gravel terraces are a relic of the Ice Ages. On the other hand, though, it also raises a few questions. This is mainly the case for solid rock outcrops at the “Seigesbach” and the “Innere Anderstalbach”, two rivers/streams that reveal some solid rock. However, it remains unclear whether or not they are bedrock since they also could be large blocks that were left behind by the Sellrain glacier, as these are the only two outcrops that show possible bedrock and simply their occurrence is not enough to come to a definitive conclusion.

When compared to any model regardless of its basis (DEM/DTM), the outcrops and the critical soil depth z_c between zero and three meters matched almost perfectly, the more so, when the precipitation was increased. However, since access to some outcrops is extremely limited due to terrain and lack of trails, it was not possible to check the steeper areas in more detail. Nonetheless, the field work in combination with the models and the literature reveals and confirms a stunning picture, namely that in the event of extreme precipitation similar to June 2015, the critical soil depth z_c between zero and three meters covers large parts of the study area and therefore increases the risk of shallow landslides. To show the close relationship between the outcrops and the calculated model(s), selected outcrops are compared to the model(s).

10.3.1 Example 1 – Outcrops along forest road to Rosskogel and the parallel trail that runs above (Outcrops 12 to 25 and outcrops 93 to 122)

This region or cluster runs from St. Quirin westward towards the Rosskogel. Each outcrop on its own does not suggest a moving slope and some of them describe the other valley flank. If all the drunken trees and smaller landslides (Figure 59) are examined together, however, there is growing evidence of a moving slope.



Figure 59: Pictures of outcrops westward of St. Quirin; namely the pictures above are from Outcrop 19 (first two upper pictures from the left) and Outcrop 110 (last upper picture from the left) and Outcrop 24 (picture below); the upper pictures describe drunken trees and the bottom picture shows a small slide along the road, approximately 4 to 5 meters high and approx. 7 to 8 meters wide

If they are now put on the same map as the calculated MEMPS-results an even clearer picture emerges, as the large map at the end shows. The resulting overlap then suggests a moving slope, although its speed and size remain unclear.

10.3.2 Example 2 – Outcrop 141

Outcrop 141 is found in the municipal forest of Neder on the forest road towards Salfeins. Although several drunken trees and smaller landslides were found in this area, this one was chosen because of its sheer size (several ten meters length). In the area in question a hummocky topography can be observed as well as several drunken trees and larger boulders (Figure 60). The lack of a clear headscarp and the fact that it is cut by a path, are a sign that it is possibly an older landslide.

Although there is no complete overlap of the outcrop's locations for the first two precipitation periods when compared to the calculated MEMPS, the situation looks different for the maximum precipitation period. Therefore, it can be argued that the slope here is moving as the other outcrops in the area suggest (Figure 32), but as it has been stated twice above, the size and speed of its movement remains unclear.

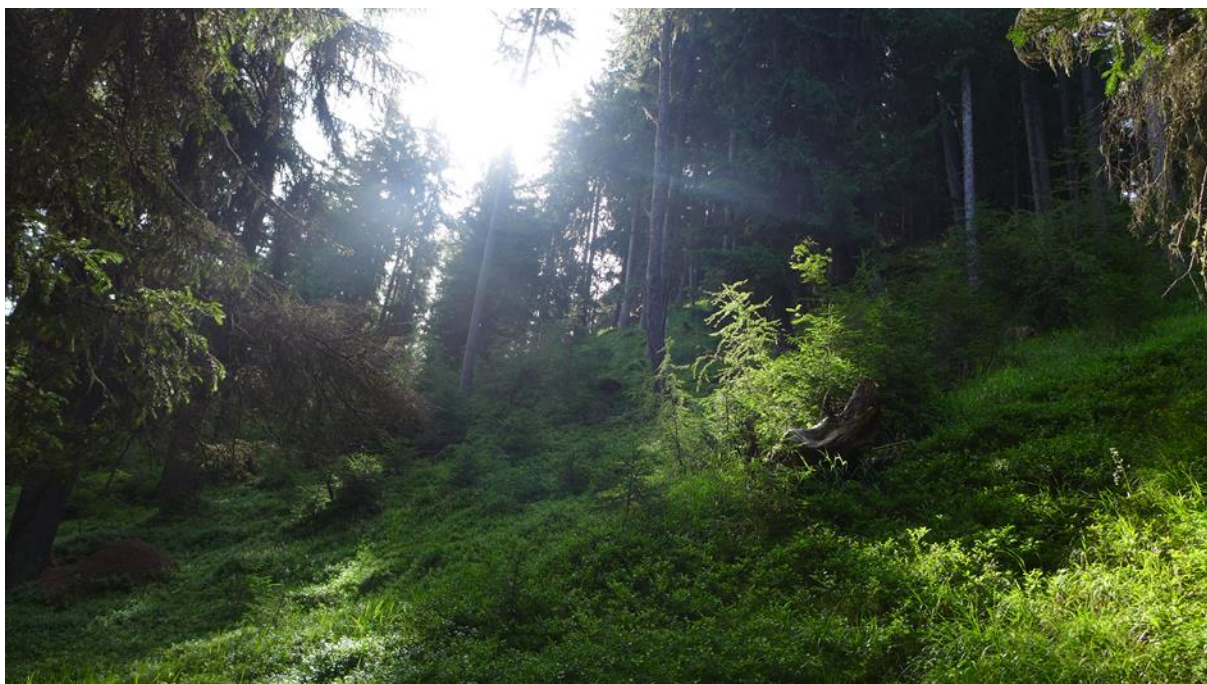
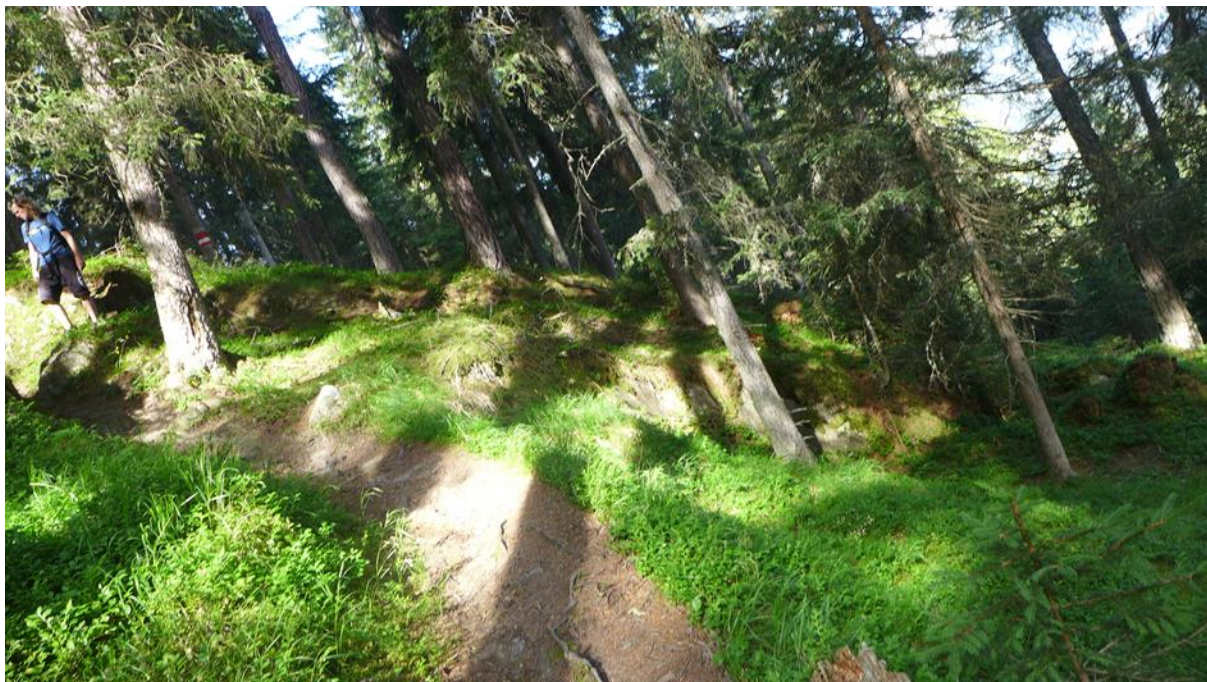


Figure 60: Outtake of outcrop 141; upper picture: Drunken trees in the background as well as hummocky topography with several boulders in between; bottom picture landslide from below -> hummocky topography; unfortunately, a full size picture was not possible

10.3.3 Example 3 – Outcrops 152/154

Found westward of Perfall in the vicinity of Durregg these two outcrops describe the same possible landslide. Its size is similar if not bigger but younger than Outcrop 141 and shows clear signs of movement because of drunken trees and its look. It also overlaps with the MEMPS - results calculated for every precipitation period (Figure 61).



Figure 61: Outcrop 152: Drunken tree(s) visible in the background (bottom pictures) plus possible headscarp in the upper and lower left picture

10.3.4 Outcrops outside the study area (Outcrops 74 to 80)

Probably the clearest sign of a moving slope was found just outside the study area in the upper parts of the Seigesbach. The outcrops are included because they show and strengthen the evidence of a moving slope, since a road that was supposedly built next to the Seigesbach which is now covered with debris. Also the dam at the border that was constructed in 2015/2016 as a result of the events in June 2015 can be interpreted as a clear indicator of the risk of slope instability in the study area which exists until today (Figure 62 & Figure 63).



Figure 62: Both pictures are taken from Outcrop 80; several smaller landslides along the Seigesbach; varying sizes (from 5 to 10 meters high and 10 to 20 meters wide)



Figure 63: Smaller slide along Seigesbach (Outcrop 79); boulder of 1- 2 meters to fine grained material (sand) possible headscarp visible in the picture; varying height (5 – 15 m) and wide up to 20 meters)

One might ask after this chapter, why the 2013 DEMs/DTMs were included, when they do not provide any new information. They are part of this thesis to highlight the differences between a study area that only focuses on the immediate surroundings of human settlements against a greater one that also includes the surroundings even more than a DEM-only model, as it has been already highlighted above with the 2013 DEMs/DTMs mostly cover Sellrain and surrounding populated areas and hardly any forests.

10.4 Possible Effects of varying Friction Angles

In this thesis a friction angle of $\varphi = 35^\circ$ was chosen, as already stated, because the soil contained material going from sand grain size to boulder size (Wikipedia.org, 2019). Furthermore, this soil was densified by glacial overload, which can further increase the friction angle (Stiftung Umwelt-Einsatz Schweiz, 2016). Therefore, $\varphi = 35^\circ$ is deemed a good enough estimation for the study area.

It is, however, clear that this friction angle is not the same for the whole area, since it is influenced by surface roughness, grain shape, the behavior during movement, dilatancy and by extension also the bulk density (Hadzalic, 2016), with all of them varying in the study area. So it is clear if a different friction angle were to be chosen, the results would look different, with an increase of values in Category II, if φ is decreased, or an increase in Category I, if φ is increased. Other soil parameters such as cohesion and density may also influence MEMPS but none in the way the friction angle does and are therefore not discussed further.

11 Conclusions

To conclude, MEMPS, as every model, is a simplification of reality as the soil parameters and precipitation may vary over the study area and a regionwide coverage of all parameters would be a waste both of resources and time since it is simply not possible to do that. But as far as models are concerned MEMPS is a more complex model that requires no assumptions on saturation levels and the vast number of input parameters make it less prone to depend on one of them.

More influence on the results, it seems, have resolution (1m/5m/10m) and the chosen base model (DTM/DEM). Whereas the 1-meter model suggests more detail than there is, the 5-meter or 10-meter models represent reality more closely. As for base models, the differences between them become less and less significant the more the resolution is decreased, so if a lower resolution is used, DTM/DEM can be used interchangeably. As for greater resolutions and overall use the DTM based models should be used since they are less influenced by the forest cover and structures which can lead to different slope angles.

As the application in the Sellrain area has shown, the amount of critical soil depths z_c beneath three meters is substantial, which means that the risk of the occurrence of a shallow landslide here is very high. To confirm these results, one only must consider the June 2015 event, when extreme precipitation occurred and hit an already saturated soil, which led to mud flows, damage to buildings and bridges and, of course, to shallow landslides. The concurring model with that amount of precipitation shows what happened then. But even when only the annual precipitation periods are considered (Period 1 and 2), the area between zero and three meters is substantial as the field work further corroborates that, which was done four years after the extreme event.

Although this shows clearly the advantages of this model it also reveals its short comings: It does not reveal the movement rate or the volume landslides and it's not possible to differentiate between areas covered with soil or where bedrock is visible based only on the model, as the outcrops near stream beds and the calculations show. The lack of soil measurements in the study area lead to a constant friction angle φ and other constant soil parameters, which can also be seen as hinderance. More soil measurements would probably lead to better results, which would of course take more time and money. Furthermore, the measuring errors for the parameters, which were not included here, since there was simply no data to work with, can falsify the results. However, the error assessment and lack of soil measurements are offset by the field work which already should suffice as a confirmation of the models' validity.

Finally, it must be emphasized that the calculated MEMPS-based models do not predict shallow landslides but gives clues where they might occur and identifies areas that are prone to them. For the future the model should only be used for soil covered areas, as it will otherwise result in false results, and also in areas, where the slope angle is larger than the friction angle. Otherwise it will result in negative or false results, too, as it did for some parts of the study area. Generally speaking, the model's applicability is undoubtedly given, and its further use may be determined by the quantity of the data provided for it as more data lead to more accurate results.

12 References

- alpen.wetter, 2015. *alpen-wetter.blogspot.com*. [Online]
Available at: <https://alpen-wetter.blogspot.com/2015/06/unwetter-und-murenabgange-juni-2015.html>
[Accessed 2 10 2019].
- Beven, K. J. & Kirkby, M. J., 1979. A physically based, variable contributing area model of basin hydrology / Un modèle à base physique de zone d'appel variable de l'hydrologie du bassin versant. *Hydrological Sciences Bulletin*, 24(1,3), p. 43–69.
- Bobek, H., 1935. Die jüngere Geschichte der Inntalterrasse und der Rückzug der letzten Vergletscherung im Inntal. In: G. Bundesanstalt, ed. Wien: s.n., pp. 135 - 189.
- Bundesministerium Nachhaltigkeit und Tourismus, 2018. *eHyd*. [Online]
Available at: <https://ehyd.gv.at/>
[Accessed 16 05 2019].
- Deb, S. K. & El-Kadi, A. I., 2009. Susceptibility assessment of shallow landslides on Oahu, Hawaii, under extreme-rainfall events. *Elsevier: Geomorphology*, Volume 108, pp. 219-233.
- Delmonaco, G. & Margottini, C., 2004. Meteorological Factors Influencing Slope Stability. In: R. Casale & C. Margottini, eds. *Natural Disasters and Sustainable development*. Berlin, Heidelberg, New York: Springer - Verlag, pp. 19-35.
- Der Bote für Tirol, 1910. Der Bote für Tirol am 17.06.1910. *Der Bote für Tirol*, 17 Juni.p. 1177.
- Dietrich, W. E., Reiss, R., Hsu, M.-L. & Montgomery, D. R., 1995. A Process-based model for colluvial soil depth and shallow landsliding using digital elevation data. *Hydrological Processes*, Volume 9, p. 383–400.
- Geologische Bundesanstalt - geologie.ac.at, 2019. *Open Data Österreich - Geologische Bundesanstalt*. [Online]
Available at: <https://www.data.gv.at/auftritte/?organisation=geologische-bundesanstalt>
[Accessed 7 10 2019].
- Geologische Bundesanstalt, 1980. *Der Geologische Aufbau Österreichs*. 1. ed. Wien: Springer-Verlag.
- Hadzalic, A., 2016. Vergleichende Untersuchungen zur Bestimmung der Scherfestigkeit verschiedener Böden mit unterschiedlichen Versuchseinrichtungen und Aussagen über den Einfluss den von Überkornanteil. *Masterarbeit*.

- Henzinger, J., 2008. *L 233 Oberperfer Straße, km 7,78 - km 8,87, Abzweigung St. Quirin - L 13 Sellraintalstraße, geotechnischer Untersuchungsbericht - Aufschlussbohrungen*, Grinzens: Amt der Tiroler Landesregierung, Landesbaudirektion, z.H. Herrn Ing. Karl Kokol.
- Heuberger, H., 1966. In: *Gletschergeschichtliche Untersuchungen in den Zentralpen zwischen Sellrain- und Ötztal*. Innsbruck: Universitätsverlag Wagner, pp. 144 - 187.
- Iida, T., 1999. A stochastic hydro-geomorphological model for shallow landsliding due to a rainstorm. *Catena*, Volume 34, pp. 293-313.
- Jäger, G., 2015. *Bergsteigerdörfer - Alpingeschichte kurz und bündig - Region Sellraintal*. s.l.:Österreichischer Alpenverein Innsbruck.
- Jenner, A., 2015. *Ereignisdokumentation nach dem Hochwasserereignis Sellrain/Tirol am 7.6.2015*. Umhausen in Tirol, Geoforum Tirol, pp. 101 - 109.
- Jong, C. d., Carletti, G. & Previtali, F., 2015. Assessing Impacts of Climate Change, Ski Slope, Snow and Hydraulic Engineering on Slope Stability in Ski Resorts (French and Italian Alps). *Engineering for Society and Territory*, Issue Volume 1, pp. 51 - 55.
- Lagger, M., 2015. *Sellraintal Juni 2015: Hangexplosionen und Muren - Eine Bestandsaufnahme*. Umhausen in Tirol, Geoforum Tirol, pp. 4 - 10.
- Land Tirol - data.tirol.gv.at, 2018. *Laserscandaten*, Innsbruck: Am der Tiroler Landesregierung - Abteilung Geoinformation - Geobasisdaten.
- Land Tirol - data.tirol.gv.at, 2019. *Open Data Österreich - Land Tirol*. [Online] Available at: <https://www.data.gv.at/auftritte/?organisation=land-tirol> [Accessed 7 10 2019].
- Lan, H. et al., 2004. Landslide hazard spatial analysis and prediction using GIS in the Xiaojiang watershed, Yunnan, China. *Engineering Geology*, Volume 76, pp. 109 - 128.
- Lindsay, J., 2009. *Whitebox GAT (Geospatial Analysis Tools) Project*. [Online] Available at: <https://jblindsay.github.io/ghrg/Whitebox/> [Accessed 2019].
- Lin, H. & Zhong, W., 2018. Influence of Rainfall Intensity and Its Pattern on the Stability of Unasaturated Soil Slope. *Geotech Geol Eng*.
- Michel, G. P. & Kobiyama, M., 2016. Development of new equation to estimate the maximum soil depth by using the safety factor. *Landslides and Engineered Slopes.Experience, Theory and Practice*, p. 1417–1421.

- Montgomery, D. R. & Dietrich, W. E., 1994. A physically based model for the topographic control on shallow landsliding. *Water Resources Research*, 30(4), p. 1153–1171.
- Neubauer, F., Genser, J. & Handler, R., 1999. The Eastern Alps: Result of a two-stage collision process. *Mitt. Österr. Geol. Ges.*, Issue 92, pp. 117-134.
- O'Loughlin, E., 1986. Prediction of Surface Saturation Zones in Natural Catchments by Topographic Analysis. *Water Resources Research*, 5(22), pp. 794 - 804.
- O'Loughlin, E., 1980. Saturation regions in catchments and their relations to soil and topographic properties. *Journal of Hydrology*, Volume 53, pp. 229 - 246.
- Piffner, O. A., 2014. Chapter 5: Tectonic Structure of the Alps & Chapter 6: Tectonic Evolution of the Alps. In: 2. ed. s.l.: Wiley Blackwell, pp. 258-329.
- QGIS, 2018 - 2019. *QGIS - Software (Versions 3.0 to 3.10.1)*. [Online] Available at: <https://www.qgis.org/en/site/>
- Quinn, P. F., Beven, K. J. & Lamb, R., 1995. The $\ln(a/\tan[\beta])$ index: How to calculate it and how to use it within the topmodel framework. *Hydrological Processes*, Volume 9, pp. 161-182.
- Rauth, C., 2015. Unwetter hinterließ Spur der Verwüstung im Sellrain und Paznaun. *Tiroler Tageszeitung*, Issue Online.
- Schmidt, K., 1965. Zum Bau der südlichen Ötztaler und Stubai Alpen. *Verh. Geol.B.-A.*, Oktober, Volume Sonderheft G, pp. 199 -233.
- Segoni, S., Rossi, G. & Catani, F., 2012. Improving basin scale shallow landslide modelling using reliable soil thickness maps. *Nat Hazards*, Volume 61, pp. 85 - 101.
- Stiftung Umwelt-Einsatz Schweiz, 2016. *Ergänzungen zum Buch Trockenmauern, Grundlagen, Bauanleitung, Bedeutung*. [Online] Available at: <http://data.umwelteinsatz.ch/T/Boden-Baugrund.html> [Accessed 10 12 2019].
- van Beek, R. et al., 2008. Hillslope Processes: Mass Wasting, Slope Stability and Erosion. In: J. Norris & et al., eds. *Slope Stability and Erosion Control: Ecotechnological solutions*. -: Springer - Verlag, pp. 17 - 64.
- Vavtar, F., 1988. Die Erzanreicherungen im Nordtiroler Stubai-, Ötztal- und Silvrettakristallin. *Arch.f.Lagerst.forsch. Geol.B.-A.*, April, Volume 9, pp. 103-153.
- von Raumer, J. & Neubauer, F., 1993. *Pre - Mesozoic Geology in the Alps*. 1 ed. Berlin, Heidelberg, New York, London, Paris, Tokyo, Hong Kong, Barcelona, Budapest: Springer - Verlag.

Wikipedia.org, 2019. *Permeabilität (Geowissenschaften)*. [Online]
Available at: [https://de.wikipedia.org/wiki/Permeabilit%C3%A4t_\(Geowissenschaften\)](https://de.wikipedia.org/wiki/Permeabilit%C3%A4t_(Geowissenschaften))
[Accessed 2019].

Wikipedia.org, 2019. *Reibungswinkel*. [Online]
Available at: <https://de.wikipedia.org/wiki/Reibungswinkel>
[Accessed 10 Dezember 2019].

Zhuang, J. et al., 2016. Assessment and mapping of slope stability based on slope units: A case study in Yan'an, China. *J.Earth Syst. Sci.*

13 Appendix

13.1 Outcrop Protocol (in German and English)

Table 2: Outcrop Protocol of the field work done by the author; It includes the number, the description and the coordinates of every outcrop (N/E/Height-> zero because not included); in German and English due to the fact that it was recorded that way

Outcrop Number	Description	Coordinates N, E and height
001	Abrisskante bei Bach; Blickrichtung Hang;	11.212168,47.21475599999999,0
002	Strecke nach St.Quirin; Risse in der Straße	11.219594,47.2193416666667,0
003	Abrisskante (?) Kreuzung Perfall-St.Quirin	11.209274,47.218288,0
004	Gemengebeschreibung: Blöcke sowie feinkörnige Matrix schlechter Rundungsgrad teils zementiert (?) -> Moränenmaterial (glaziale Ablagerung, Mächtigkeit unbekannt) teils auch große Blöcke keine Schichtung/Schieferung stark zerklüftet wahrscheinlich nicht anstehen (?)	11.20704,47.218437,0
005	Abrisskante St. Quirin Blick Berg	11.212453,47.2184361111111,0
006	mögl. Rutschung	11.215086,47.21833600000001,0
007	Hummocky Topography	11.216758,47.219564,0
008	Drunken Trees	11.217084,47.219755,0
009	Blickrichtung Berg/NW; Abrisskante (?)	11.213886,47.21932999999999,0
010	2x Abrisskante (bereits fotografiert)	11.209231,47.218194,0
011	A11.1 Kirche St.Quirin; Moränenmaterial A11.2 Andere Talseite; in Blickrichtung von Fotschertal westlich; mögl. Abrisskanten	11.21441,47.22121199999999,0
012	Straße Richtung Rosskogel verschieden große Blöcke; teils zementiert wahrscheinlich Terrassenschotter	11.207474,47.21967599999999,0
013	Forststraße; Drunken Tree	11.206628,47.220288,0
014	Forststraße kleine Rutschung mögl. anstehendes Gestein; Glimmerschiefer ÖSK Mögliche Rutschung	11.205592,47.22037399999999,0
015	mögl. Rutschung	11.202902,47.218632,0

Outcrop Number	Description	Coordinates N, E and height
016	Rutschung /Hummocky Topography mit Vegetationswechsel	11.201837,47.21827,0
017	Mögl. Rutschungen andere Talseite; mögl. Rutschung unterhalb (fehlender Baumbewuchs und andere Vegetation)	11.197965,47.217024,0
018	mögl. Schuttkegel + Drunken Tree	11.19465,47.216695,0
019	mögl. Rutschung Drunken Trees veränderte Vegetation kleinere Abrisskante (?)	11.192103,47.216291,0
020	mögl. Abrisskante	11.191099,47.21660800000001,0
021	mögl. Abrisskante	11.188677,47.216253,0
022	Drunken Trees	11.18693997177506,47.2162785845041,0
023	mögl. Rutschung /Kante	11.188773,47.217344,0
024	Ausbruch an Straße;	11.189186,47.217694,0
025	Drunken Trees	11.183274,47.217694,0
026	Drunken Trees Gefügebrauch sandig bis grobkörnig; ungeordnet	11.242254,47.225179,0
027	Hummocky Topography Andere Talseite: Hummocky Topography; mögl. Rutschung	11.243113,47.225197,0
028	Andere Talseite, Tiefentalbach	11.24142,47.224427,0
029	Drunken Tree	11.239477,47.223868,0
030	Risse in Straße; Hammer senkrecht zu Hang	11.240599,47.224114,0
031	Drunken Trees and Hummocky Topography	11.239894,47.22242,0
032	Drunken Tree	11.239358,47.223612,0
033	kleinere abgenetzte Rutschung	11.237599,47.222441,0
034	Andere Talseite, Sellrain Gasse	11.231625,47.22059,0
035	Drunken Trees and Hummocky Topography	11.230672,47.220244,0
036	Drunken Tree	11.229482,47.219733,0
037	kleine Rutschung (ca.3m) und Drunken Trees	11.228905,47.22005300000001,0
038	Drunken Trees	11.228222,47.219461,0
039	Drunken Trees und kleine Risse in Straße (Hammer senkrecht zum Hang)	11.227874,47.218822,0
040	Drunken Trees	11.226538,47.21849199999999,0
041	Drunken Trees	11.225215,47.217817,0

Outcrop Number	Description	Coordinates N, E and height
042	Drunken Trees	11.225042,47.21779399999999,0
043	mögl. Rutschung- größere Blöcke und mögl. Abrisskante mit mehreren Drunken Trees ca. 10 m Breite, ca. 10- 15m Höhe	11.224901,47.217686,0
044	Gefügebrauch- blockig bis sandig; ungeordnet Abrisskante(?), Drunken Tree	11.22492,47.217529,0
045	Drunken Trees bei Roter Kapelle -> Hummocky Topography und Risse in Gebäude	11.223497,47.21766300000001,0
046	mögl. Rutschung und Drunken Trees	11.222644,47.217177,0
047	Gegenhang gegenüber Kirche Sellrain Hummocky Topography	11.222484,47.21712200000001,0
048	mögl. Rutschungen; Blickrichtung Gasse/St.Quirin	11.217514,47.21593800000001,0
049	Drunken Trees	11.220721,47.215667,0
050	Drunken Tree	11.220715,47.215628,0
051	Drunken Trees	11.220865,47.215165,0
052	Vegetationswechsel Wald	11.221138,47.214577,0
053	Vegetationswechsel	11.221786,47.214493,0
054	Mögliche Rutschung; westliche Flanke Fotschertal mögliche Rutschung bei St.Quirin	11.221193,47.21278099999999,0
055	Hummocky Topography	11.221269,47.210831,0
056	St. Quirin -> Hummocky Topography und mögliche Rutschungen	11.223207,47.211471,0
057	Tanneben: Drunken Trees und Hummocky Topography	11.223428,47.210762,0
058	mögl. Rutschung - Anderstalbach - Blickrichtung St. Quirin Drunken Tree (Straßenrand)	11.22274,47.21008299999999,0
059	Drunken Trees	11.221892,47.208735,0
060	mögliche Rutschungen - Blickrichtung Perfall	11.220871,47.207098,0
061	Mögl. Rutschung bei St. Quirin Hummocky Topography - Tanneben	11.220301,47.208837,0
062	mögl. Rutschung, westliche Seite Fotschertal	11.217896,47.207826,0
063	Drunken Trees Mögl. Abrisskante	11.217896,47.204976,0
064	mögl. kleinere Rutschung /Drunken Tree(?)	11.215614,47.207402,0
065	Sellrain 63/mögl. Rutschung	11.215233,47.208649,0
066	Blickrichtung Gasse/ gleiche Rutschung wie A48	11.21501,47.209928,0
067	Drunken Trees/Weg Seigesalm	11.21456,47.20997,0

Outcrop Number	Description	Coordinates N, E and height
068	Drunken Trees	11.213461,47.210043,0
069	Drunken Tree	11.210563,47.20967700000001,0
070	Drunken Trees (?)	11.212378,47.208846,0
071	Abrisskante/oder temporäres Gewässer Drunken Trees	11.210962,47.207722,0
072	mögliche Rutschung bei Perfall (?)	11.210297,47.20735799999999,0
073	Rutschung (Rückhaltebecken Seigesbach) Drunken Trees mögl. Rutschung	11.209171,47.205122,0
074	Blick auf Perfall- mehrere mögl. Rutschungen oberhalb	11.209782,47.203667,0
075	Blickrichtung Sellraintal Rutschung Seigesbach	11.209155,47.20292200000001,0
076	Rutschung Seigesbach (Außerhalb des Gebietes) Blickrichtung Berg kleinere mögliche Rutschung am Straßenrand sandig bis blockig ungeordnet	11.208854,47.20262500000001,0
077	Rutschung Seigesbach (außerhalb)	11.208706,47.20224,0
078	Rutschungen bei Seigesbach (mögl. außerhalb des Gebietes) Rutschung Straße	11.20776,47.201477,0
079	Rutschungen Seigesbach (Außerhalb des Gebietes) zwischen 5 - 15m hoch blockiges Material(1-2m) bis sandig	11.206819,47.201069,0
080	Rutschungen Seigesbach (außerhalb des Gebietes) Material gleichbleibend - etwas kleiner	11.206989,47.20292,0
081	Drunken Trees	11.205616,47.204652,0
082	Drunken Trees und Vegetationswechsel	11.20415,47.20494599999999,0
083	mögliche Rutschungen auf anderer Talseite / links von Perfall	11.202787,47.205285,0
084	Drunken Trees	11.198657,47.20409,0
085	Drunken Trees	11.200337,47.204591,0
086	Seigesbach: beidseitig Rutschungen; unterschiedlich blockiges Material - cm bis m Bereich Abrisskanten beidseitig ca. 5 - 10 m über Bach felsige Umgebung aufgrund von Bach	11.206513,47.207203,0
087	Drunken Trees	11.205013,47.20780600000001,0
088	Drunken Trees	11.205087,47.20863300000001,0
089	Drunken Trees	11.204366,47.209141,0

Outcrop Number	Description	Coordinates N, E and height
090	kleine Rutschung - Drunken Trees Auf anderer Talseite - mögl. Rutschungen (?)	11.204413,47.209305,0
091	mögliche Rutschungen oberhalb Sportplatz	11.204603,47.210388,0
092	Drunken Trees	11.203018,47.209372,0
093	Blickrichtung Seigesbach; mehrere mögliche Rutschungen am Hang - wahrscheinlich bereits aufgenommen	11.211178,47.220186,0
094	Drunken Trees (mögl.)	11.209001,47.220468,0
095	Drunken Trees	11.210102,47.221968,0
096	Hummocky Topography	11.208007,47.222834,0
097	Drunken Trees	11.207944,47.22374800000001,0
098	Drunken Trees	11.208205,47.224345,0
099	Drunken Trees	11.206539,47.224725,0
100	Drunken Tree	11.205613,47.224843,0
101	Drunken Trees	11.204488,47.224906,0
102	Drunken Trees Mögliche Rutschung/Hummocky Topography	11.20299,47.22476,0
103	Drunken Trees	11.202112,47.224341,0
104	Drunken Trees (mögl.)	11.20042,47.22375900000001,0
105	Drunken Trees	11.199429,47.223642,0
106	Wahrscheinliche Rutschungen (eher nicht) und Drunken Trees	11.198899,47.222175,0
107	mögliche Rutschungen	11.198762,47.22179,0
108	Drunken Trees	11.198246,47.221248,0
109	Drunken Trees	11.196784,47.220305,0
110	Drunken Trees	11.19553734668247,47.219986864 62196,0
111	mögliche Rutschungen aufgrund der Topografien und Drunken Tree	11.194016,47.219554,0
112	Mögliche Rutschung und Drunken Tree	11.193885,47.219642,0
113	Drunken Trees	11.192606,47.219538,0
114	Bei Bodenbach: Drunken Trees mögliche Rutschung (Hummocky Topography und Unebenheit) mögliche Abrisskante (?) ca. 10 m Länge	11.190755,47.219724,0
115	Rutschender Hang bei Straße bis ca. A116	11.186247,47.219014,0
116	Blickrichtung Gries: Rutschung wahrscheinlich außerhalb des Gebietes Blickrichtung Tal (Sellrain)	11.18421664552013,47.218349867 26916,0

Outcrop Number	Description	Coordinates N, E and height
	mögliche Rutschungen - relativ großräumig	
117	mögliche Rutschungen andere Talseite (Seigesbach ?)	11.185435,47.21832500000001,0
118	Drunken Trees	11.188495,47.217083,0
119	mögliche Rutschung / Blickrichtung Gries	11.186161,47.216178,0
120	mögliche Rutschung/Blickrichtung Tal	11.190622,47.215612,0
121	Blickrichtung Tal - Rutschung Seigesbach	11.194436,47.216678,0
122	Blickrichtung Tanneben - mögliche Rutschungen	11.204436,47.218925,0
123	Risse bei Straße St. Quirin	11.21414,47.22088999999999,0
124	Hummocky Topography Drunken Tree	11.215913,47.221519,0
125	Hummocky Topography - mögliche Rutschung Brandögg (Grinzens) -> mögliche Rutschungen	11.21775,47.22245100000001,0
126	Hummocky Topography mögliche Rutschung aufgrund mehrerer Felslinsen;	11.220271,47.223803,0
127	Hummocky Topography	11.221194,47.224569,0
128	Blickrichtung Grinzens - mögliche Rutschungen	11.221652,47.225143,0
129	Hummocky Topography	11.221968,47.22648100000001,0
130	Risse bei Straße - Hammer senkrecht zu Hang	11.221572,47.22807399999999,0
131	Risse bei Straße - Hammer senkrecht zu Hang	11.223166,47.226741,0
132	Risse bei Straße - Hammer senkrecht zu Hang	11.223302,47.225945,0
133	Risse bei Straße - Hammer senkrecht zu Hang	11.222954,47.224427,0
134	Risse bei Straße - Hammer senkrecht zu Hang	11.222741,47.224027,0
135	Risse bei Straße - Hammer senkrecht zu Hang	11.221425,47.222153,0
136	Drunken Tree	11.251539,47.222537,0
137	Drunken Trees	11.247454,47.221911,0
138	Drunken Trees	11.244912,47.22093,0
139	Drunken Trees	11.242924,47.22008,0
140	Drunken Trees	11.241603,47.217547,0
141	Drunken Trees und mögliche größere Rutschung aufgrund der Topografie	11.243886,47.21597299999999,0

Outcrop Number	Description	Coordinates N, E and height
142	mögliche Rutschung blockig (max. 0.5 m) bis sandige Größe	11.239897,47.21468800000001,0
143	Drunken Trees	11.23221,47.212708,0
144	mögliche Rutschung feinkörnig, 2 Blöcke größer ca. 5m breit und 0.5 m hoch	11.230798,47.21144799999999,0
145	mögliche Rutschung und Drunken Trees ca. 10m breit und 5m hoch blockiges Material (0.5 m groß) bis sandig	11.2307,47.211083,0
146	mögliche Rutschung oberhalb der Straße	11.207894,47.21847,0
147	Drunken Trees	11.200587,47.215232,0
148	mögliche Rutschung, relativ groß, mehrere Abrisskanten	11.19893,47.214821,0
149	mögliche Rutschung, relativ groß; mehrere Abrisskanten Blöcke in der Regel im 0.5 m Bereich	11.196215,47.213876,0
150	Drunken Trees	11.196062,47.213449,0
151	Drunken Trees	11.194307,47.21243,0
152	mögliche Rutschung und Drunken Trees und auch mögliche Headscarp	11.193357,47.211477,0
153	mögliche Rutschung	11.191888,47.21106,0
154	mögliche Rutschung (bereits aufgenommen in A152)	11.195571,47.209978,0
155	Risse auf Straße; Hammer senkrecht zu Hang	11.197566,47.21105,0
156	mögliche Rutschungen oberhalb der Bushaltestelle; auch bei A148	11.1989086710755,47.20678780588738,0

13.2 DEM – maps

13.2.1 5m resolution

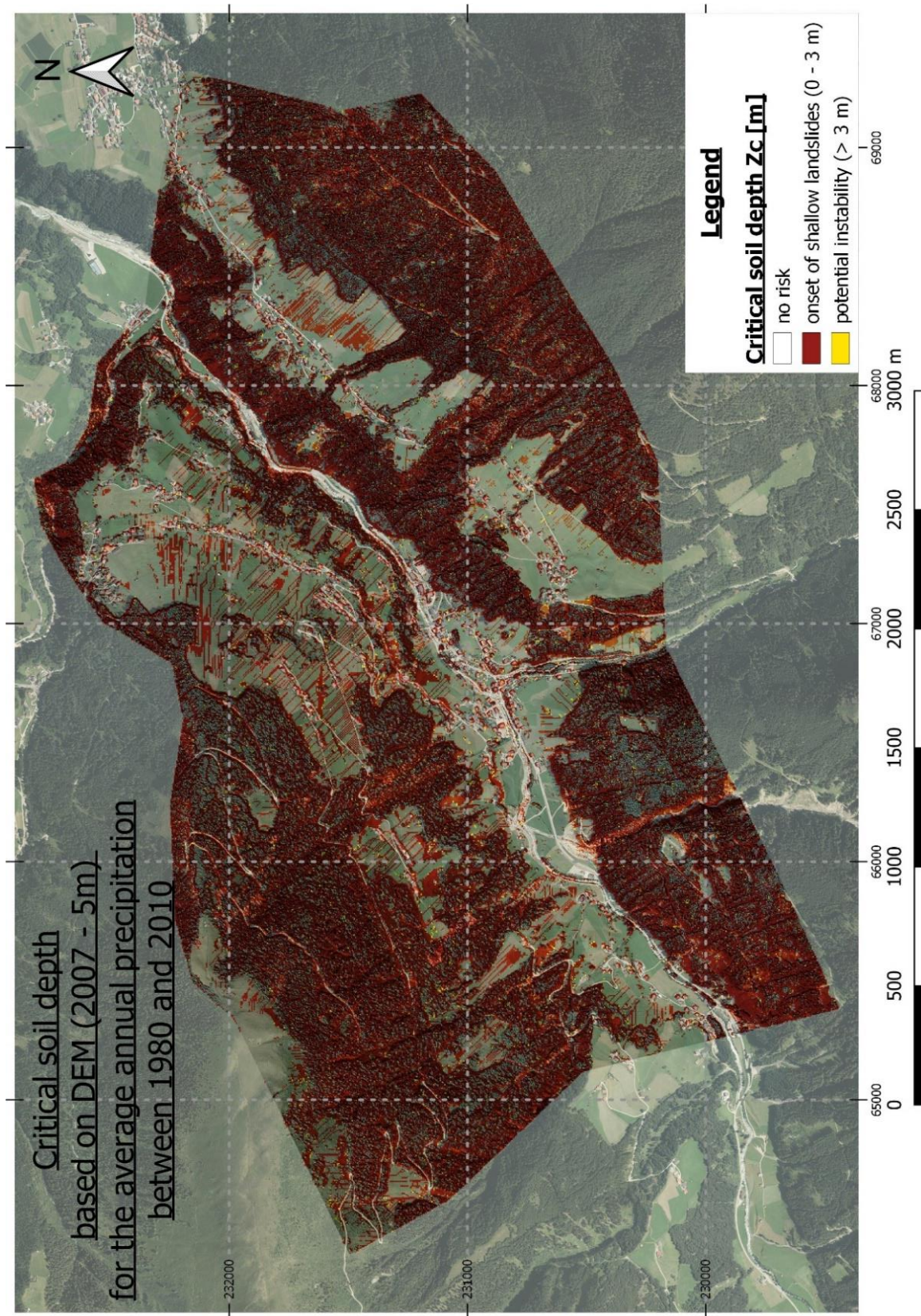


Figure 64: Map of the critical soil depth z_c for the average annual precipitation between 1980 and 2010 (2007 - DEM, 5m); raw data: © (Land Tirol - data.tirol.gv.at, 2018), orthophoto: © (Land Tirol - data.tirol.gv.at, 2019)

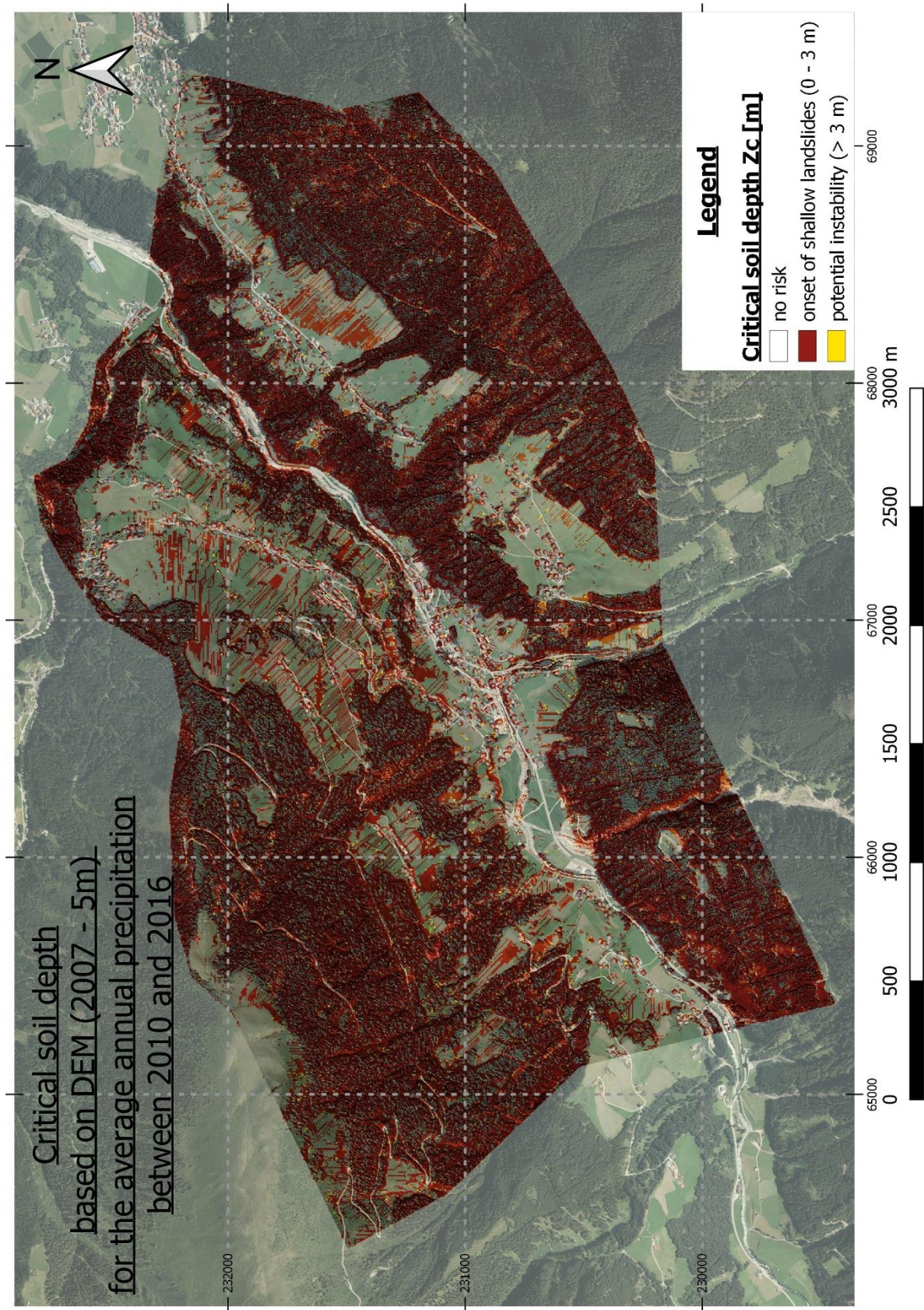


Figure 65: Map of the critical soil depth z_c for the average annual precipitation between 2010 and 2016 (2007 - DEM, 5m); raw data: © (Land Tirol - data.tirol.gv.at, 2018), orthophoto: © (Land Tirol - data.tirol.gv.at, 2019)

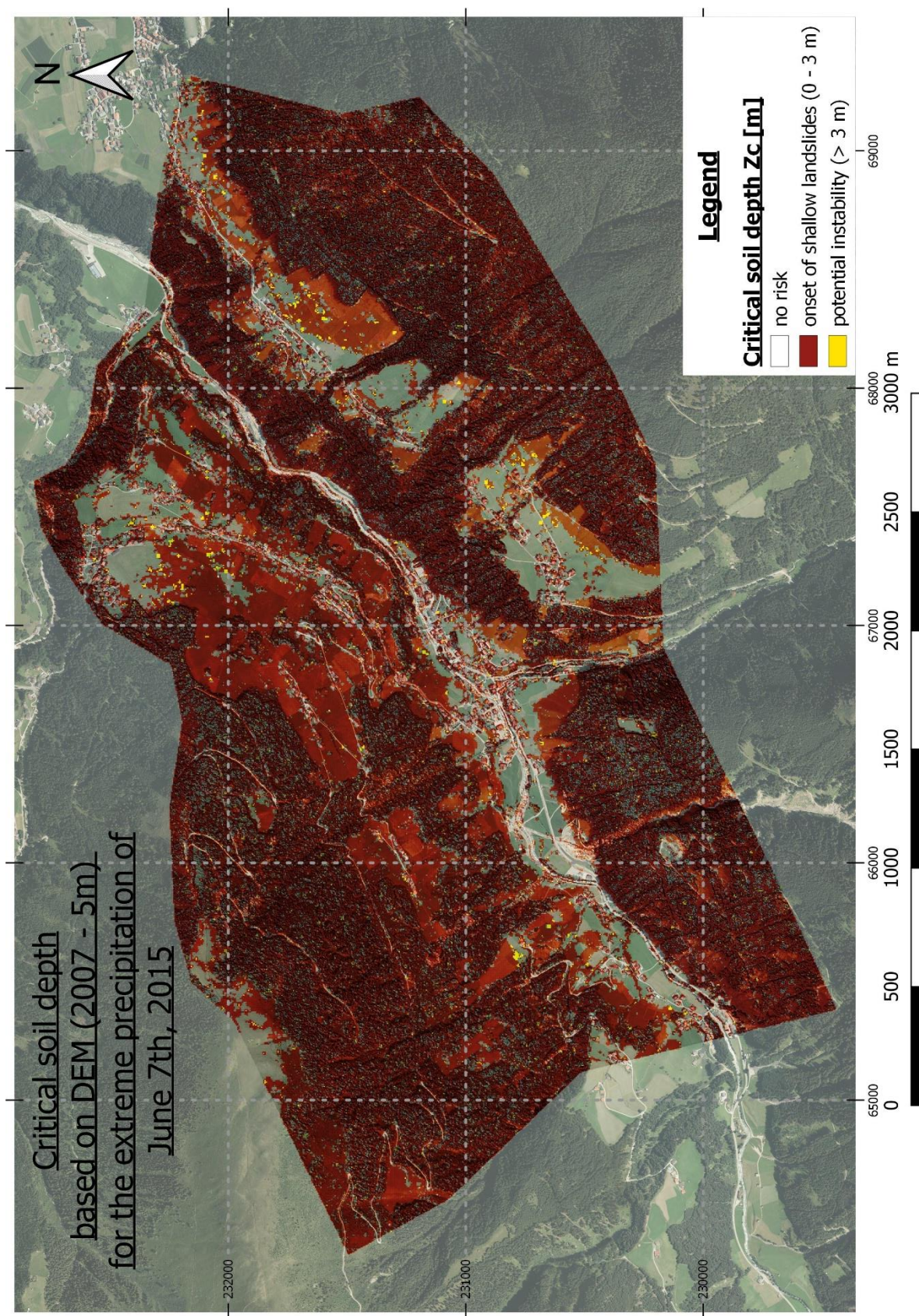


Figure 66: Map of the critical soil depth z_c for the Extreme Precipitation of June 2015 (2007 - DEM, 5m); raw data: © (Land Tirol - data.tirol.gv.at, 2018), orthophoto: © (Land Tirol - data.tirol.gv.at, 2019)

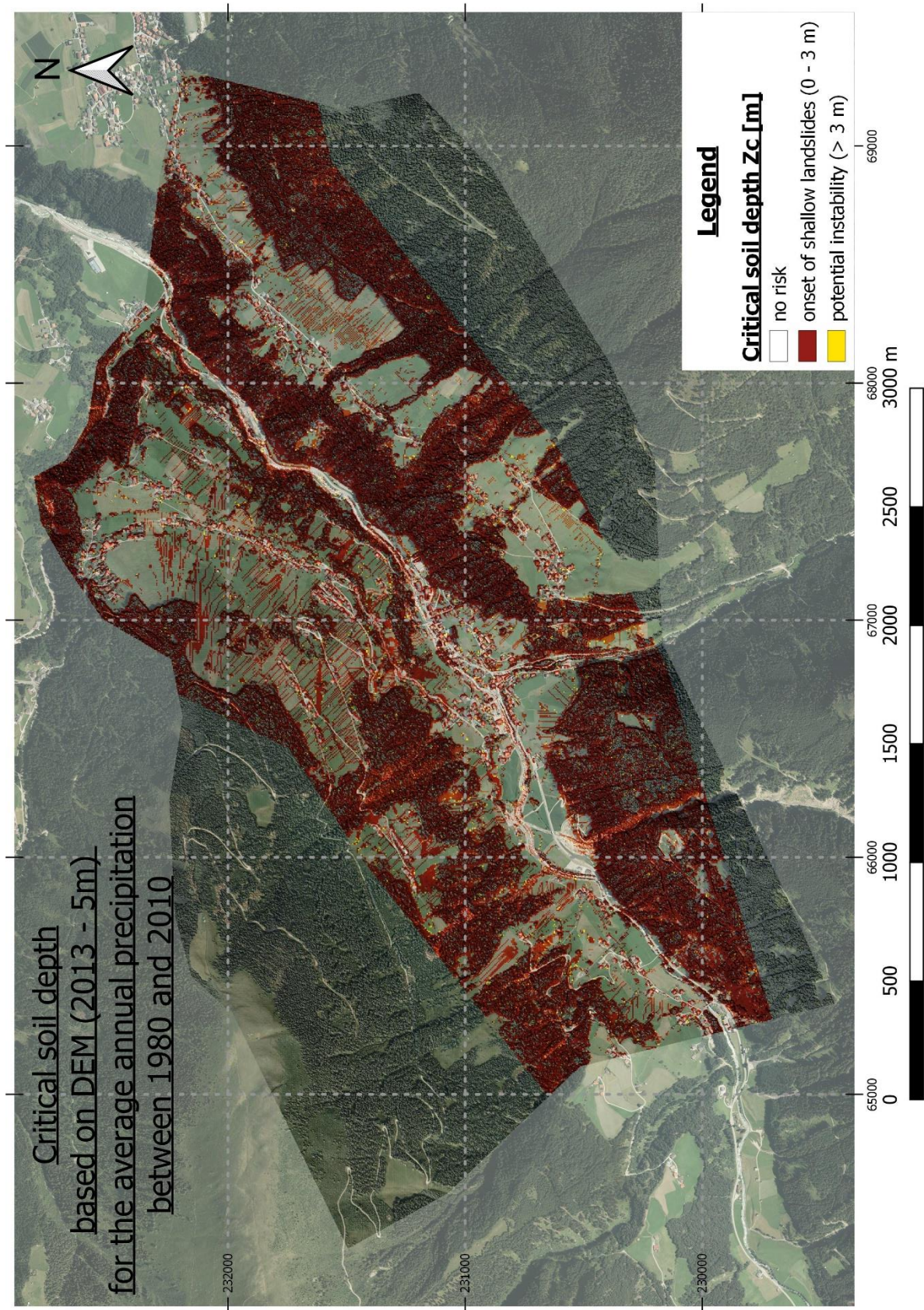


Figure 67: Map of the critical soil depth z_c for the average annual precipitation between 1980 and 2010 (2013 - DEM, 5m); raw data: © (Land Tirol - data.tirol.gv.at, 2018), orthophoto: © (Land Tirol - data.tirol.gv.at, 2019)

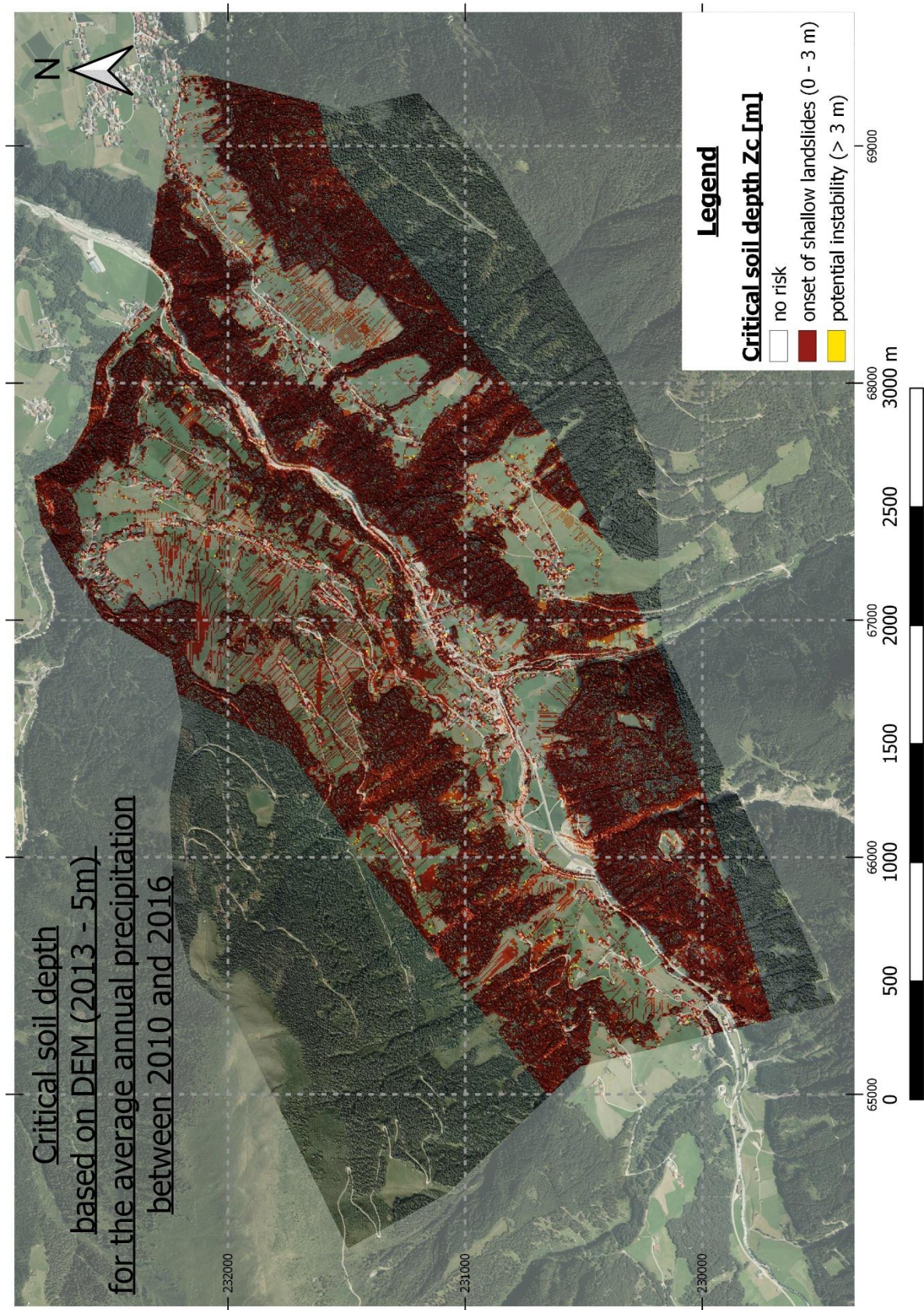


Figure 68: Map of the critical soil depth z_c for the average annual precipitation between 2010 and 2016 (2013 - DEM, 5m); raw data: © (Land Tirol - data.tirol.gv.at, 2018), orthophoto: © (Land Tirol - data.tirol.gv.at, 2019)

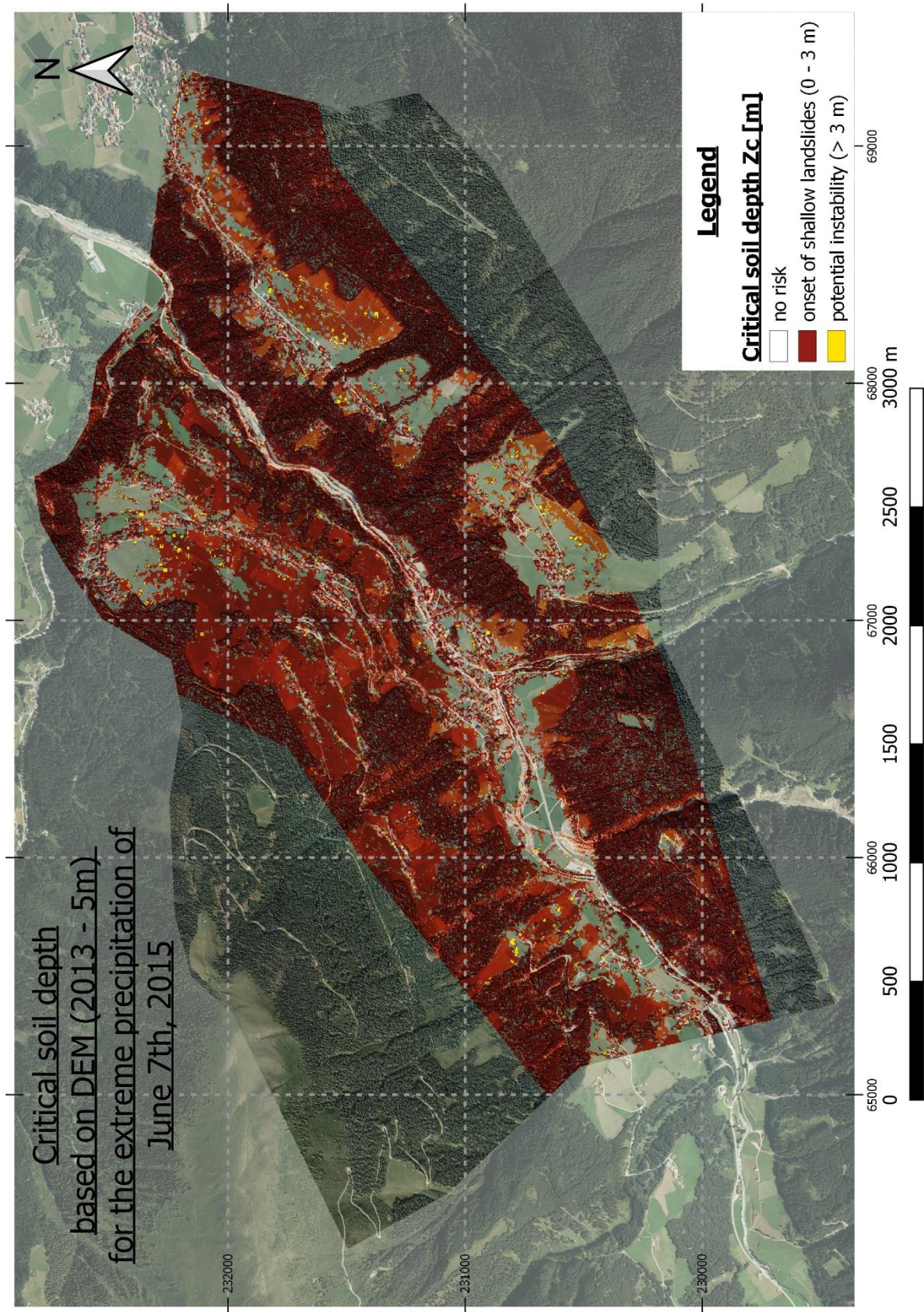


Figure 69: Map of the critical soil depth z_c for the extreme precipitation of June 2015 (2013 - DEM, 5m); raw data: © (Land Tirol - data.tirol.gv.at, 2018), orthophoto: © (Land Tirol - data.tirol.gv.at, 2019)

13.2.2 10m resolution

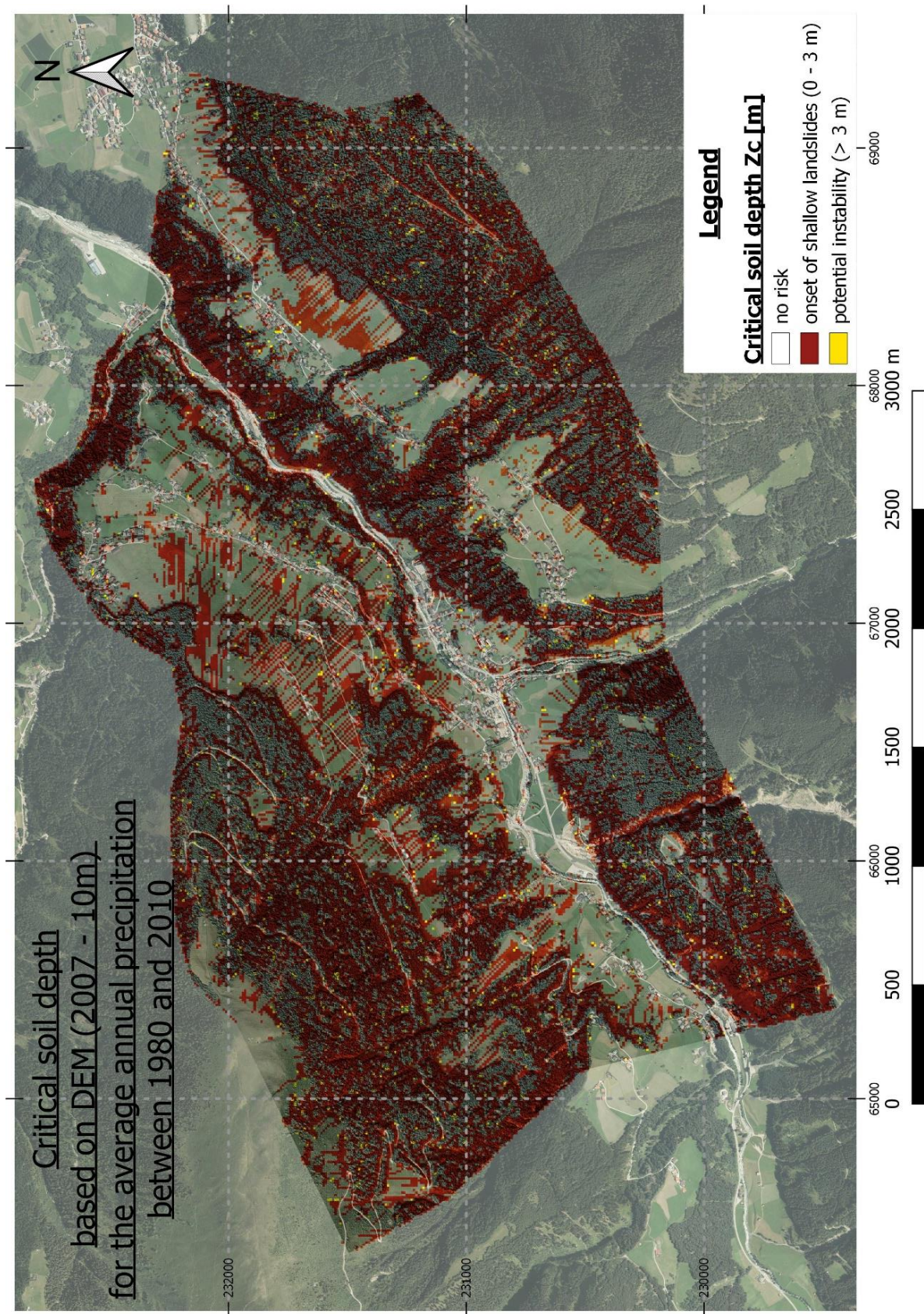


Figure 70: Map of the critical soil depth z_c for the average annual precipitation between 1980 and 2010 (2007 - DEM, 10m); raw data: © (Land Tirol - data.tirol.gv.at, 2018), orthophoto: © (Land Tirol - data.tirol.gv.at, 2019)

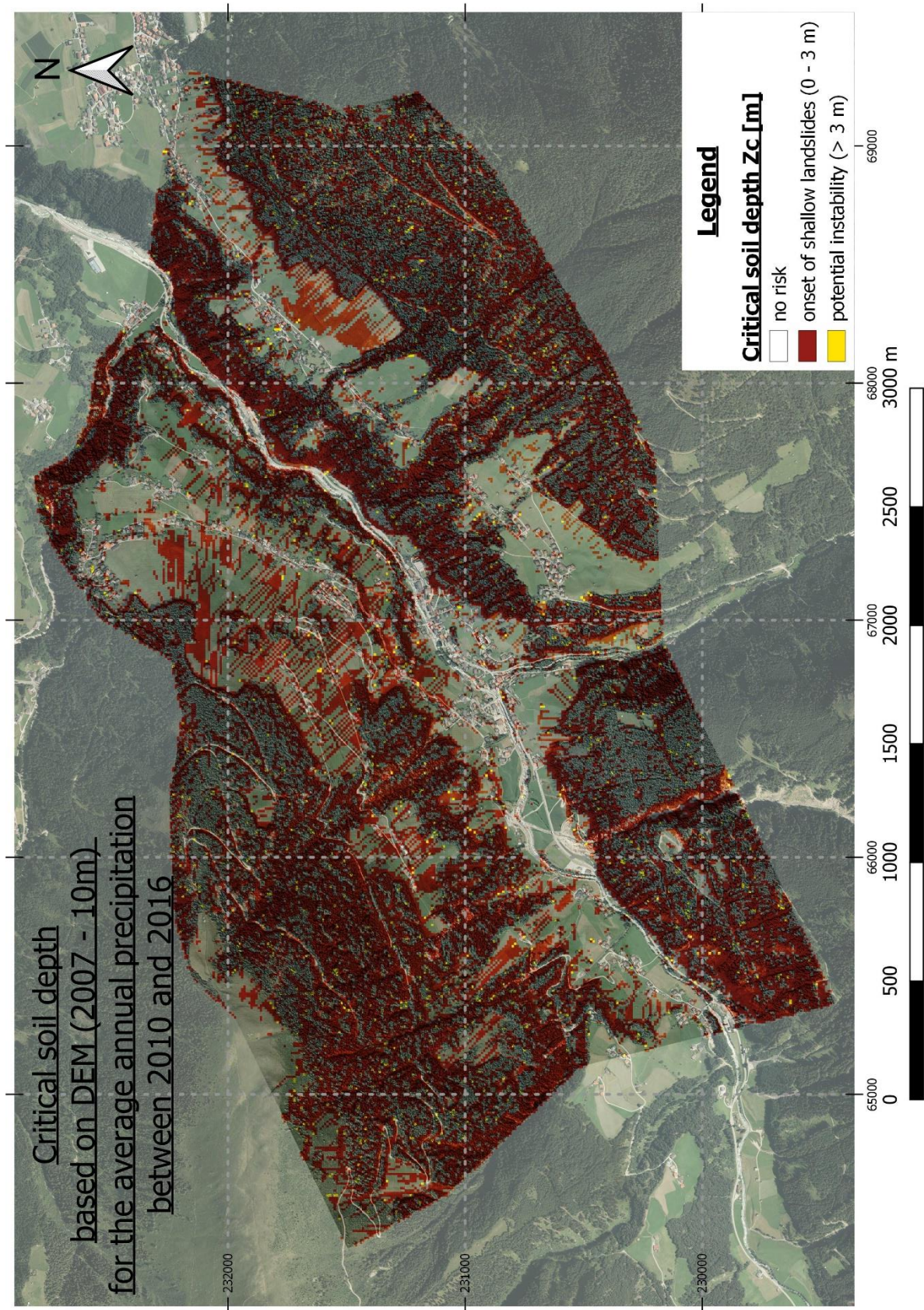


Figure 71: Map of the critical soil depth z_c for the average annual precipitation between 2010 and 2016 (2007 - DEM, 10m); raw data: © (Land Tirol - data.tirol.gv.at, 2018), orthophoto: © (Land Tirol - data.tirol.gv.at, 2019)

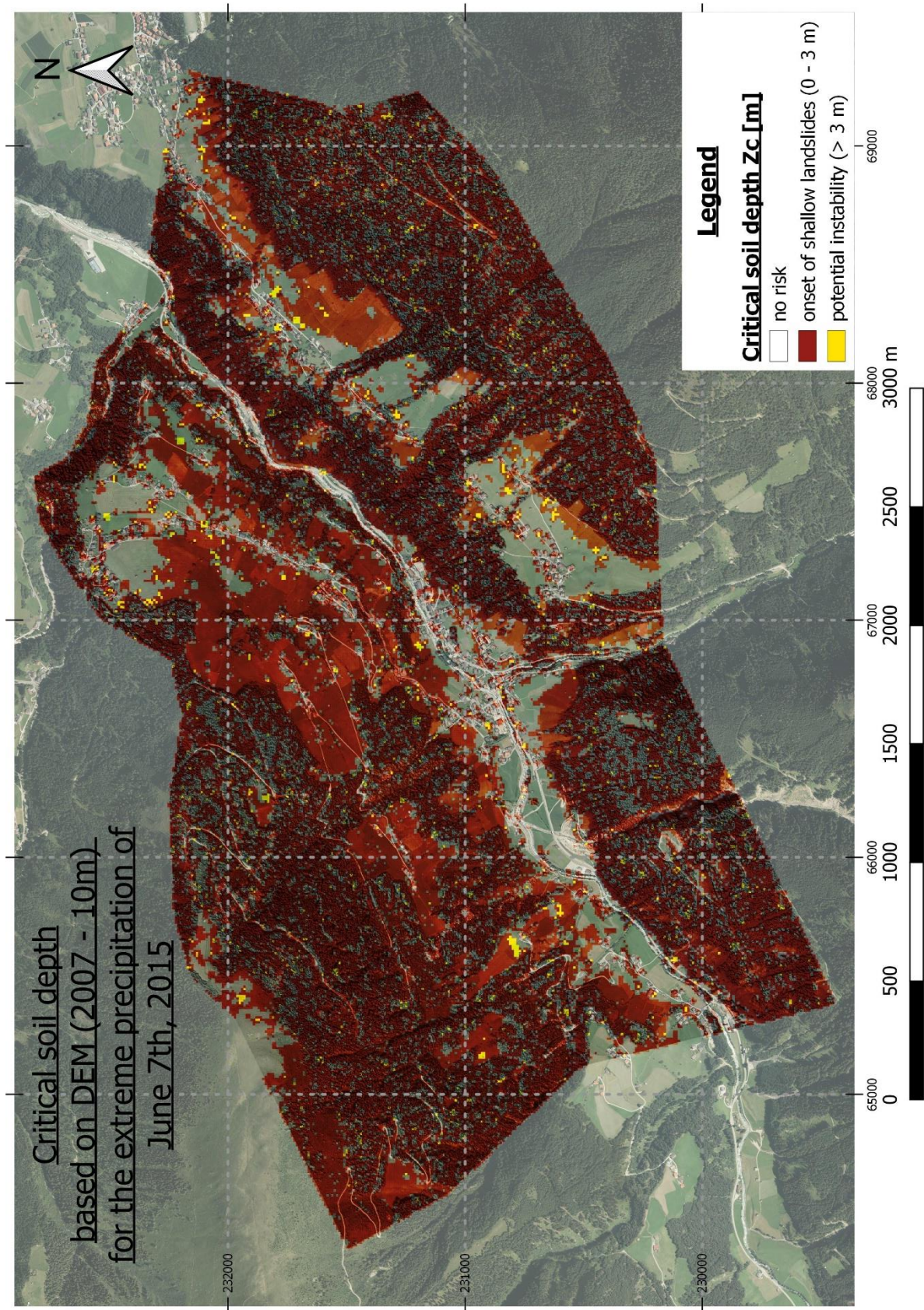


Figure 72: Map of the critical soil depth z_c for the extreme precipitation of June 2015 (2007 - DEM, 10m); raw data: © (Land Tirol - data.tirol.gv.at, 2018), orthophoto: © (Land Tirol - data.tirol.gv.at, 2019)

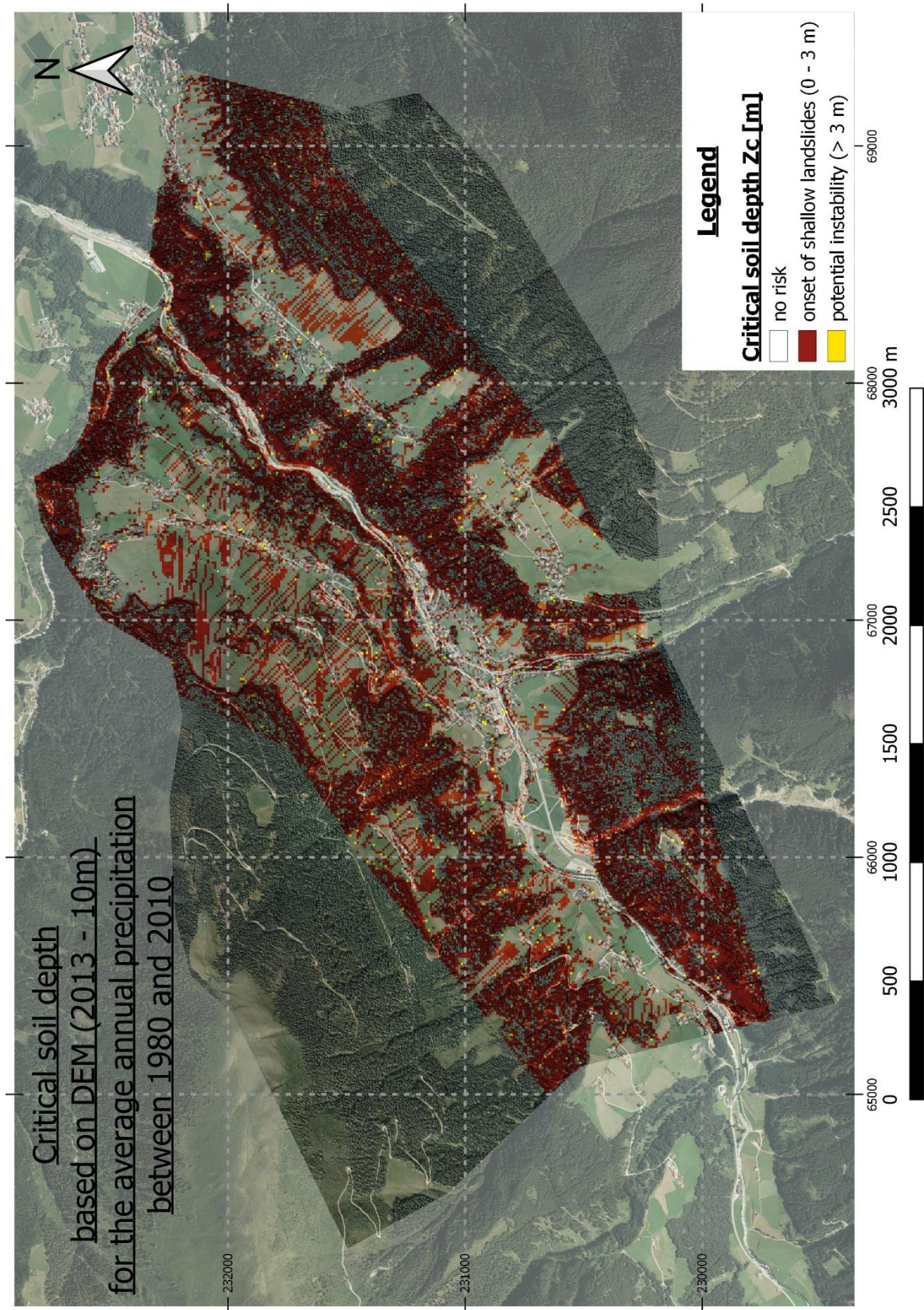


Figure 73 Map of the critical soil depth z_c for the average annual precipitation between 1980 and 2010 (2013 - DEM, 10m); raw data: © (Land Tirol - data.tirol.gv.at, 2018), orthophoto: © (Land Tirol - data.tirol.gv.at, 2019)

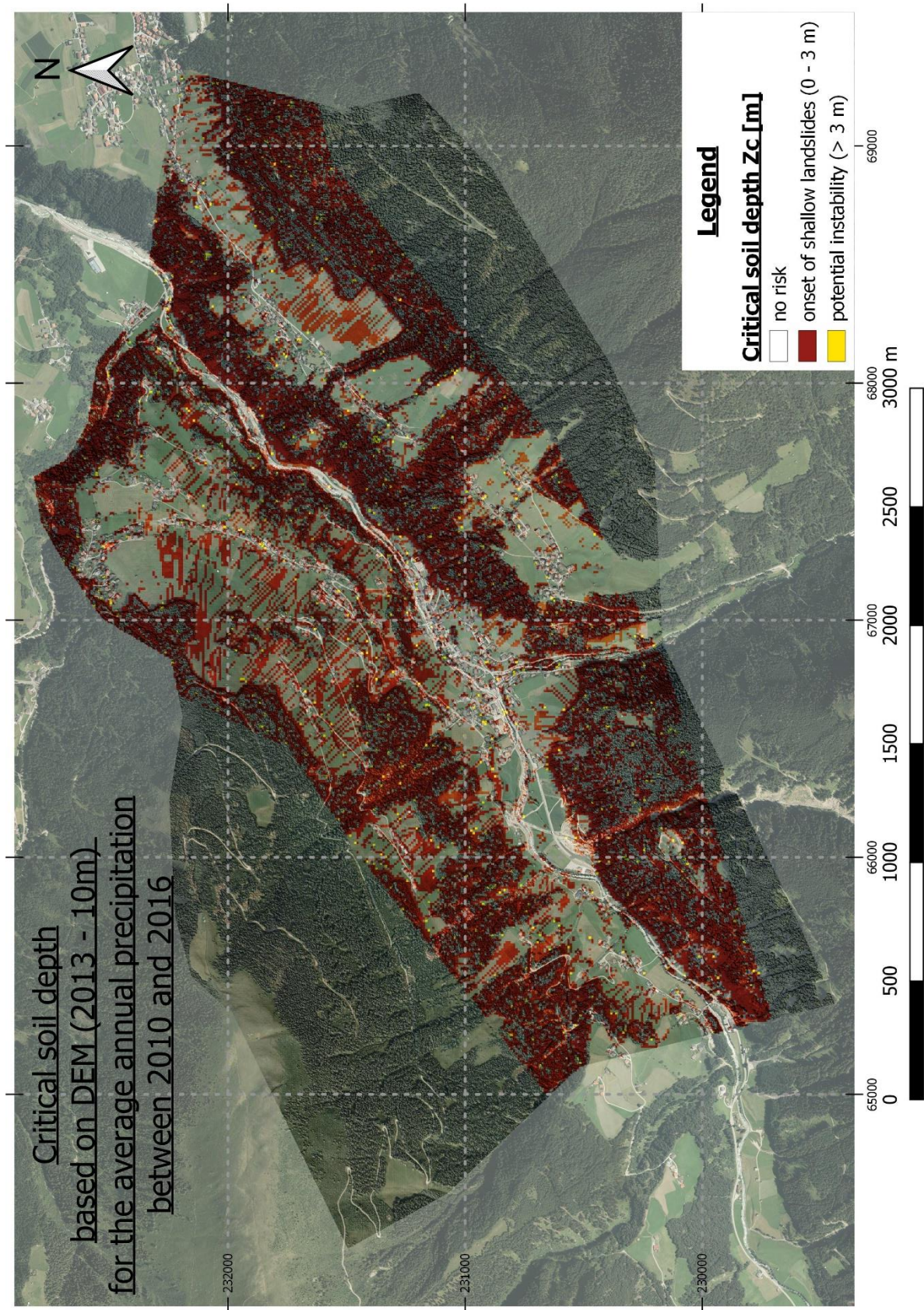


Figure 74: Map of the critical soil depth z_c for the average annual precipitation between 2010 and 2016 (2013 - DEM, 10m); raw data: © (Land Tirol - data.tirol.gv.at, 2018), orthophoto: © (Land Tirol - data.tirol.gv.at, 2019)

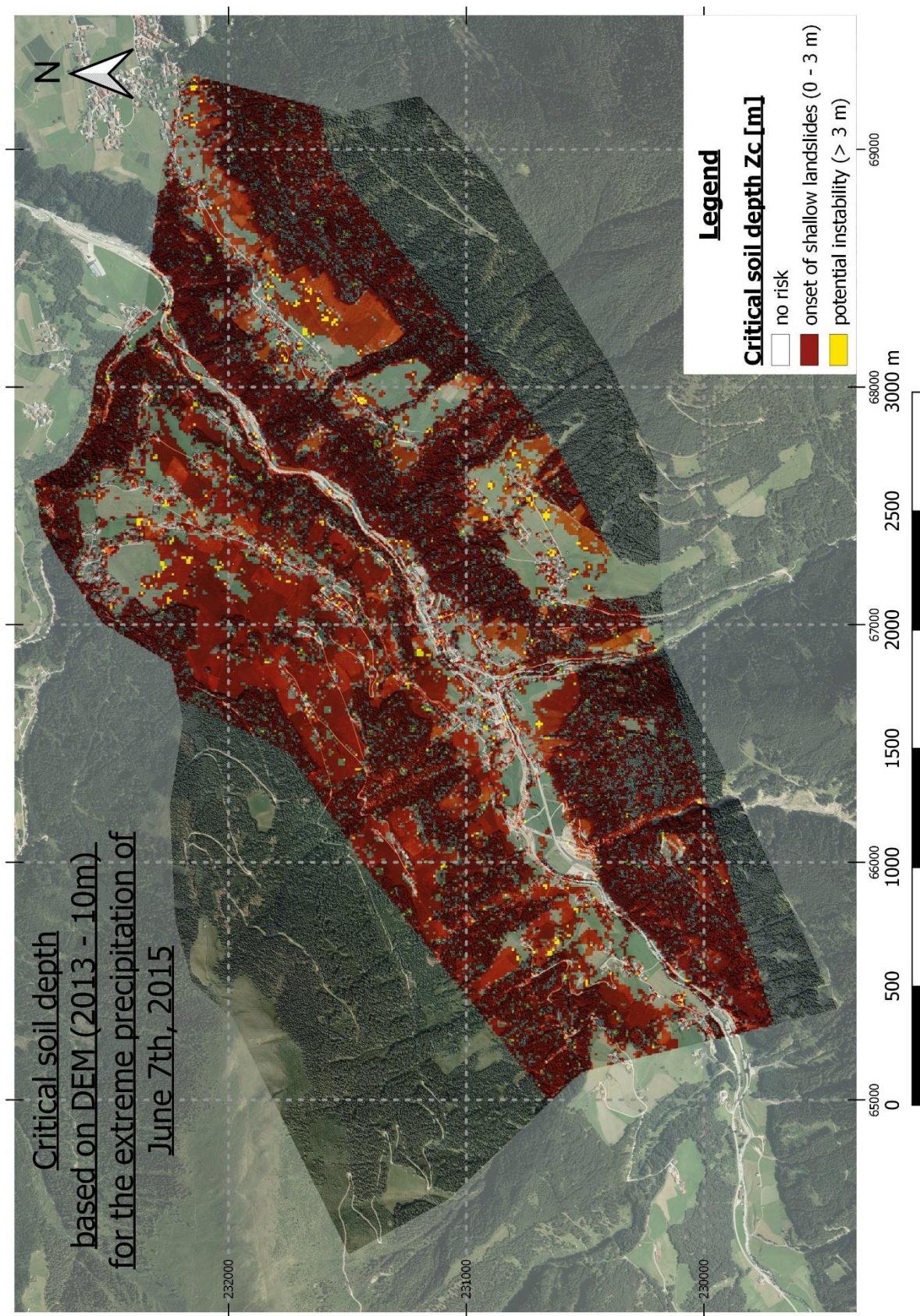


Figure 75: Map of the critical soil depth z_c for the Extreme Precipitation of June 2015 (2013 - DEM, 10m); raw data: © (Land Tirol - data.tirol.gv.at, 2018), orthophoto: © (Land Tirol - data.tirol.gv.at, 2019)

13.3 DTM – maps

13.3.1 5m resolution

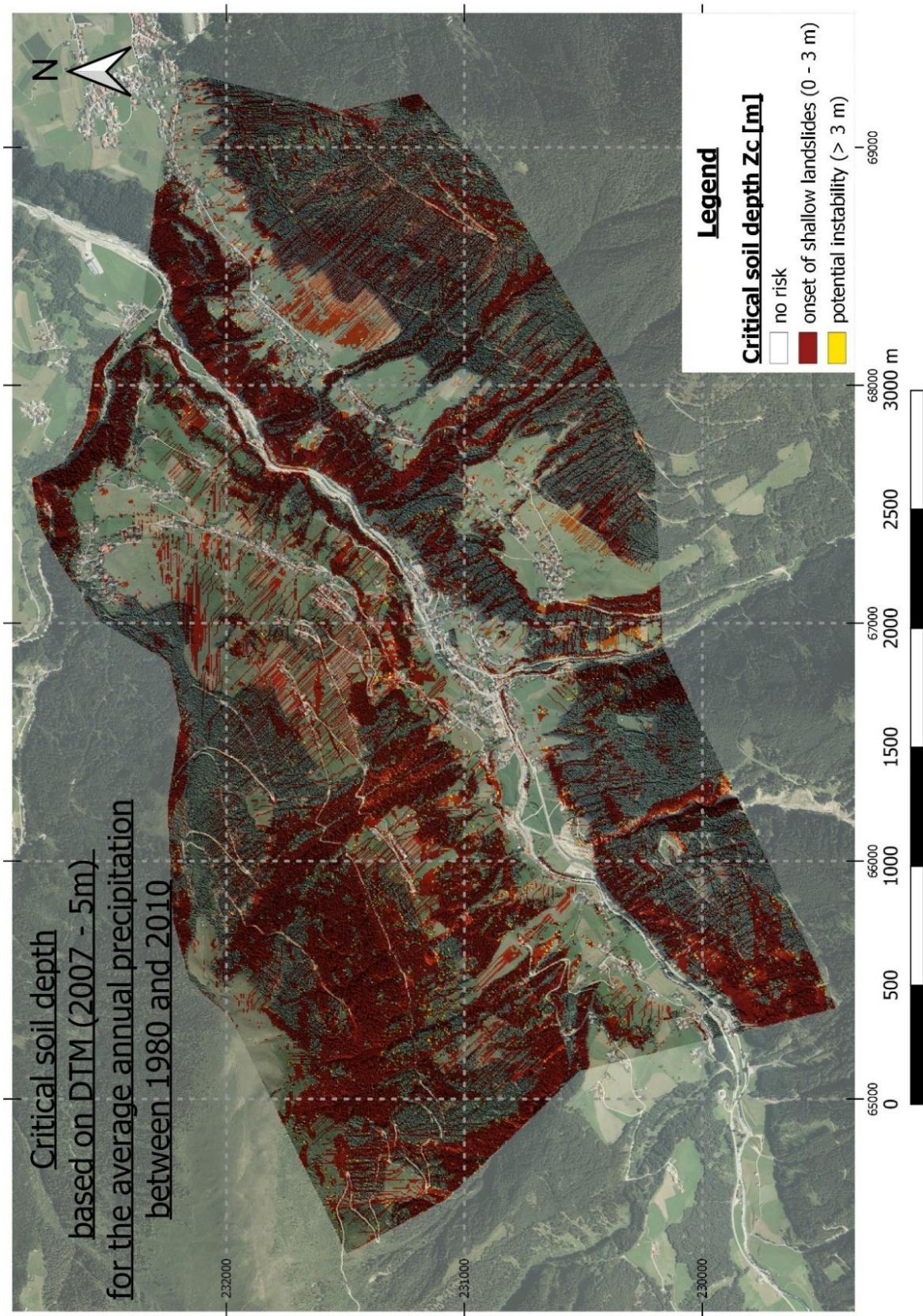


Figure 76: Map of the critical soil depth z_c for the average annual precipitation between 1980 and 2010 (2007 - DTM, 5m); raw data: © (Land Tirol - data.tirol.gv.at, 2018), orthophoto: © (Land Tirol - data.tirol.gv.at, 2019)

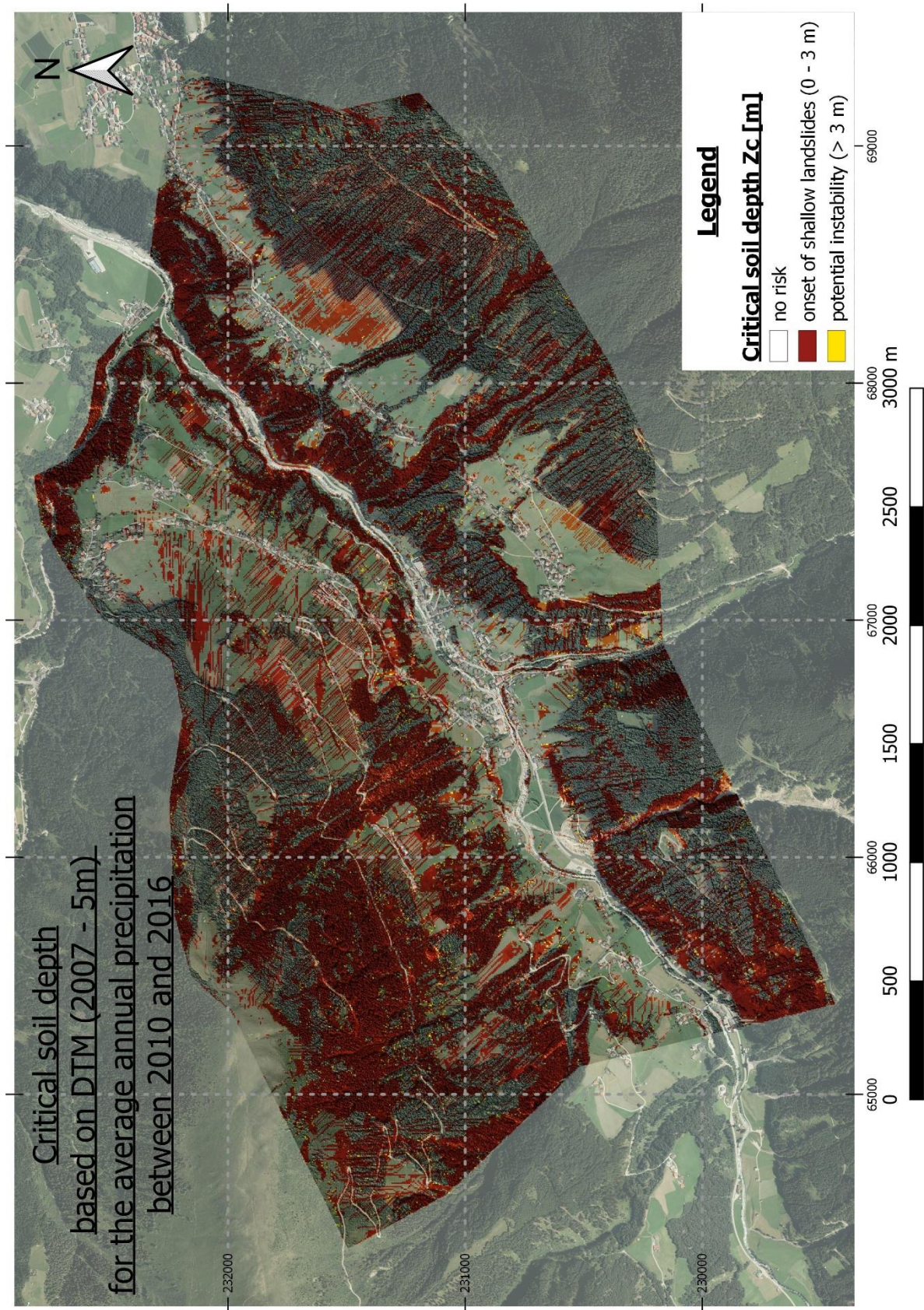


Figure 77: Map of the critical soil depth z_c for the average annual precipitation between 2010 and 2016 (2007 - DTM, 5m); raw data: © (Land Tirol - data.tirol.gv.at, 2018), orthophoto: © (Land Tirol - data.tirol.gv.at, 2019)

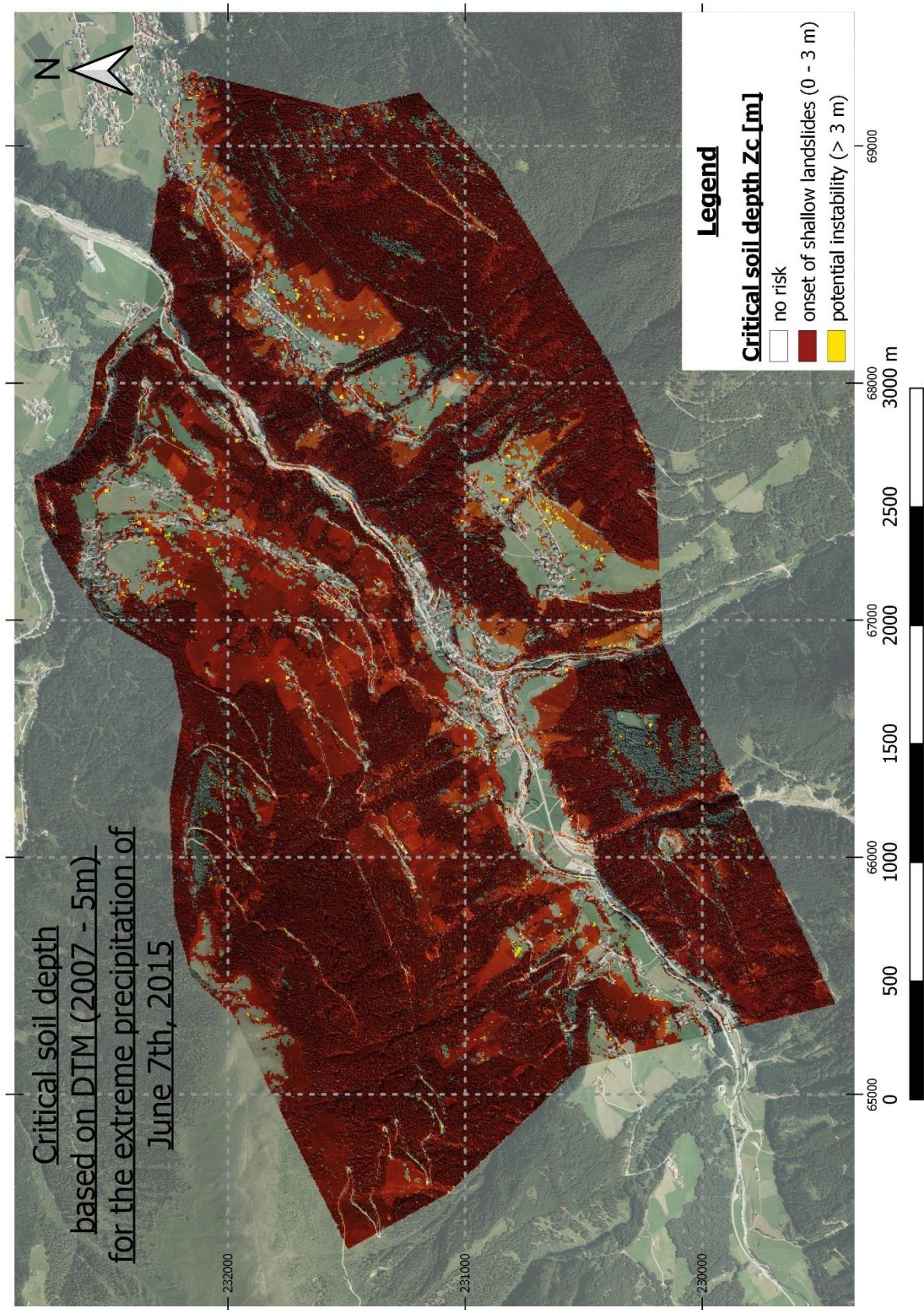


Figure 78: Map of the critical soil depth z_c for the extreme precipitation of June 2015 (2007 - DTM, 5m); raw data: © (Land Tirol - data.tirol.gv.at, 2018), orthophoto: © (Land Tirol - data.tirol.gv.at, 2019)

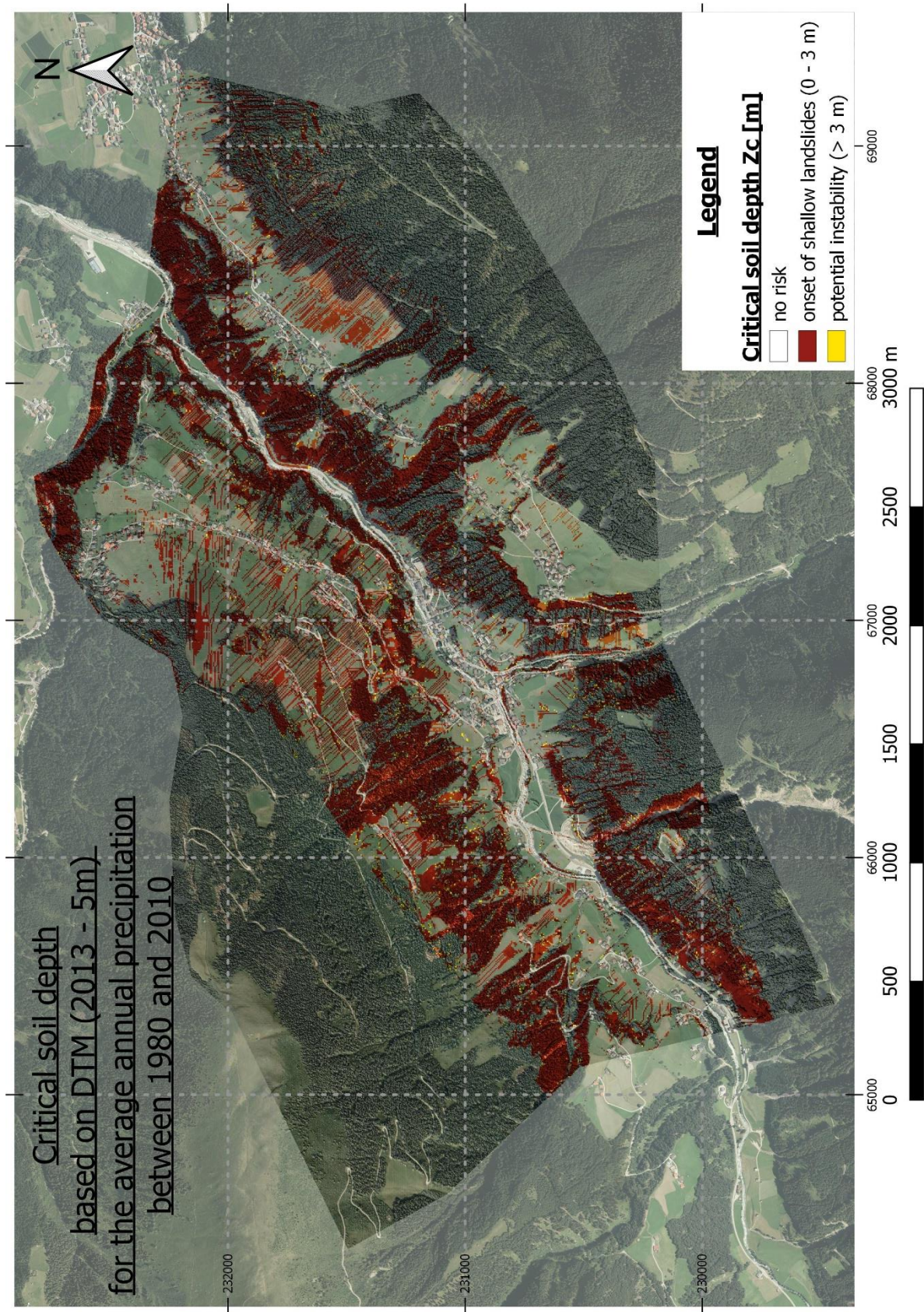


Figure 79: Map of the critical soil depth z_c for the average annual precipitation between 1980 and 2010 (2013 - DTM, 5m); raw data: © (Land Tirol - data.tirol.gv.at, 2018), orthophoto: © (Land Tirol - data.tirol.gv.at, 2019)

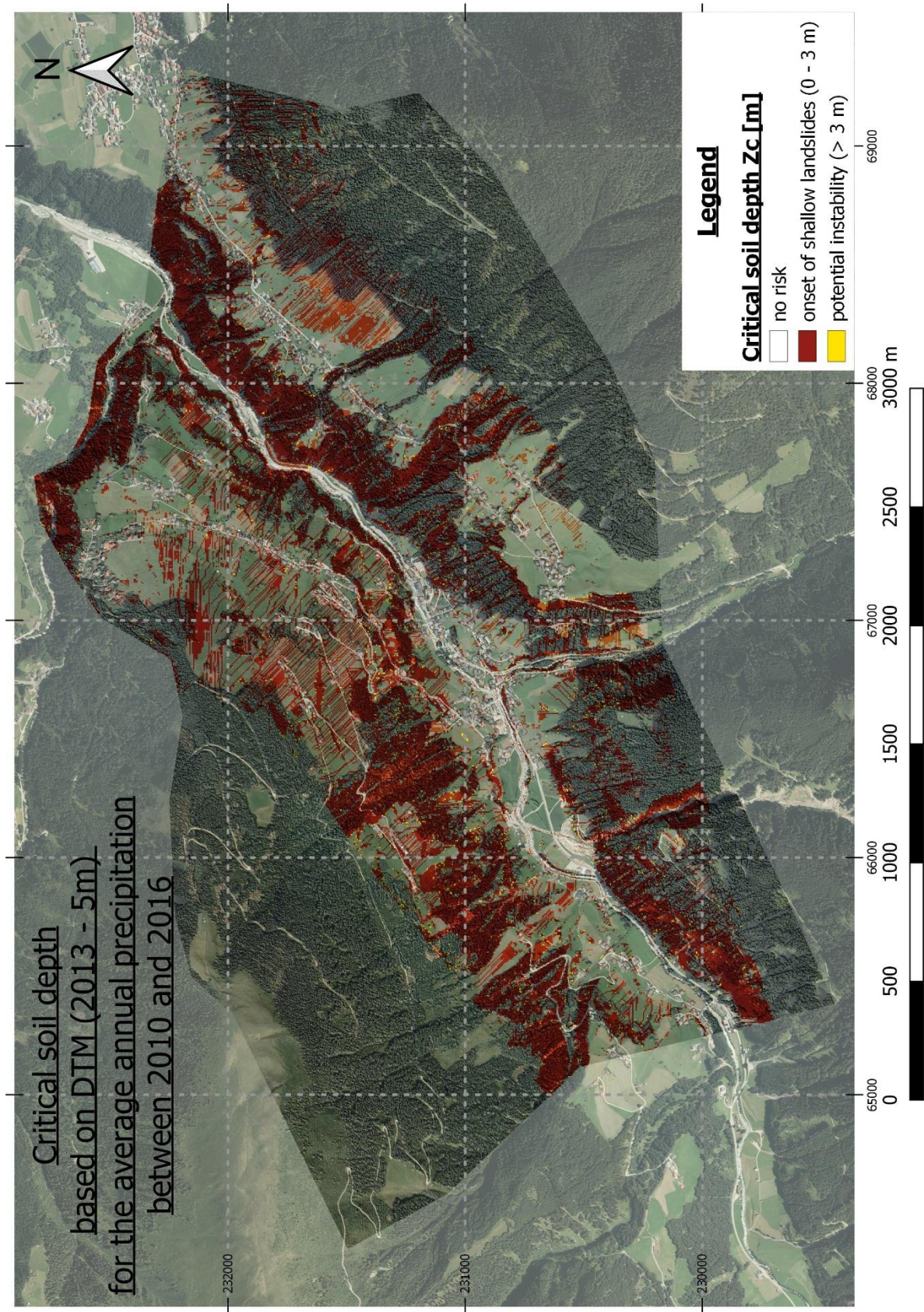


Figure 80: Map of the critical soil depth z_c for the average annual precipitation between 2010 and 2016 (2013 - DTM, 5m); raw data: © (Land Tirol - data.tirol.gv.at, 2018), orthophoto: © (Land Tirol - data.tirol.gv.at, 2019)

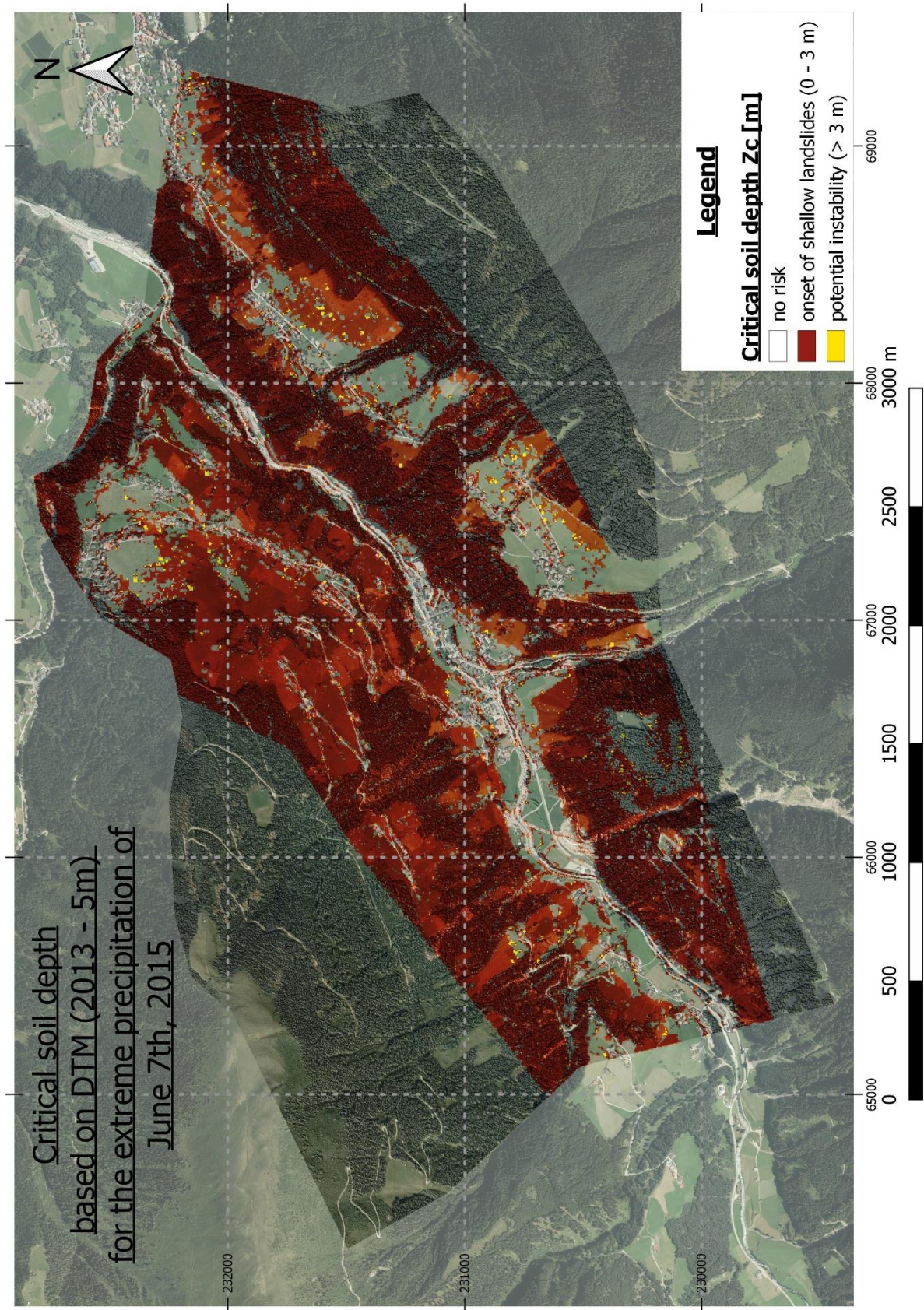


Figure 81: Map of the critical soil depth z_c for the extreme precipitation of June 2015 (2013 - DTM, 5m); raw data: © (Land Tirol - data.tirol.gv.at, 2018), orthophoto: © (Land Tirol - data.tirol.gv.at, 2019)

13.3.2 10m resolution

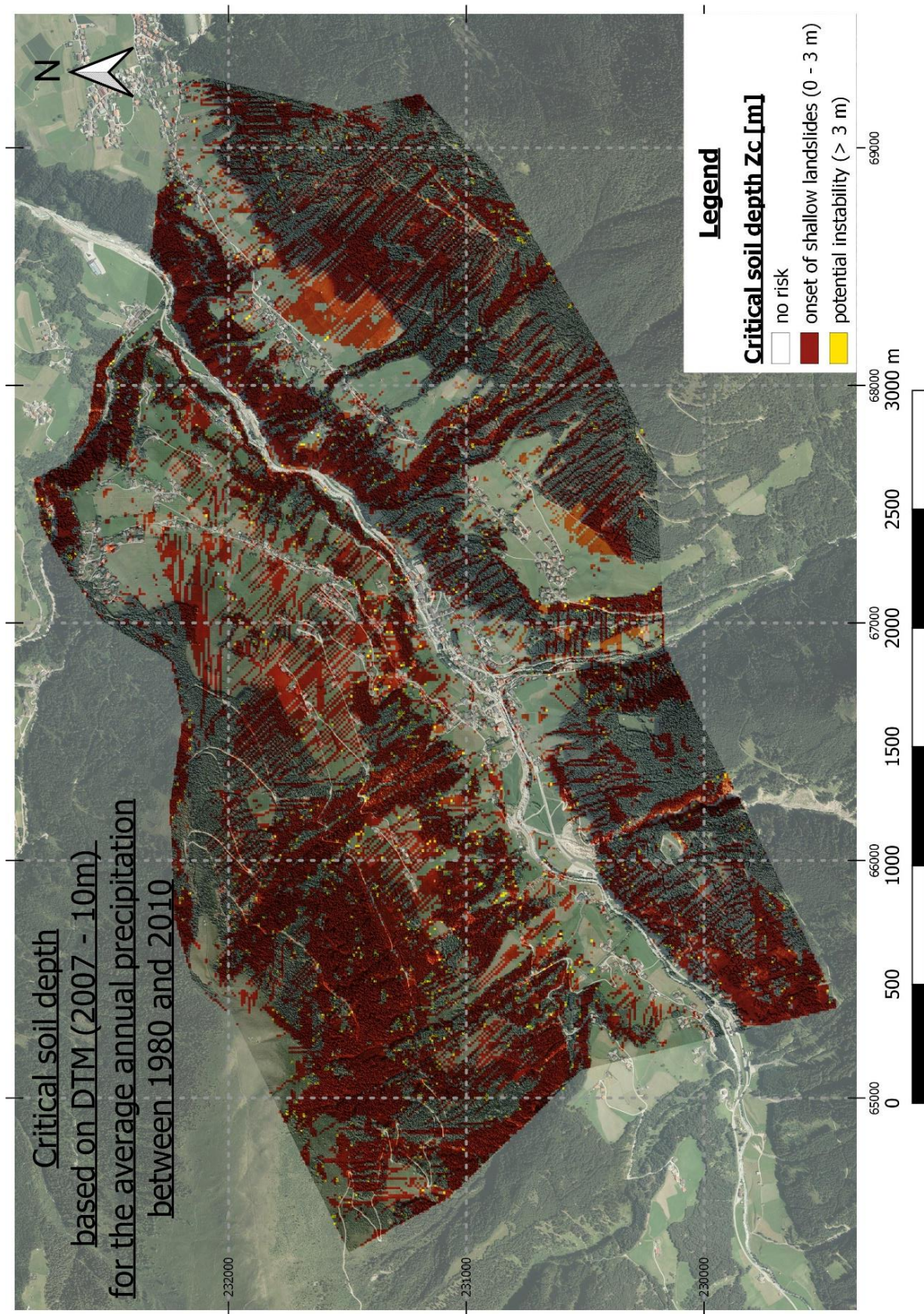


Figure 82: Map of the critical soil depth z_c for the average annual precipitation between 1980 and 2010 (2007 - DTM, 10m); raw data: © (Land Tirol - data.tirol.gv.at, 2018), orthophoto: © (Land Tirol - data.tirol.gv.at, 2019)

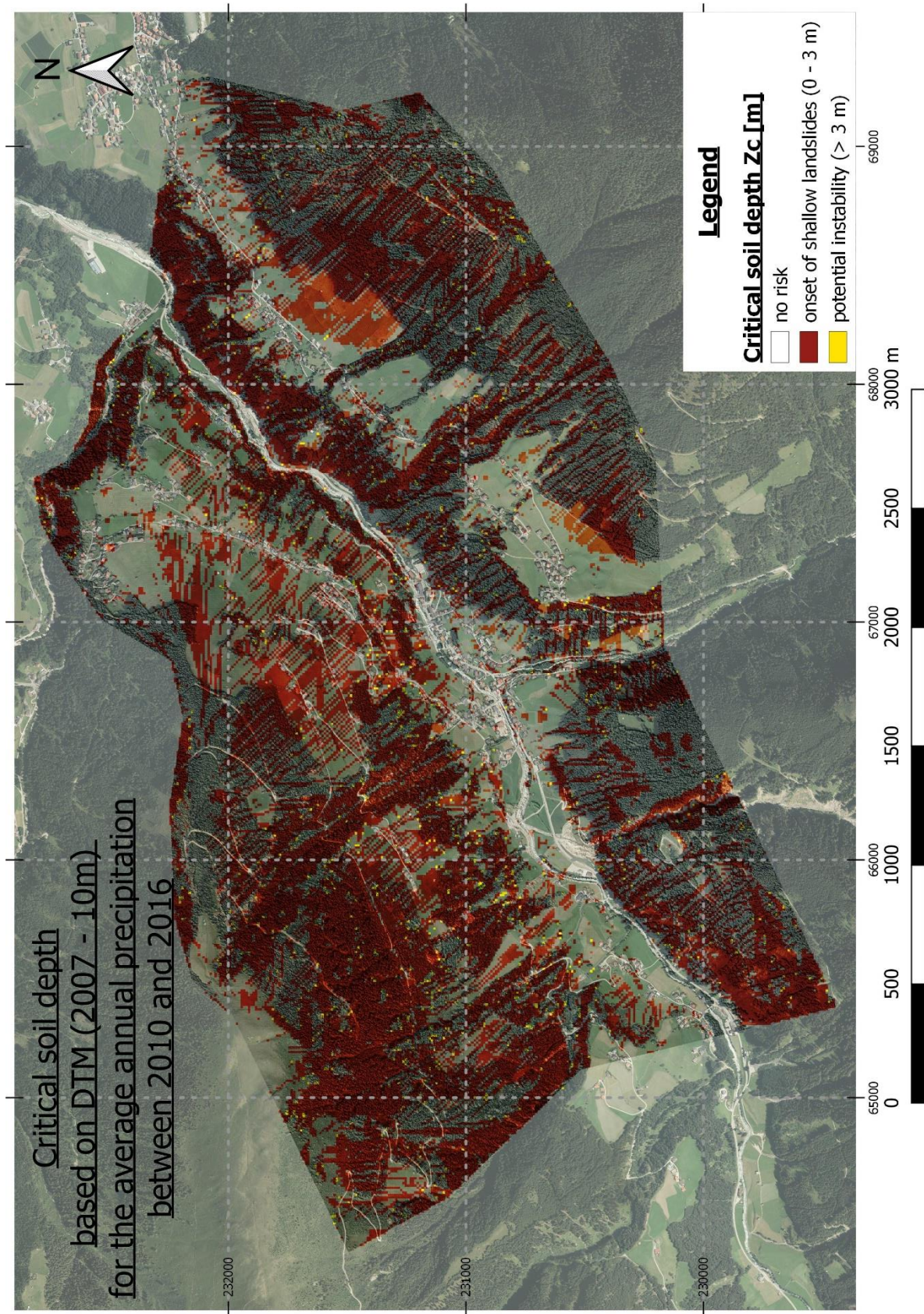


Figure 83: Map of the critical soil depth z_c for the average annual precipitation between 2010 and 2016 (2007 - DTM, 10m); raw data: © (Land Tirol - data.tirol.gv.at, 2018), orthophoto: © (Land Tirol - data.tirol.gv.at, 2019)

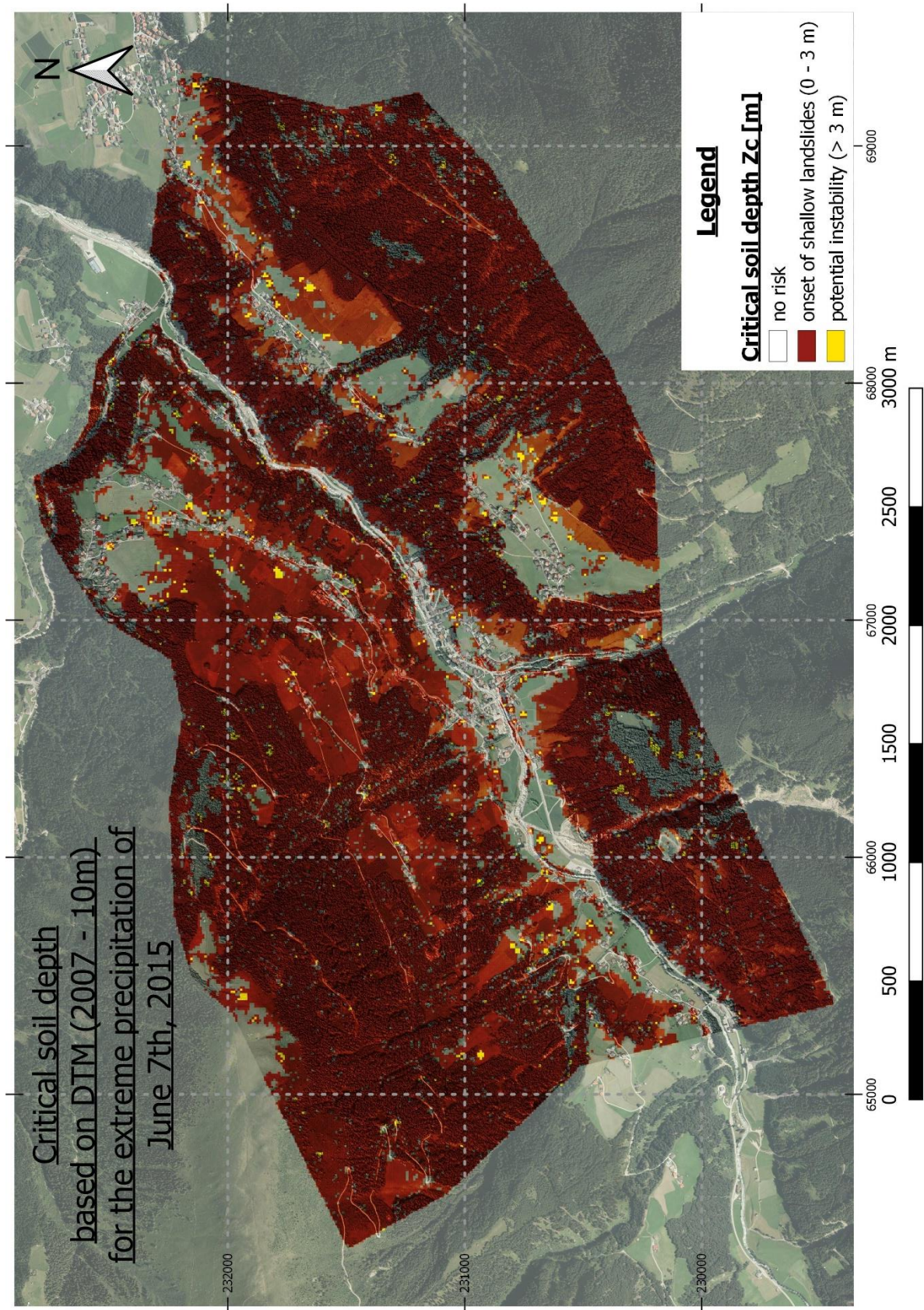
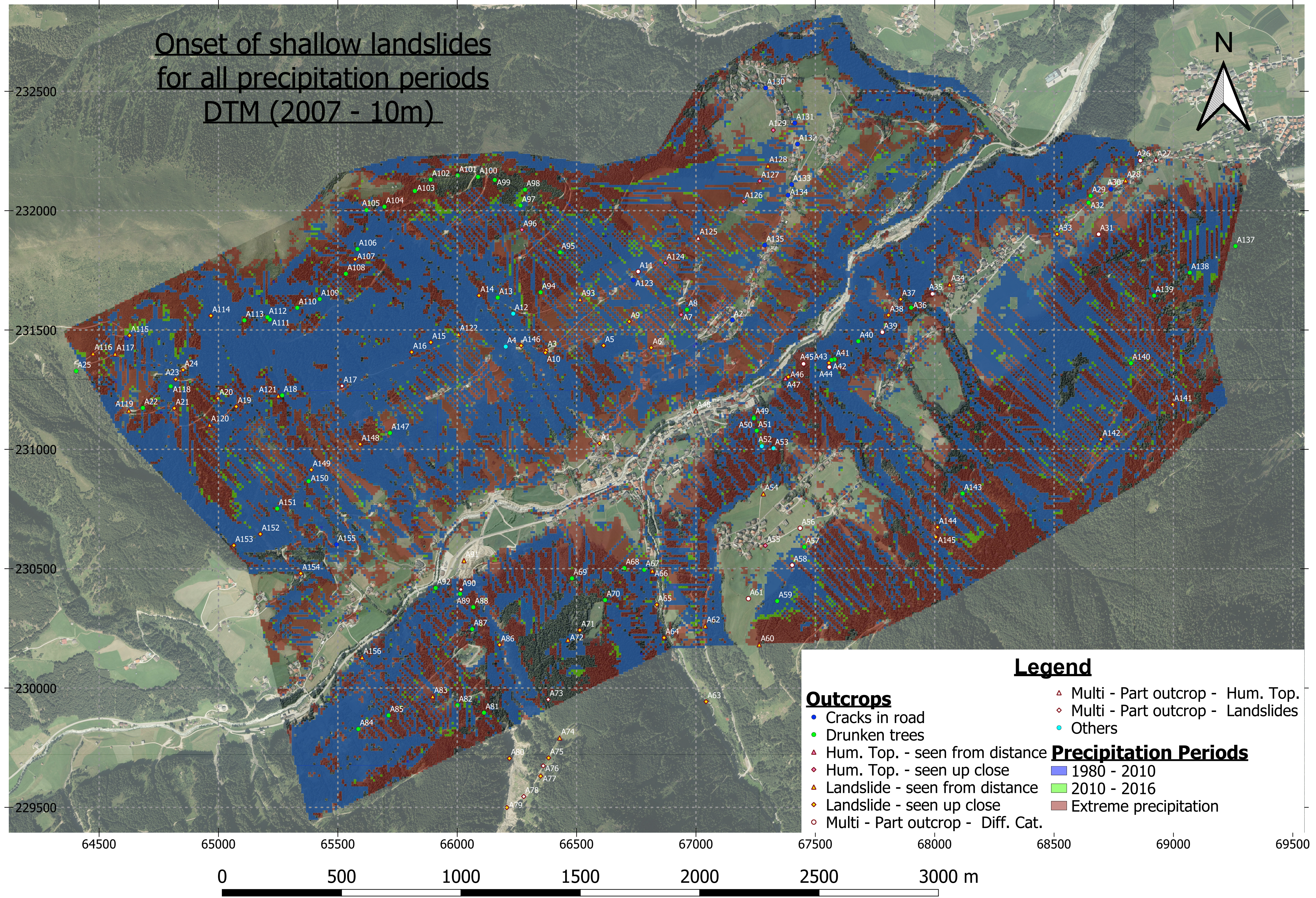


Figure 84: Map of the critical soil depth z_c for the extreme precipitation of June 2015 (2007 - DTM, 10m); raw data: © (Land Tirol - data.tirol.gv.at, 2018), orthophoto: © (Land Tirol - data.tirol.gv.at, 2019)

Onset of shallow landslides for all precipitation periods DTM (2007 - 10m)



Legend

Outcrops

- Cracks in road
- Drunken trees
- ▲ Hum. Top. - seen from distance
- ◆ Hum. Top. - seen up close
- ▲ Landslide - seen from distance
- ◆ Landslide - seen up close
- Multi - Part outcrop - Diff. Cat.
- ▲ Multi - Part outcrop - Hum. Top.
- ◆ Multi - Part outcrop - Landslides
- Others

Precipitation Periods

- 1980 - 2010
- 2010 - 2016
- Extreme precipitation